

**NEURO-FUZZY BASED MPPT FOR SOLAR PV PANEL  
HYBRID COOLING SYSTEM**

A Project Proposal Presented to the Faculty of  
Electronics Engineering Department  
College of Engineering  
Technological University of the Philippines

In Partial Fulfillment of the Subject Requirements for the Degree of  
**Bachelor of Science in Electronics Engineering**

Gratela, Rickric O.

Martes, Joyce Ann S.

Pagatpatan, Gerome I.

Pagkaliwangan, Jessa P.

Torcuato, Diether Kyle A.

August 2020

## APPROVAL SHEET

This project study entitled "**Neuro-Fuzzy Based MPPT for Solar PV Panel Hybrid Cooling System**", has been prepared and submitted by the following proponents:

Gratela, Rickric O.

Pagatpatan, Jerome I..

Martes, Joyce Ann S.

Pagkaliwangan, Jessa P.

Torcuato, Diether Kyle A.

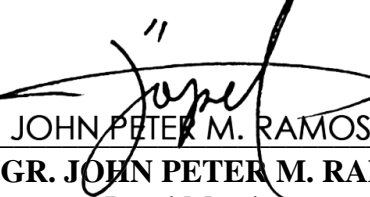
In partial fulfillment of the requirements for the degree of **Bachelor of Science in Electronics Engineering** is hereby recommended for approval.



DR. IRA C. VALENZUELA  
Adviser

---

ENGR. EDMON O. FERNANDEZ  
Panel Member



JOHN PETER M. RAMOS

ENGR. JOHN PETER M. RAMOS  
Panel Member

---

ENGR. TIMOTHY M. AMADO  
Panel Member



---

ENGR. GLENN CALVIN VIRREY  
Panel Member

Accepted and approved in partial fulfillment of the course requirements for the degree of **Bachelor of Science in Electronics Engineering**.

---

ENGR. EDMON O. FERNANDEZ  
Head, ECE Department

---

ENGR. BENEDICTO N. FORTALEZA  
Dean, College of Engineering

## **ACKNOWLEDGEMENT**

The researchers would like to express deepest gratitude to the individuals who contributed to the success of this study.

To Dr. Ira C. Valenzuela, our dearest thesis adviser, for giving her precious time during consultations throughout the completion of the study, for her effort and support which resulted for this research to be presented in an international conference, for her notions and skills that aided the proponents to attain a successful research. Lastly, to her knowledge and guidance that is truly inspiring not only as an engineer but also as a researcher.

To our Methods of Research and Project Study professors: Engr. Aaron U. Aquino and Engr. Nilo M. Arago, for sharing their proficiency, wisdom, provisions, and references that made this research feasible and fruitful.

To Engr. Edmon O. Fernandez, Engr. Timothy M. Amado, and Engr. John Peter C. Ramos for their approval of this project study, constructive criticisms, perceptions, support, and recommendations to help and improve the competence of the researchers and the study.

To the Electronics Engineering Department faculty, who unceasingly supported and contributed to the continuous excellence of the researchers.

To the head of Balangkas Material Recovery Facility, Ms. Nelda Gabiaso, and co-facilitators for permitting the researchers to deploy and conduct experiments in this location. Most of all, for their warm welcome and support during and after deployment which greatly eased the accomplishment of this study.

To the endless love, prayers, and support of the proponents' families which served as an inspiration and motivation all throughout this course. For morally believing and financially aiding the researchers, thank you very much.

On top of all, to God Almighty our Creator, for the opportunity, strength, blessings, grace, and unending guidance He provided to us all throughout this time. To God be the glory and honor.

The Researchers

## **ABSTRACT**

The project study aimed to develop a Neuro-Fuzzy based MPPT solar charge controller and hybrid cooling system for solar PV panel. The proposed algorithm, Adaptive Neuro-Fuzzy Inference System (ANFIS) uses voltage, current, temperature and irradiance as inputs in tracking the maximum power point as a prediction model to obtain the power cycle to regulate the output. The hybrid cooling system is composed of air cooling and water-cooling mechanisms to mitigate the negative effects of temperature that will increase the efficiency and lifespan of the solar panel. The cooling system is activated through a microcontroller that detects the temperature of the solar panel surface when it exceeds the threshold. Based on the testing procedures and data gathering done, the proposed 150 W solar PV system with hybrid cooling and ANFIS-MPPT gained the highest efficiency value of 24.005 % compared to the standard setups. For the AI-based prediction model using ANFIS, the training phase showed an RMSE value of 0.0015666 % while the testing phase showed an error value of 0.086933 %. The results conclude that the proposed system has a great fit in terms of precision.

## TABLE OF CONTENTS

TITLE PAGE.....	i
APPROVAL SHEET.....	ii
ACKNOWLEDGEMENT.....	iii
ABSTRACT.....	v
TABLE OF CONTENTS.....	vi
CHAPTER 1 .....	1
INTRODUCTION .....	1
1.1 Background of the Study.....	1
1.2 Statement of the Problem .....	2
1.3 Objectives.....	3
1.4 Significance of the Study .....	3
1.5 Scope and Limitations of the Study .....	4
CHAPTER 2 .....	6
REVIEW OF RELATED LITERATURE.....	6
2.1 Conceptual Literature .....	6
2.2 Related Literature .....	19
CHAPTER 3 .....	26
METHODOLOGY .....	26
3.1 Theoretical Framework .....	26
3.2 Conceptual Framework .....	27
3.3 Research Process Flow .....	28
3.4 Hardware Design .....	29
3.5 Software Development .....	38
3.6 Testing Procedure .....	43
3.7 Evaluation Procedure .....	44
3.8 Gantt Chart .....	45

<b>CHAPTER 4 .....</b>	<b>46</b>
<b>RESULTS AND DISCUSSION .....</b>	<b>46</b>
4.1 Project Technical Description .....	46
4.2 Project Structural Organization .....	46
4.3 Project Capabilities and Limitations .....	48
4.4 Project Evaluation.....	49
4.5 Tabulation of Results and Interpretation .....	50
<b>CHAPTER 5 .....</b>	<b>54</b>
<b>SUMMARY OF FINDINGS, CONCLUSIONS AND RECOMMENDATIONS.....</b>	<b>54</b>
5.1 Summary of Findings .....	54
5.2 Conclusion.....	54
5.3 Recommendation .....	55
<b>REFERENCES.....</b>	<b>56</b>
<b>APPENDIX A BILL OF MATERIALS.....</b>	<b>63</b>
<b>APPENDIX B PROGRAM CODES .....</b>	<b>65</b>
<b>APPENDIX C SPECIFICATIONS AND DATASHEET .....</b>	<b>83</b>
<b>APPENDIX D DOCUMENTATION .....</b>	<b>103</b>
<b>APPENDIX E CURRICULUM VITAE .....</b>	<b>106</b>

## LIST OF TABLES

<b>Table No.</b>	<b>Title</b>	<b>Page</b>
<b>Table 2.1</b>	Maximum Power Changes of PV panel	6
<b>Table 2.2</b>	Annual electric energy and energy generation efficiency of conventional PV and PV-PCM Panel	13
<b>Table 3.1</b>	Data Comparison of 3 Different Setups	44
<b>Table 3.2</b>	Activities from November to March 2020	45
<b>Table 4.1</b>	Summary of efficiency per setup	50
<b>Table 4.2</b>	Summary of efficiency comparison	50
<b>Table 4.3</b>	Training Data for different FIS Functions	51
<b>Table 4.4</b>	Cost saved for each setup	53

## LIST OF FIGURES

Figure No.	Title	Page
<b>Figure 2.1</b>	Effect of humidity (%) on the output power of the PV solar module at the 800 W/m <sup>2</sup> level	8
<b>Figure 2.2</b>	Effect of dust on solar cell efficiency at the 800W/m <sup>2</sup> irradiation level	8
<b>Figure 2.3</b>	Net Radiation according to geographical location	9
<b>Figure 2.4</b>	Monthly efficiency of different types of silicon solar cells	10
<b>Figure 2.5</b>	CV Technique Flowchart	14
<b>Figure 2.6</b>	P&O Flowchart	15
<b>Figure 2.7</b>	Fibonacci Search Algorithm	16
<b>Figure 2.8</b>	Neural Network	17
<b>Figure 2.9</b>	Fuzzy Logic System	17
<b>Figure 2.10</b>	Surface view created by ANFIS	18
<b>Figure 2.11</b>	Rule base of ANFIS controller	19
<b>Figure 3.1</b>	Closely Related to the Present Study under Investigation	26
<b>Figure 3.2</b>	Input-Process-Output Diagram of the System	27
<b>Figure 3.3</b>	Process Flow Chart of the System	28
<b>Figure 3.4</b>	Block Diagram of the System	29
<b>Figure 3.5</b>	Detailed Design of the Solar Panel Rack	31
<b>Figure 3.6</b>	Schematic Diagram	32
<b>Figure 3.7</b>	Restar Solar 150W Monocrystalline	33
<b>Figure 3.8</b>	Buck-boost Converter	33
<b>Figure 3.9</b>	Lead-Acid Battery	34
<b>Figure 3.10</b>	DC Brushless Fan and DC Water Pump	34
<b>Figure 3.11</b>	Mega ATmega2560-16AU CH340G	35
<b>Figure 3.12</b>	Voltage Detection Sensor Module 25V	35

<b>Figure 3.13</b> Current Sensor ACS712T-20A	36
<b>Figure 3.14</b> Temperature Sensor DS18B20	36
<b>Figure 3.15</b> Adafruit TSL2591 Light Sensor	37
<b>Figure 3.16</b> Cooling System Flowchart	38
<b>Figure 3.17</b> Fuzzy Interference System	39
<b>Figure 3.18</b> ANFIS Network Design	39
<b>Figure 3.19</b> Triangular Membership Functions	40
<b>Figure 3.20</b> ANFIS Program Flow Chart	41
<b>Figure 3.21</b> Buck-Boost Program Flow Chart	42
<b>Figure 4.1</b> Front Side of the Panel	47
<b>Figure 4.2</b> Rear Side of the Panel	47
<b>Figure 4.3</b> Solar Panel Setups	48
<b>Figure 4.4</b> Power output of setups 1,2, & 3	49
<b>Figure 4.5</b> Surface Plot of Duty Cycle with Respect to Voltage and Irradiance	50
<b>Figure 4.6</b> Surface Plot of Duty Cycle with Respect to Current and Temperature	51
<b>Figure 4.7</b> Test Plot	51

## **CHAPTER 1**

### **INTRODUCTION**

Energy consumption and demand increases with the continuous population growth. Fossil fuels are mostly the source of the world's energy but are limited and therefore lead to continuously price increase that directly impacts inflation [1]. Using air, solar, and hydro power as renewable energy sources is important in developing a more viable environment. The solar energy is an effective renewable energy due to its abundance, convenience, cleanliness, and reliability. It has been paid more attention since the availability of the swiftly emerging technology in catering the energy demands of the evolving world and society [2].

An electrical device that directly converts light energy to electrical energy is called a solar cell. It is the production of voltage or current in a material from exposing the material to sunlight. Solar cells produce electric current even without external voltage source. The solar cell performance can be affected by its crystalline structure, intensity of light, angle of sunlight irradiation, and surface temperature [3].

#### **1.1 Background of the Study**

A traditional photovoltaic (PV) system receives 80 % of immediate solar radiation, which is either reflected or absorbed as heat energy by the glass cover of the PV module. This results to a great influx of PV module temperature [4]. According to a study, for every rise of 1 degree Celsius in PV cell temperature, its efficiency falls by 0.45 % [5]. Truthfully, most panels on the market has an efficiency of about 6 %-20 % as a result from the conversion of solar energy into waste heat. Since the PV panel temperature surges with any gradual increase of solar radiation level, the PV system

requires an integration of a cooling system that will effectively maintain the appropriate working temperature.

Variety of methods for cooling are used and the most common are air and water. Air cooling has an average capacity and needs less energy compared to water cooling. On the contrary, water is more effective as coolant than air though it requires more expensive equipment than air cooling [6]. According to a study, a PV module yields greater output energy with a hybrid cooling system compared to just using fan as coolant [7]. Another method used in aiming greater efficiency is the use of different algorithms for Maximum Power Point Tracking (MPPT). Maximum Power Point Tracking algorithms are applied to the nonlinear power output of a solar panel caused by environmental constraints [8]. These include techniques such as the Fuzzy Logic Control (FLC) [9], the Artificial Neural Network method (ANN method) [10], the Perturbation and Observation method (P & O method) [11], and the Ripple Correlation Control algorithm (RCC algorithm) [12].

There are various studies that apply automatic cooling systems to mitigate efficiency loss of solar PV panels. Through a system of weather station and wireless nodes, the module temperature and atmospheric parameters such as ambient temperature, irradiation intensity, relative humidity, and wind speed are processed as data to activate the cooling system [13].

## **1.2 Statement of the Problem**

Due to the increasing price and decreasing reserve of the current energy sources, this study concentrates in renewable energy. Solar power remains to be one of the most lavish and auspicious type of renewable energy that allows the production of electricity from the unbounded sunlight. Unfortunately, Solar PV panels are not able to reach its maximum efficiency due to the excessive heat that can significantly reduce the power

production. The efficiency goes down by about 0.45 % per °C increase in the temperature of the panel [14]. From the occurrence of irradiation, 80% is being utilized by the PV, portion of it is used for power production, and the remaining just turned into heat energy which results to power loss [15]. Also, the non-linearity of solar radiation and ambient temperature yields to a variation of PV solar panel outputs that causes inefficiency [16].

### **1.3 Objectives**

#### **1.3.1 General Objective**

This study aims to develop a Neuro-Fuzzy Based MPPT Solar Charge Controller and Hybrid Cooling System for Solar PV Panel.

#### **1.3.2 Specific Objectives**

1. To develop a Neuro-Fuzzy-controlled algorithm to implement maximum power point tracking in a solar charge controller.
2. To design hybrid air- and water-cooling system and optimize the activation time.
3. To compare the three different setups of PV system with MPPT, with Hybrid Cooling, and with both MPPT and Hybrid Cooling System in terms of efficiency.
4. To develop cost-benefit analysis for the three different setups of PV system with MPPT, with Hybrid Cooling, and with both MPPT and Hybrid Cooling System.

### **1.4 Significance of the Study**

The technology being used daily is evolving and requires efficient energy sources. As each day progresses, energy scarcity is becoming evident and renewable

energy as alternative is becoming a trend. These generators of renewable energy resources are made to last long enough until further inventions are created.

The study will help increase the efficiency of solar PV panel for longer usage as an energy source. This study will benefit owners of solar PV panels and those who plan to use solar PV panels as their energy source in their household or for commercially use. This design of the study will provide a self-sustaining automated cooling system that will help lessen the expenses for energy usage and a neuro-fuzzy based charge controller to maximize the power output under different atmospheric conditions.

The study will also provide data containing the critical parameters of solar PV system that needs to be observed. These data will be able to help future researchers in determining the best setup for the enhancement of the efficiency of a solar PV panel.

## **1.5 Scope and Limitations**

The primary focus of this study is to develop a neuro-fuzzy based MPPT charge controller for the hybrid air- and water-cooling system of the solar PV panels. The fan and water spray will be activated by the microcontroller using the PV system itself as power source. The activation starts when the temperature sensor attached to the PV module is triggered which is greater than  $35^{\circ}$ . The output of the PV panel will be regulated by the MPPT charge controller using Neuro-Fuzzy algorithm.

It is proven that to generate maximum electricity, the optimum tilt angle of the solar PV panel is calculated with respect to the geographical location of the setup. For this project, the solar PV panel will be mounted on a fixed angle. Due to the rotation of the Earth, the light radiation harnessed is lesser compared to a moving counterpart using a sun-tracking system.

This research includes the comparison of efficiencies of each setup to prove the significance of using a hybrid cooling system and maximum power point algorithm. Above all, this study aims to exceed the efficiencies of the previous studies that uses an MPPT which has an average power efficiency of 88.235 %, a DC brushless fan cooling system with 32.23 % efficiency increase in power output, and a DC water pump cooling system with 38.98 % increase in power output efficiency.

## CHAPTER 2

### REVIEW OF RELATED LITERATURE

#### 2.1 Conceptual Literature

##### 2.1.1 Environmental Factors

###### 2.1.1.1 Solar Radiation Level

As solar radiation increases, the output power also increases thus higher efficiency of solar PV panel is achieved [17]. The solar radiation level absorbed by a PV panel varies depending on the location of the setup and time intervals in a day. A MATLAB simulation [18] of an equivalent circuit of a PV panel using the manufactured data results show that with increased rating of solar radiation ( $\text{W/m}^2$ ) yields greater output power (W). For the simulation, the following parameters for rating a manufactured PV panel is used: 1,000  $\text{W/m}^2$  solar irradiance, 1.5 Air Mass, and 20 °C ambient temperature at 10 m above ground level and 1 m/s wind speed. Table 2.1 shows the maximum power changes of PV panel under various solar radiation levels and ambient temperature.

**Table 2.1** Maximum Power Changes of PV panel [18]

Matlab Simulation Results						
Max Power	Solar Radiation ( $\text{W/m}^2$ )					Temperature
	200	400	600	800	1000	
Pmax (W)	20.49	42.64	65.46	88.84	112.2	0 °C
Pmax (W)	18.02	38.03	58.57	79.83	101.1	25 °C
Pmax (W)	15.59	33.29	51.54	70.6	89.66	50 °C

### **2.1.1.2 Ambient Temperature**

Ambient temperature is one of the most prominent parameters that affect the solar PV panel efficiency. There is an inverse relation between ambient temperature and solar PV panel efficiency. As the ambient temperature increases, the power yield also decreases [19]. The optimal setup of floating solar PV panels installed on water surface [20] benefits from the effect of evaporation while also cooling down the overall temperature of the module. According to the table of the MATLAB simulation results, [18], a rating of solar radiation of  $1000 \text{ W/m}^2$  under varying ambient temperature conditions  $0\text{--}50^\circ\text{C}$ , yielded the most output power of  $112.2 \text{ W}$  at the lowest temperature  $0^\circ\text{C}$ . The output power decreased significantly with  $25^\circ\text{C}$  higher temperature at constant solar radiation levels.

### **2.1.1.3 Wind Velocity, Humidity and Dust Density**

Ambient humidity has a negative effect on solar PV panel performance. In an experiment [21], it is observed that with a 20 % increase in relative humidity and dust accumulation on the surface of the solar PV module, the power output is reduced by  $3.16 \text{ W}$  and  $7.70 \text{ W}$ . The setup is in a thermal laboratory with  $27^\circ\text{C}$  ambient temperature. Varieties of range in levels of irradiance intensity, water flow rate, and humidity were  $400\text{--}1000 \text{ W/m}^2$ ,  $40\text{--}160 \text{ L/h}$ , and  $40\text{--}60 \%$ . Figure 2.1 shows that with 40 % level of humidity, the power generated is  $25.31 \text{ W}$ ; increasing to 50 % and 60 % humidity and the output power consequently decreased by  $23.76 \text{ W}$  and  $22.15 \text{ W}$ . Dust accumulation of  $0.012 \text{ g/cm}^2$  on the PV module surface resulted to a 1.47 % efficiency drop. Figure 2.2 shows the difference in efficiency between a PV module with and without dust on its surface.

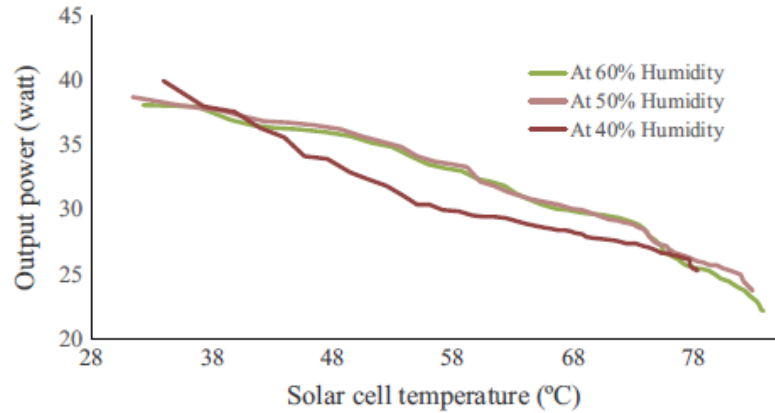


**Figure 2.1** Effect of humidity (%) on the output power of the PV solar module at the  $800 \text{ W/m}^2$  level [21]

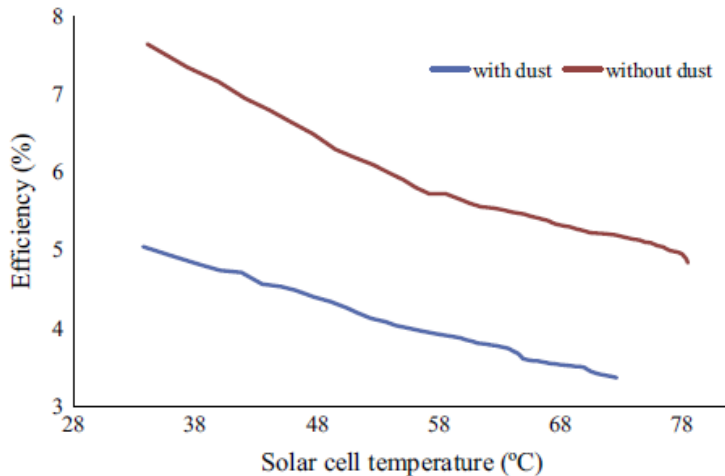


**Figure 2.2** Effect of dust on solar cell efficiency at the  $800 \text{ W/m}^2$  irradiation level [21]

A study [22] observed that increased wind velocity directly caused the decrease in humidity resulting to greater efficiency. Though increased wind speed causing the scattering and lifting of dust surrounding the PV module lowered its performance.

#### 2.1.1.4 Geographical Location and Tilt Angle for PV Panel Orientation

The Philippines as a tropical country mostly has an abundance of solar radiance throughout the year. According to NASA, the amount of light energy absorbed is higher compared to the amount of heat radiated, resulting to a net solar energy surplus for tropic regions. However, in polar regions, there is an energy deficit because heat radiated is greater than the light energy absorbed. Figure 2.3 shows the intensity of net radiation according to geographical location.

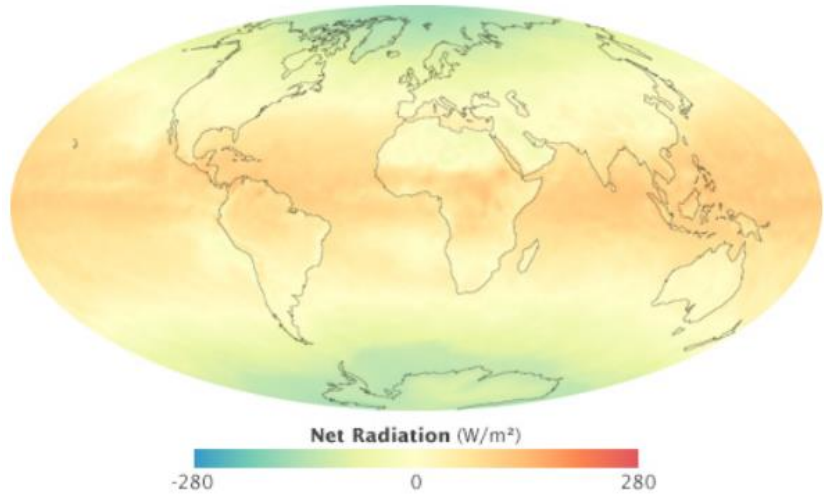


**Figure 2.3** Net Radiation according to geographical location

<https://earthobservatory.nasa.gov/features/EnergyBalance/page1.php>

To maximize power output in static installation of solar PV panels, the optimum angle of the PV panel setup is calculated using the latitude depending on geographical location. The research conducted through mathematical model for estimating the solar radiation at different tilt angles [23] concluded that the tilt angle should be adjusted at least twice a year. For the 80 cities of Iran, compared with a horizontal PV panel, the solar radiation

average gained annually for daily, monthly, seasonal, and yearly adjustments were 21.3 %, 21 %, 19.6 %, and 13.3 %.

### 2.1.2 PV System Devices

#### 2.1.2.1 Photovoltaic Cell

Solar PV panel efficiency depends on the PV cell type it is composed of. According to a market analysis, 90 % of the PV technologies developed used commercially available monocrystalline and multicrystalline solar PV cells 33 % and 53 % of the market, respectively. The efficiency of different types of silicon solar cells is graphed below for each month of the year [24]. Both types have excellent reliability – for monocrystalline silicon cell, a 24.7 % efficiency and for multicrystalline silicon cell, a 19.8 % efficiency. Figure 2.4 shows the monthly energy yield of monocrystalline, multicrystalline and amorphous type of PV cells.

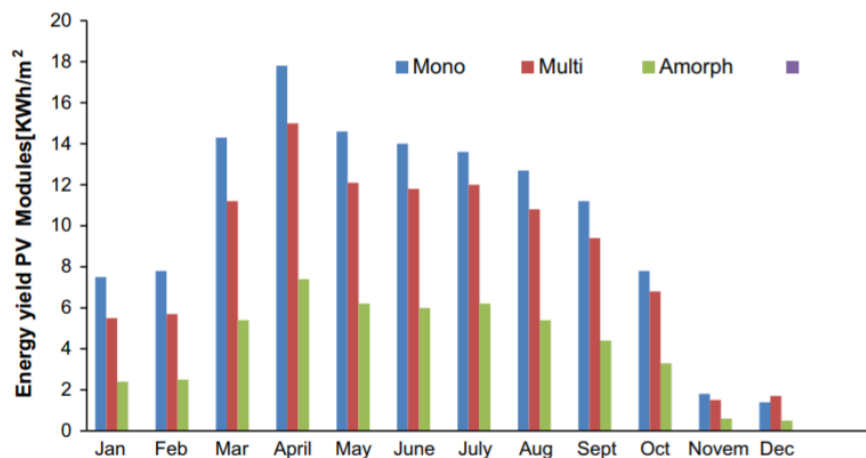


**Figure 2.4** Monthly efficiency of different types of silicon solar cells [24]

#### 2.1.2.2 Charge Controller

Solar PV charge controller is employed to protect the battery from overcharging and undercharging by using interrupt technique. It uses a

protection circuit that activates itself over current and short circuit characteristics. Due to the nonlinearity of solar PV characteristics and environmental factors such as temperature and solar irradiance, there is lesser efficiency produced. Maximum Power Point Tracking (MPPT) is integrated to charge controllers to efficiently extract the peak power value to supply the battery. According to a comparative study [25], P & O method for MPPT is the most common in research and in market.

#### **2.1.2.3 Battery**

Due to the scarcity of non-renewable energy, researchers find ways to design a small-scale solar PV system composed of solar PV panel and storage batteries. An array of photovoltaic panels is used as the primary energy source and batteries as backup energy sources. The importance of battery in this study is for storing electricity from the PV panel source to be consumed by the load [26].

#### **2.1.2.4 Inverter**

Power generation is essential to supply electricity for low-powered electronic consumption used in domestic applications. In a study, PIC16F72 is used to generate a 10 kHz PWM signal, which serves as a sine wave inverter while the IRFZ44MOSFET and 6N137 is used as a MOSFET driver. Since the study aims to power AC appliance, it is required to use an inverter. The load connected across a 12 V DC sine inverter input and 220 VAC output transformer considered several important results of P & O MPPT method and sine wave inverter for evaluation [26].

### **2.1.3 Cooling System**

For every increase of the PV module temperature by 1 °C, there is a relative decrease of 0.45 % in efficiency [27]. The integration of a cooling system maintains the optimal temperature for solar PV surfaces. According to a research under a cooled condition, there is an increase up to 47 % efficiency for a typical 4 kW PV system. The said cooling system is proposed for residential applications with a return of investment reduced by 2.9 years [28].

#### **2.1.3.1 Geothermal Cooling**

An efficiency of 18.90 % is achieved by geothermal cooling system subjected to hot climate. The study concluded that power efficiency increased with the corresponding air flow rates by 4.54 % for 0.0228 m<sup>3</sup>/s, 9.19 % for 0.0248 m<sup>3</sup>/s, 13.99 % for 0.0268 m<sup>3</sup>/s, and 18.90 % for 0.0288 m<sup>3</sup>/s. The setup includes a buried earth-to-air heat exchanger (EAHE) that precools ambient air and is implemented to flow at manually set rates into the encased surface under the solar PV module [29].

#### **2.1.3.2 Phase Change Material**

PCM is a passive cooling that is integrated to complex systems to remove the requirement of additional energy for controlled cooling systems though preferred conditions are low outdoor temperature, low wind speed, and high solar radiation. It is mainly used to decrease the PV module temperature directly with convective heat transfer coefficient as the limiting factor for the PCM material. According to the study, the PV-PCM system under outdoor climatic conditions has 0.8 % higher annual energy generation and 7.3 % increase of electric energy is produced compared to a conventional PV panel

[30]. Table 2.2 shows annual results of electric energy production and generated efficiency of PV and PV-PCM panel.

**Table 2.2** Annual electric energy and energy generation efficiency of conventional PV and PV-PCM panel [30]

Slovenia Month	Ljubljana Hglob [kWh]	Electric energy [kWh]		Energy generation efficiency [%]		Difference		Increase [%]
		Conventional PV	PV-PCM	Conventional PV	PV-PCM	[kWh]	[%]	
January	52.43	10.58	11.03	12.6	13.1	0.45	0.5	4.3
February	83.37	15.88	16.84	11.8	12.6	0.96	0.8	6.0
March	138.11	25.21	27.25	11.3	12.3	2.04	1.0	8.1
April	133.61	23.82	25.9	11.1	12.1	2.08	1.0	8.7
May	170.04	29.56	32.09	10.8	11.7	2.53	0.9	8.6
June	167.45	28.73	30.77	10.7	11.4	2.04	0.7	7.1
July	173.05	29.5	31.6	10.6	11.4	2.1	0.8	7.1
August	167.81	28.52	30.83	10.6	11.4	2.31	0.8	8.1
September	110.24	19.63	21.23	11.1	12.0	1.6	0.9	8.2
October	77.82	14.49	15.42	11.6	12.3	0.93	0.7	6.4
November	42.45	8.35	8.71	12.2	12.8	0.36	0.6	4.3
December	40.79	8.09	8.47	12.3	12.9	0.38	0.6	4.7
Total	1357.17	242.36	260.17	11.4	12.2	17.81	0.8	7.3

### 2.1.3.3 Water Cooling

In an experimental setup composed of water-cooling sprinkler across the back of a polycrystalline PV module, the activation of the sprinklers is done manually with a constant flowrate at scheduled time intervals. The water pipe is buried underground to keep the water temperature constant at 18 °C. Comparing the PV module with and without the water sprinkler system, there is a relative increase in efficiency of 12.17 % for high irradiation level and 9.09 % for low irradiance level [31].

### 2.1.4 MPPT Techniques

#### 2.1.4.1 Constant Voltage Method

The Maximum Power Point Tracking algorithm is installed in PV solar panel to achieve maximum available photovoltaic output power with a non-linear state due to the external environment effects. It aims to produce low efficiency of constant voltage method and having a hard time finding the next frequentative step will have the same effect of the increasing conductance method. Increasing of conductance and constant voltage were presented, to

manipulate the varying voltage with the overwhelming change in outside environment. With the use of the constant voltage method, the increase in conductance method with optimized step in iteration was suggested to eradicate the power variation. Using this technique, the efficiency of the system was said to be improved and the PV panel generated a steady and a momentary variation in characteristics with the suggested maximum power point tracking [8]. Figure 2.5 shows the flowchart of constant voltage technique.

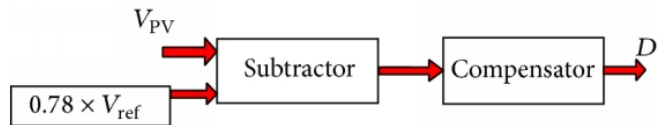


**Figure 2.5** CV Technique Flowchart [32]

#### 2.1.4.2 Perturb and Observe Method

This method is under the hill climbing based method which promotes an arbitrary solution in a problem and resort to a more useful solution by making an incremental variation in the given solution. Solar panel power output keeps varying with solar irradiation and temperature that causes the PV panel to receive a non-linear power characteristic. Due to the advancement of technology particularly to the field of power electronics, it is now possible to achieve PV power at its maximum power point for the improvement of its efficiency. Figure 2.6 shows the flow diagram of P&O.

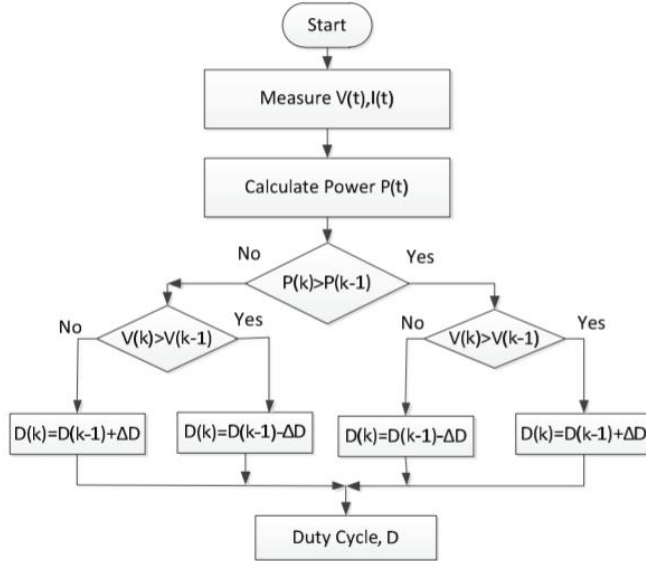


**Figure 2.6 P&O Flowchart [33]**

Based on Perturb and Observe method with the use of Fuzzy Logic Controller, the simulated result of the combined Fuzzy Logic Controller algorithm and Perturb and Observe method shows an improvement in maximum power point compared to the conventional Perturb and Observe method. Furthermore, it is easy to be implemented in PIC microcontroller that keeps up into fast variation results [33].

#### 2.1.4.3 Fibonacci Search

This method suggests an algorithm of topmost power tracking that produces withdrawal of the solar PV panel peak power under every conditions of solar radiation. The dynamic attributes of the solar PV panel show several steps and output under a small portion of shaded conditions caused by the inclusion of bypass diodes. Moreover, it also depends on the size of the panel and its configurations aside from the shade intensity and pattern. The normal Maximum Power Point Tracker has no means of differentiating the global maximum and the local maximum. This algorithm based on Fibonacci has always been suggested for its accuracy but fails with such shading conditions.

Changes in the algorithm is suggested by applying more than one search points to improve its accuracy in tracking and identification with reliability of global maximum with regards to its interval of searching. The algorithm suggested the introduction of a few shade patterns which are evaluated [34].

Figure 2.7 shows the algorithm of a Fibonacci Search.

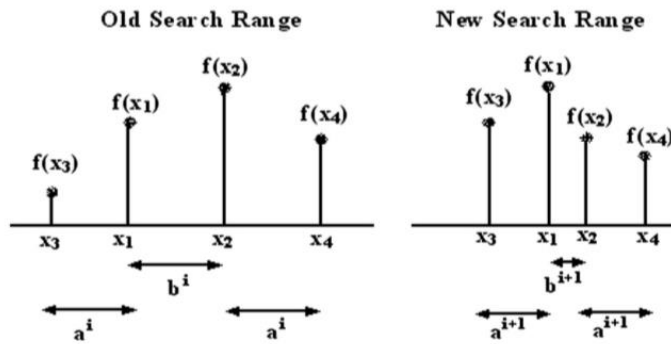


**Figure 2.7** Fibonacci Search Algorithm [35]

#### 2.1.4.4 Artificial Neural Network (ANN)

To mitigate efficiency loss and enable the system to operate optimally, another type of Artificial Intelligence (AI) is implemented for maximum power point tracking of a PV module. In this study [36], a MATLAB/Simulink simulation consisting of PV module, DC-to-DC boost converter and ANN based MPPT charge controller are used to control the whole system. The ANN technique used the atmospheric parameters, solar radiation level, and ambient temperature as nonlinear inputs; also combining Perturb and Observation algorithm to determine the incremental values of the energy output. It trains the data samples online since a small-scale device comes with an insufficient storage. The simulation underwent abrupt variations of solar radiation levels to evaluate the MPPT algorithm's response time and efficiency. Figure 2.8 shows a block diagram of the Neural Network.

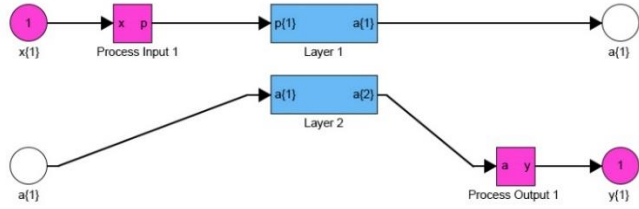


**Figure 2.8** Neural Network [36]

#### 2.1.4.5 Fuzzy Logic

FL implementation in MPPT method is developed for the solar panel output power maximization with the use of combination of fuzzy logic MPP Tracker algorithm to achieve a constant voltage and a cooling system for the improvement of solar panel output efficiency. The PV panel solar irradiation has an interrelation with its temperature which produces power oscillation. This variation is the main purpose of using maximum power point tracker within every state of weather. It presents that some point of MPPT can be achieved using the solar panel, particularly its Voltage-Current and Voltage-Power relation. Moreover, the Fuzzy logic-based implementation in Maximum Power Point Tracker improves overall efficiency of the panel and its performance compared to the common nonlinear controllers. This integrated fuzzy logic implementation in maximum power point tracker proved the accuracy and effectiveness in the improvement of its performance [37]. Figure 2.9 shows the framework of a fuzzy logic system.

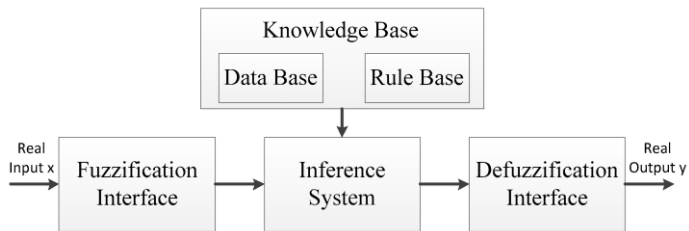


**Figure 2.9** Fuzzy Logic System [38]

#### 2.1.4.6 Adaptive Neuro-Fuzzy Interference System (ANFIS)

An existing study [39] designed an AI-controlled Maximum Power Point Tracking based on adaptive neuro-fuzzy interference system which is a stable and fast method. The proposed algorithm is implemented into a MATLAB/Simulink simulation, which consists of a PV module, ANFIS controller, boost converter and voltage inverter with a three-phase load as the output. The input conditions are PV module temperature and solar radiation levels are varied from 10 to 70 °C and 50 to 1000 W/m<sup>2</sup>. After 100 sets of data are trained, membership functions for the solar irradiance and PV module temperature with low, medium, and high levels are generated. A surface view is created and shows how the values of two atmospheric factors affect the maximum power output of the PV system shown in Figure 2.10. Figure 2.11 shows that the ANFIS system is limited to nine rules which proves to be efficient and accurate.

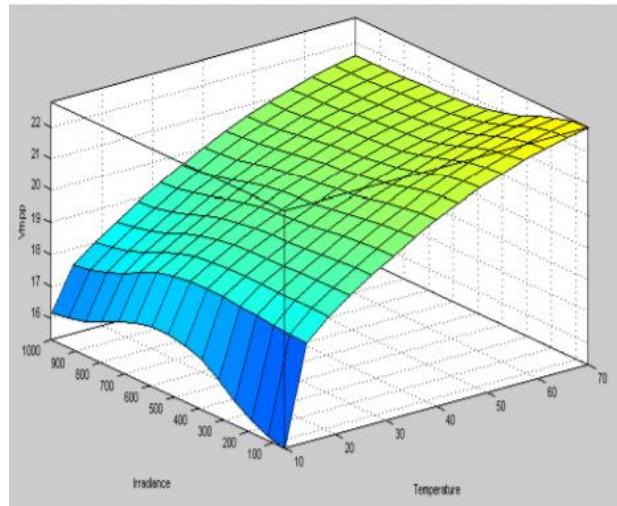


**Figure 2.10** Surface view created by ANFIS [39]

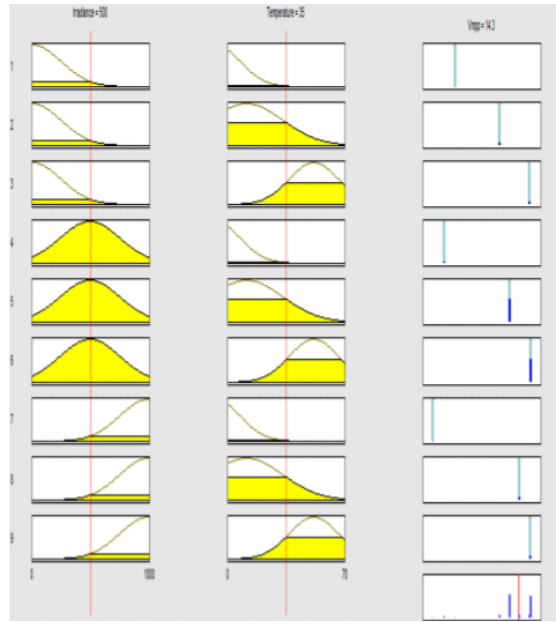


**Figure 2.11** Rule base of ANFIS controller [39]

## 2.2 Related Literature

### 2.2.1 Hybrid Cooling System

On a study of how cooling works using air and water fluids affects the solar panel, a fan is used on the backside of the panel while the water is flown on the front side. The water flows through a piping system and was set up to test along with the fan under various flow rates. The result shows a comparison between no cooling, air cooling, and water cooling at 1 gpm and 2 gpm, consecutively. A theoretical analysis is observed to determine the efficiency of each cooling process through its parameters [40].

Another study compared which the most optimal and efficient cooling system is between air-cooling technique, water-cooling technique, and hybrid cooling in decreasing the temperature of the solar PV panel. In this study, the air-cooling system will use the Ground Coupled Central Panel Cooling System or GC-CPCS that uses forced convection through a blower and uses earth tubes [41] like the

behavioral study of solar photovoltaic under different intensities of solar irradiance.

It also used a fan supplied by the panel itself [42].

For the water-cooling system, water nozzles will initiate the water flow from the upper side of the panel. It is a water cycle process that returns water to the tank to minimize consumption [41]. Similarly, using water for evaporative cooling technique wherein the water needs to evaporate to attain phase equilibrium. This method is cheap and easy to achieve and is effective for countries of dry climates [43].

The system of the study operates every fifteen minutes of either blower or pump or both as hybrid for two minutes. The data logger then records the data every five minutes and is stored every fifteen minutes. The result shows that though the hybrid system is more effective, it is costly than the other cooling method [41].

Another study deals with the comparison of photovoltaic cell output with and without cooling systems. Using hybrid photovoltaic/thermal system, the system aims to maintain the maximum allowable temperature which is 35 °C. The pump starts to work when the temperature exceeds the MAT until cooled below 35 °C by using LM35 temperature sensor [44].

A research using DC brushless fan aided with a water pump improved the efficiency and reduced the temperature of the panel. The PV module will provide the battery with electrical charge and the battery will supply the cooling system. The DC brushless fan is installed at the back while the DC water pump is installed in front of the PV module. The DC cooling system increases the output by 4.99 %, the output current by 39.9 %, and the output power by 42.65 %. This will help the payback period to reduce and the PV module lifespan to be [45].

Hybrid cooling system has also been compared with an automatic water-cooling system in a study of developed prototype. The combination of electrical and thermal energy output denotes the decrease in temperature of 11.42 % and greater energy production of about 8.22 % – greater than a common module resulting to an overall efficiency of 33.28 % [46].

### **2.2.2 Automated Cooling System**

Artificial neural network was used in numerous studies for automation to implement network training and testing while the man-machine communication interface is based on LabVIEW. Data gathering is used as input and output device for temperature control signals and drives the control unit to complete flow speed control. The trained neural network can predict fluid viscosity and the coefficient of thermal conductivity at different temperatures and pressures. Based on the results, temperature and fluid cooling control systems are more accurate [47].

As stated by a study, the concept of fuzzy logic can also be used to solve several types of control system which contains a series of if-then rules. According to fuzzy logic principles, the fuzzy if-then rules are used to map fuzzy sets in the input universe of discourse to the fuzzy sets in the output universe of discourse. The fuzzy model can control the speed of the hydraulic system and optimal operations of the cooling system [9].

The fuzzy logic controller can also be used as a base constant voltage MPPT algorithm. A research combined the two systems where the cooling system will reduce the temperature of the PV panel and the Fuzzy Logic Constant Voltage MPPT algorithm will track the peak power of the PV panel. The combination of the two systems showed better efficiency and performance of the panel. The output increased when it worked on the optimal temperature. This proves that Fuzzy Logic-

based controllers are effective in improving the efficiency of solar PV panels in any weather conditions [16].

Automated cooling systems requires regular monitoring and maintenance. The proposed system used microcontroller to display critical parameters that can be monitored real-time. The AT89S52 microcontroller that acquires and display real-time parameters was the basis of the module. The Hall Effect sensor ACS712, a 25-V Voltage Sensor, and DS18B20 digital temperature sensor is also used. The control circuit observed the state of the PV modules automatically without the help of any operator [48].

Enhancement in collection of energy is achieved by an integration of an automatic cooling system for PV modules. A method that estimates temperature was developed to determine the temperature of the PV module according to the data of wireless nodes or Wireless Sensor Network (WSN) on the PV modules that collects the environmental parameters and module temperature that transmits data to the gateway to control the sprinkling time for cooling. Seventeen point seventy-five percent energy output was produced more than the PV module without the cooling mechanism [49].

### **2.2.3 Maximum Power Point Tracking (MPPT)**

An MPPT controller is an algorithm in charge of battery charging regulation wherein it extracts the maximum energy a PV module can produce. MPPT helps produce more power regardless of climatic variations. There is an increase in the system voltage through the series connection with the PV modules. A study used a fuzzy controller in tracking the PV module's maximum power point. The outputs were compared to a P & O controller which shows that the proposed study has less

energy losses and by simulation, evaluated the consistency of the MPP of all cases [50].

A research [51] introduced the different techniques used in MPPT. It includes different algorithm flowcharts that may be used for each different unique condition. Another study used fuzzy logic MPPT to simplify PV modeling and directly control its duty cycle. Three stated PV modules were applied by the proposed technique for modeling and with boost converter. This system application significantly reduced the cost of the system while enhancing the efficiency of the PV system.

Artificial Neural Network (ANN) is also one of the AI-based techniques used for maximum power point tracking. A study [52] focused on mitigating the effects of non-uniform irradiance distribution for PV modules integrated on e-vehicles. The inputs for the multilayer feed-forward ANN are the PV module voltage and current used to compute the variation in power. A power threshold is set as a condition that will decide when to use the ANN controller to obtain the working voltage. The response time of the MPPT is based on the learning process and hardware specifications of the system.

Another cost-effective and reliable algorithm for MPPTs commonly used is the Adaptive Neuro-Fuzzy Inference System or ANFIS. The study [53] proposed to evaluate this method through a MATLAB simulation composed of the PV panel and DC-to-DC converter connected to the load. The proposed AI technique has voltage, current, and temperature as data training inputs and duty cycle as the output that will regulate the converter to sustain the maximum power. It was concluded that the proposed method produced minimum oscillations and response time.

One of the most common techniques to extract maximum power point is constant voltage method using the formula of  $V_{mpp}/V_{oc} = K$ , where  $K$  is the

percentage of the optimal value. In a study [54], an isolated solar panel is simulated to get the value of open circuit voltage to avoid disconnection to the load reducing power inefficiency. A Proportional Integrator (PI) controller is included in a feedback control system to obtain the correct duty cycle. The PWM signal is the input to the gate of the MOSFET driver in the DC-to-DC converter circuit.

FLC MPPT method is used to control a boost converter circuit to operate at maximum power point. A study [55] used varying temperature and irradiance to test the algorithm's accuracy and tracking speed. The control in voltage depended on the value of change in power and change in voltage of the solar PV panel. The inputs for the FLC is the error and change of error while the output is duty cycle, which is input into the switch of the DC-to-DC converter circuit. The study concluded that using fuzzy logic was 94.8-99.4 % accurate.

A study [56] proposed a new method by combining Perturb and Observe (P & O) and Fractional Short-Circuit Current (FSCC) method. ISC is measured using sensor. The signal decided by the system is controlled by calculation of  $I_{mpp}$  and compared through limit subroutine. The simulation underwent steady and dynamic weather; showed 97.56 % and 95.71 % efficiency, respectively.

A bio-inspired algorithm is proposed in a study [57] where Enhanced Leader-Particle Swarm Optimization (EL-PSO) method for MPPT proved to be more efficient in tracking speed than PSO. The input data is trained so the swarm agent can learn and follow the best power output varying in every iteration and the output is applied to a boost converter circuit

Improved Increment Conductance (InC) algorithm is used in a study [58] for the MPPT charge controller. MPP is obtained by equating incremental

to the instantaneous conductance. The system also included solar tracking to maximize power output under varying irradiation and temperature values – concluded to be 43.27 % more efficient.

## CHAPTER 3

### METHODOLOGY

#### 3.1 Theoretical Framework

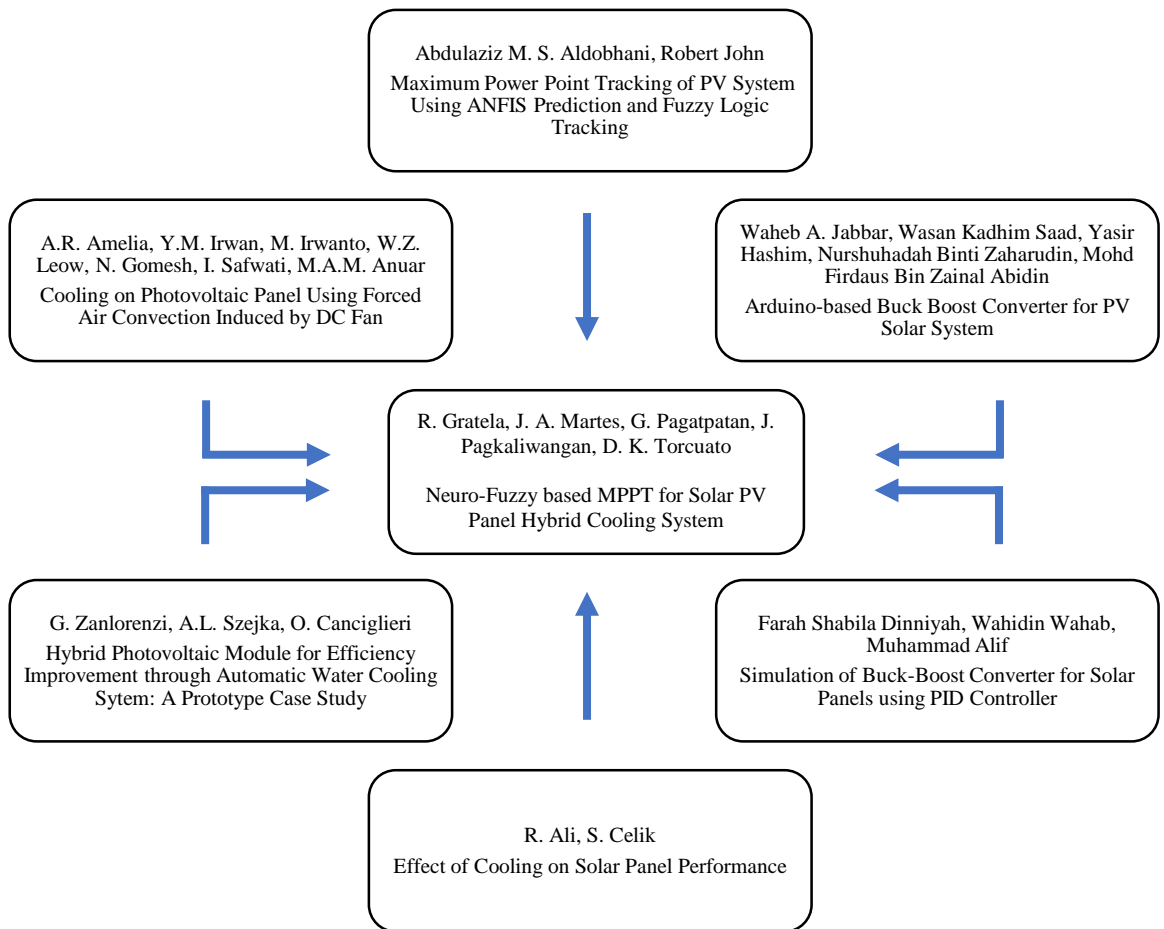


**Figure 3.1** Closely Related to the Present Study under Investigation

Figure 3.1 shows the theoretical framework of the study. The diagram consists of literatures closely related to the present study. Authors of each literature are also cited.

The integration of the ANFIS-based MPPT was derived from the study conducted by Abdulaziz M. S. Aldobhani and Robert John which primarily focused on mitigating the environmental effects and nonlinearity of the voltage output that decreases the power efficiency of the PV system [59]. The design of the DC-to-DC

converter circuit for the output voltage regulation controlled by duty cycle is fabricated from the study by Jabbar et al. [60]. For the selection of component values for the buck-boost converter circuit, the formulas used are based on the paper by Dinniyah et al. [61].

The design of the hybrid cooling system became an influence from the studies on the effect of cooling on solar PV performances by R. Ali and S. Celik [62]. Applying the concept of automation of the cooling system is based on the published research articles done by G. Zanlorenzi et al. and Amelia et al. [63] [64].

### 3.2 Conceptual Framework

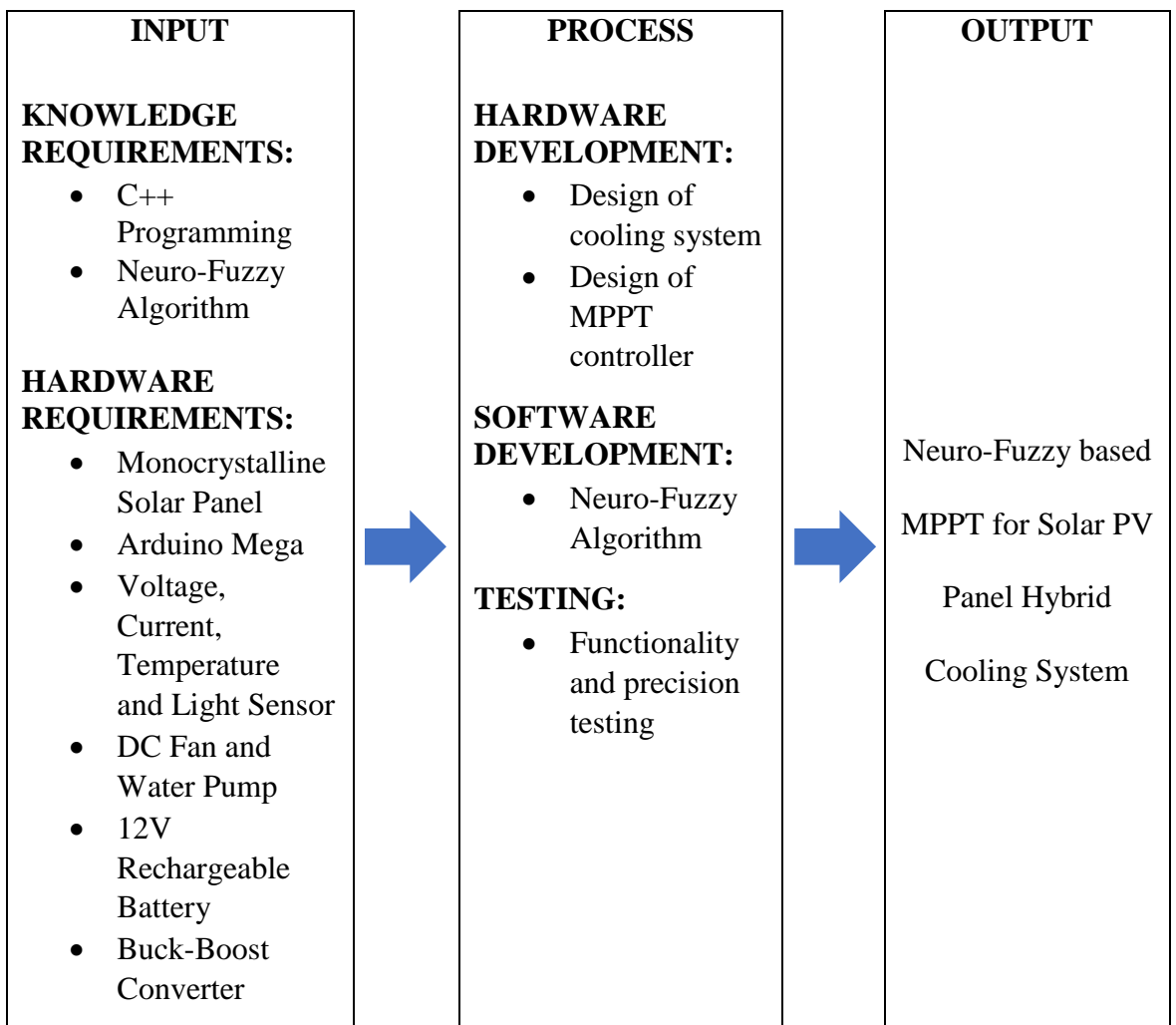


**Figure 3.2** Input-Process-Output Diagram of the System

Figure 3.2 shows the input of the microcontroller for the cooling system was the panel surface temperature, wherein the air and water mechanisms were automatically activated when the set temperature is exceeded. The ANFIS inputs were voltage, current, temperature, and irradiance which were fed to the neuro-fuzzy algorithm for the buck-boost converter circuit under the Maximum Power Point Tracking system to attain duty cycle or voltage linearity of 13.8V.

### 3.3 Research Process Flow

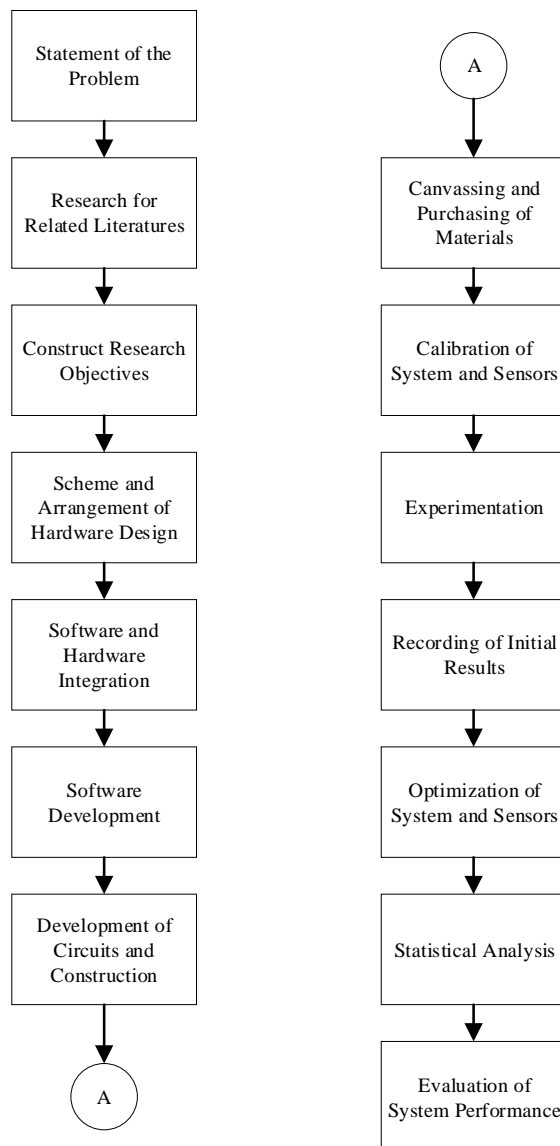


**Figure 3.3** Process Flow Chart of the System

Figure 3.3 shows the development of the research. Progressively, it was followed for the completion of the objective.

### 3.4 Hardware Design

This part shows the combination of materials which built the research study. It includes the block diagram, circuit diagram, and design consideration of the MPPT and cooling system.

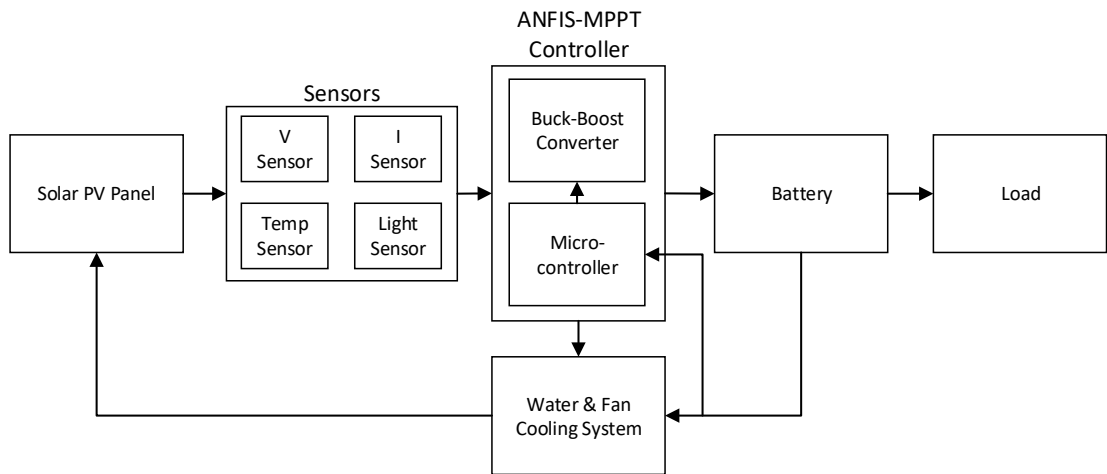


**Figure 3.4** Block Diagram of the System.

Figure 3.4 represents the Block Diagram of the System. The following sensors installed in the solar PV panel collected the data which was processed by the microcontroller. The MPPT was composed of buck-boost converter and a microcontroller which replaced the task of a commercially available solar charge controller. The Buck-Boost converter's function was to stabilize the output voltage of the solar panel which uses step up/step down method. In this study, the desired voltage is 13.8 V, and the maximum output voltage of the solar PV panel is 21 V. The maximum power point tracker extracted the peak available power from the PV panel by operating it at the most efficient stable voltage using the algorithm executed by the microcontroller. The whole system equipment – including the hybrid cooling system

drew portion of the power generated by the solar panel which made it a standalone system.

### **3.4.1 Design Considerations**

Complexity of the system comes with costs. This study aims to provide higher efficiency with system of cost-efficient approach. The higher the power rating of the solar panel, the larger the physical dimensions. This also affected the components' size, power and/or quantity for cooling method. In short, the provided solar panel was computed in terms of efficiency – larger enough to cater the power usage of the fan, water pump and the DC load provided.

Each setup used four fans which are installed at the back of the panel while eight nozzles are placed at the top face of the panel spaced evenly for full coverage.

The setup used an adjustable angle bracket for the solar panel frame and stand which made it convenient in transferring since it can be disassembled. The solar panel frame is expected to be at exactly  $15^{\circ}$  with respect to the horizontal but was assembled with at least  $\pm 5\%$  allowance as shown in Figure 3.5. The setup also used a pot as container considering the water return from cooling the panel may eventually affect the temperature of the stored water. It shall help maintain the stored liquid's temperature.

A fixed flow rate for the water cooling depending on the water pressure can cover the whole solar cell module. 2 L/min was the most appropriate flow rate for the system considering the size of the solar module since the pressure can be modified depending on the area for water coverage. A study also suggested using 2 L/min, without cooling apparatus, the photovoltaic panel

produced 62 Wh. After using a water flow rate of 2 L/min the energy produced increased to 77 Wh, a gain of 24 %.

The DC brushless fan was used with inlet configuration, making it more effective than outlet configuration, in lowering the photovoltaic panel temperature. The selection of the number of units of fan to be installed depends on the surface area of the PV panel which is 1487x666x35 mm. According to a study, with 4 units of fan installed, the temperature average decreased from 51.31 °C to 35.28 °C, also increasing the power output by 44.34 %. Considering the power consumption of for the operation of air cooling, only 4 units of fan were installed.

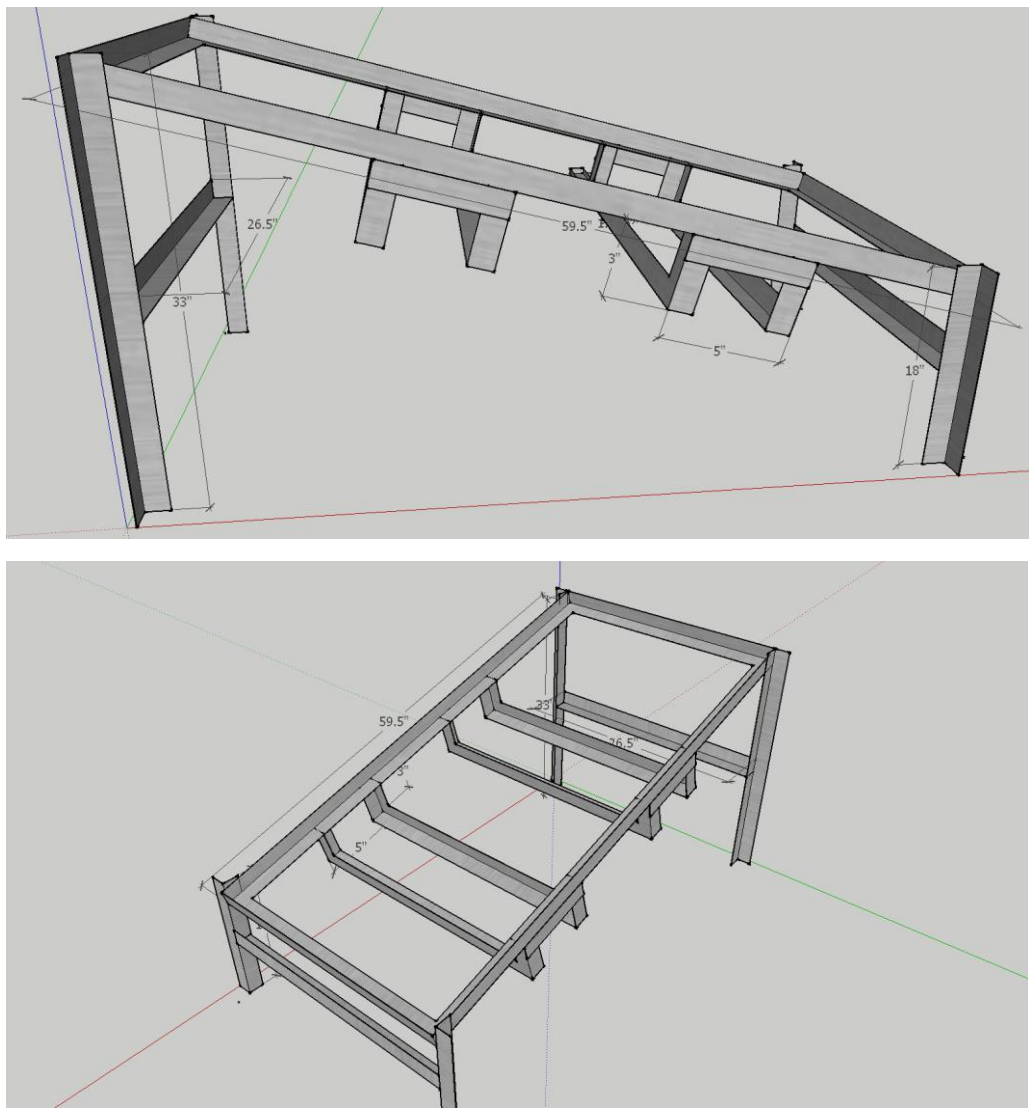


**Figure 3.5** Detailed Design of the Solar Panel Rack

### 3.4.2 Circuit Diagram

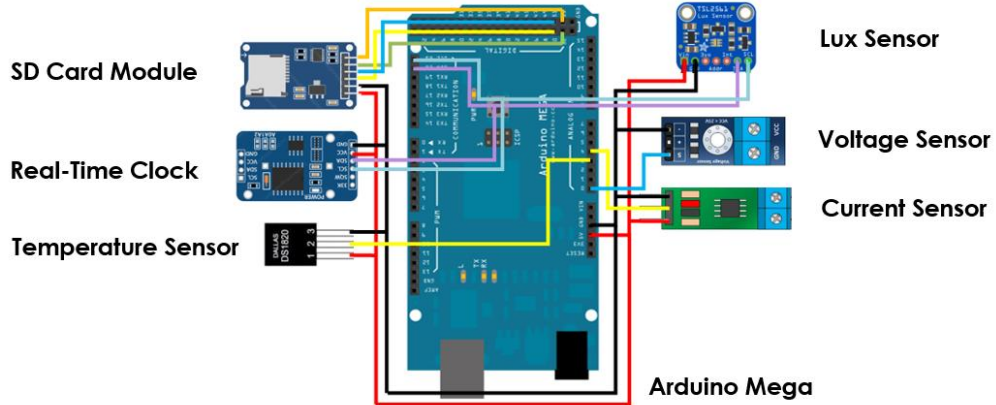


**Figure 3.6** Schematic Diagram

Figure 3.6 shows the composition of the components which includes buck-boost converter and microcontroller. The Arduino served as the central processing unit of the system, it accommodated the program for data storing and algorithm for data processing manipulation. The microcontroller algorithm made appropriate adjustments depending on the data parameters received from the sensors for the duty cycle output which was fed to the MOSFET component of the buck-boost converter. The produced output of the microcontroller was necessary to control the duty cycle of the buck-boost converter MOSFET for acquiring high efficiency maximum power point with low fluctuation.

### 3.4.3 Project Components

#### 3.4.3.1 Solar PV Panel

Solar PV Panel holds the responsibility of converting solar irradiation directly into electrical energy. Its power output depends on the material used, size, and quantity of photovoltaic cells.



**Figure 3.7** Restar Solar 150W Monocrystalline

### 3.4.3.2 Buck-Boost Converter

Figure 3.8 shows the components of a buck-boost converter. The Buck-boost Converter was used to stabilize the output voltage coming from the photovoltaic module. The buck converter served as a DC-to-DC stepping down converter of the voltage that was greater than the threshold voltage. Voltage stepped down as the current rises due to its inversely proportional relationship. Conversely, the boost converter increased the voltage when the output was less than the threshold voltage.

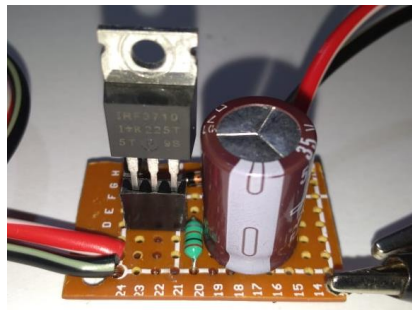


**Figure 3.8** Buck-Boost Converter

### 3.4.3.3 Battery

Figure 3.9 served as the power storage for the energy generated by the solar panel. It reserved the power for the upcoming consumption that was fully charged by a connected charge controller directly from the solar panel. The stored energy was consumed every time the solar panel stops the power generation due to lack of sunlight during the power demand or during power

failures occurrence. This Lead-Acid battery was charged with 13.8 V which is the stable voltage coming from the buck boost converter.



**Figure 3.9 Lead-Acid Battery**

#### 3.4.3.4 Fan and Water Cooling Devices

Figure 3.10 shows the hybrid cooling system devices. It is composed of fan and water sliding served as the coolant. The fan was placed at the rear portion of the solar panel which provided enough pulsed air. Meanwhile, the pump was placed in the water storage which provided the water supply in the surface layer of the solar panel. Both devices gave the cooling effect to maintain the solar panel temperature.



**Figure 3.10 DC Brushless Fan and DC Water Pump**

### 3.4.3.5 Controller Device

Figure 3.11 shows an Arduino Microcontroller. It analyzed the extracted data from the solar module and inverter as bases for the cooling method by controlling the temperature of the PV module in order to attain best performance of the system. It served as the central processor of the system which provided the calculations and decisions using the parameters provided by the sensors.



**Figure 3.11** Mega ATmega2560-16AU CH340G

### 3.4.3.6 Voltage Sensor

Figure 3.12 shows the voltage sensor. It was used to measure the DC output voltage of the solar photovoltaic panel. The supply voltage for the module is 5 V and can measure up to 25 V DC. It received the voltage signal directly from the output terminals of the solar panel and registered it through the microcontroller.



**Figure 3.12** Voltage Detection Sensor Module 25V

### **3.4.3.7 Current Sensor**

Figure 3.13 shows an ACS712 current sensor. It was used to measure the AC or DC current generated by a source. To obtain the current value, the sensor must be in series with the solar PV panel. The supply voltage for the 20 A model sensor is 5 V and can measure between 20 A to 20 A range, with a sensitivity of 66 mV/A. It received the current signal directly from the solar panel terminal and records the value through the microcontroller.



**Figure 3.13 Current Sensor ACS712T-20A**

### **3.4.3.8 Temperature Sensor**

Figure 3.14 shows the waterproof temperature sensor. It was the waterproof counterpart of the DS18B20 sensor, which is advantageous when the system to be measured is exposed to natural wet state such as rain. The sensor is digital; meaning signal attenuation is avoided over long-range measurements. The supply voltage for the sensor is 3-5 V. It can measure up to 125 C and has a +-0.5 C discrepancy.



**Figure 3.14 Temperature Sensor DS18B20**

### 3.4.3.9 Lux Sensor

Figure 3.15 shows the TSL2591. It was used to measure light precisely to detect values between 188 Lux to 88,000 Lux. It is composed of both infrared and full spectrum diodes which can measure infrared and visible light separately. 3-5 V is needed to supply the sensor. It served as the irradiance meter for the system.



**Figure 3.15** Adafruit TSL2591 Light Sensor

## 3.5 Software Development

### 3.5.1 Cooling System

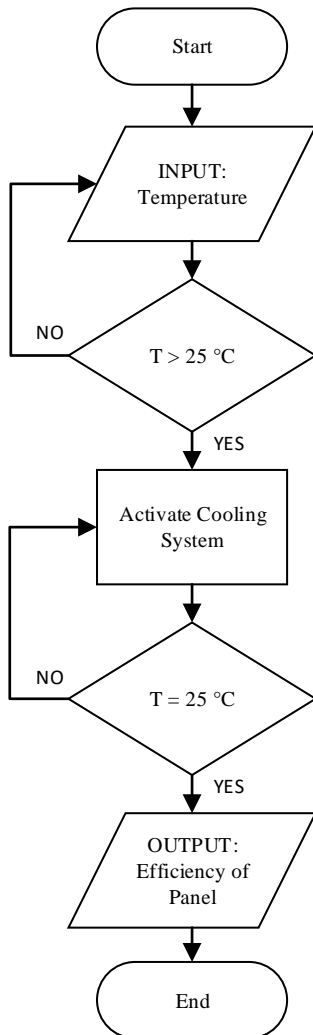


**Figure 3.16** Cooling System Flowchart

Figure 3.16 shows the Cooling System Flowchart. In its most basic form, the cooling system operated depending on the surface temperature of the solar PV panel. When the panel reached its threshold temperature that caused the power generation efficiency to decrease, the cooling system automatically turned on to cool down the surface of the panel. The temperature of the panel was maintained by activating the cooling system based on its standard threshold temperature.

### 3.5.2 Adaptive Neuro-Fuzzy Inference System

ANFIS algorithm is a hybrid of Artificial Neural Network (ANN) and Fuzzy Logic. ANN was used to train the data sample for it to learn while the fuzzy logic was used to assign the input and output variables into different membership functions or degree. Figure 3.17 shows the Fuzzy Inference System.

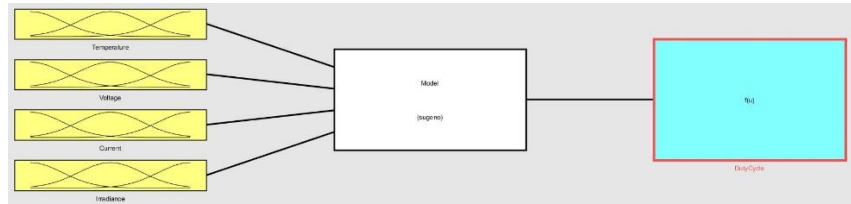


**Figure 3.17** Fuzzy Inference System

Figure 3.18 shows the ANFIS model structure for the integration of MPPT charge controller. The inputs were voltage, current, temperature, and irradiance. The ANFIS algorithm generated the duty cycle output to regulate the output voltage based on the rules automatically set.

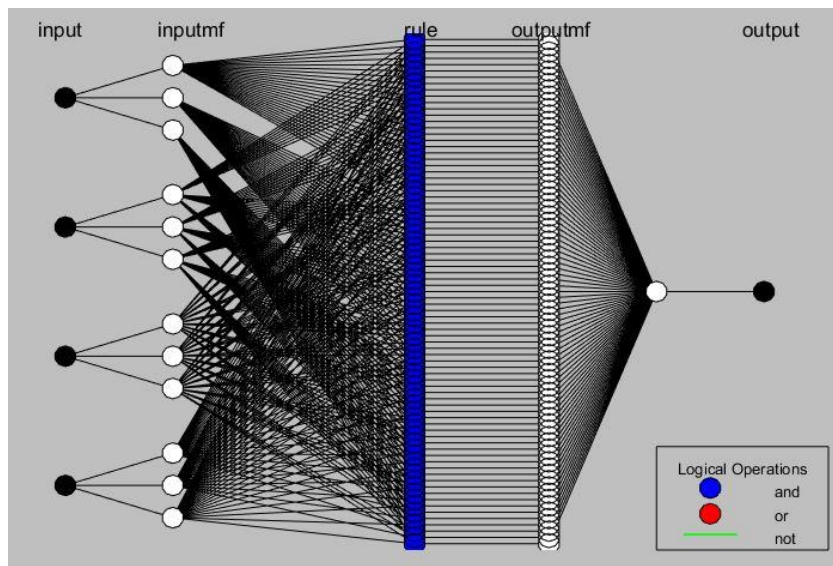


**Figure 3.18** ANFIS Network Design

The membership function plotted the input variable for the fuzzy inference method. A function included a fuzzy range which were categorized as low, medium,

and high. The output was determined by the rules generated. In order to obtain the lowest percentage of error in the training phase, it is important to choose the type of membership functions for the FIS structure. Figure 3.19 visualizes the Membership Functions (MFs) of the variable input temperature from Cold (24.25 °C), Normal (30.75 °C), and Hot (37.25 °C). The MFs for voltage and current were: (10.91 V, 0.952 A) (14.66 V, 1.41 A), and (18.41 V, 1.868 A) identified as Low, Medium, and High. The MFs of the Irradiance were Weak (-373.3 W.m<sup>-2</sup>), Medium (773.3 W.m<sup>-2</sup>), and Strong (1919 W.m<sup>-2</sup>)

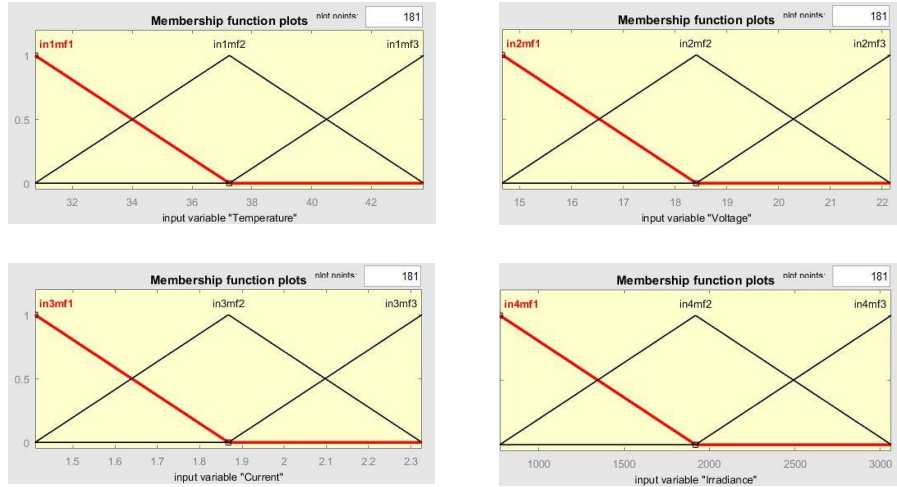


**Figure 3.19** Triangular Membership Functions

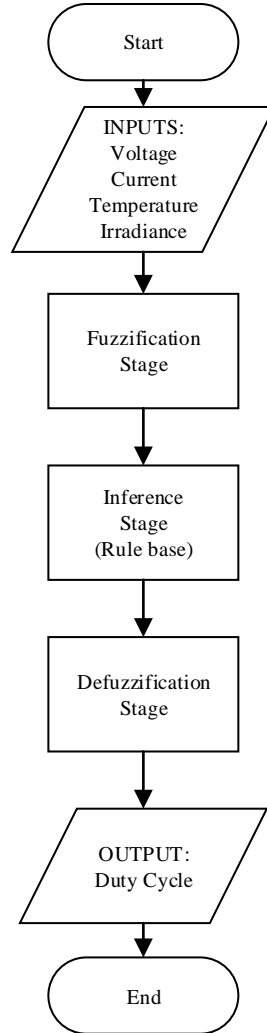


**Figure 3.20** ANFIS Program Flow Chart

Figure 3.20 shows the Program Flowchart. This is the process where the ANFIS algorithm functions as voltage stabilizer was accomplished by a boost/buck converter. The actual voltage and current gathered under various conditions was utilized for the fuzzification process – it converted the crispy values into fuzzy variable which presented the characteristics of power-voltage and current-voltage in several conditions while the features of the system were recognized by a certain implementation of rules and conditions. The system outputs as duty cycle and the voltage maximum power point which controls the whole functionality of the solar panel were recognized.

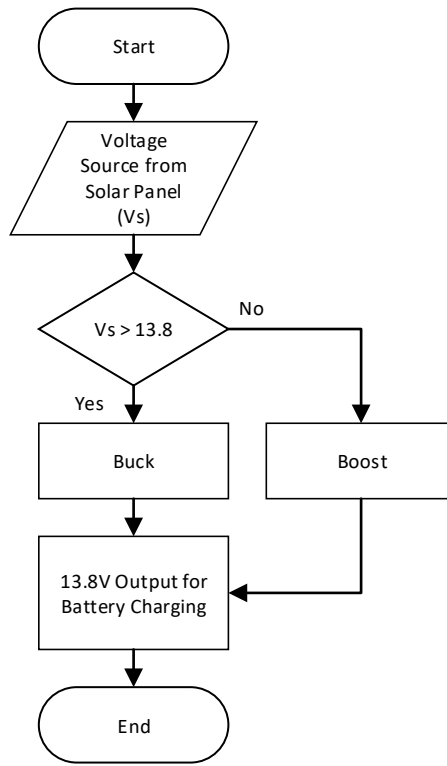


**Figure 3.21** Buck-Boost Program Flow Chart

Figure 3.21 shows the Buck-Boost converter operation with its voltage source produced by a 150 W monocrystalline Solar PV panel. The Solar panel can produce 0 V-21 V depending on the solar irradiance which underwent step-down or step-up conversion to meet the voltage requirement for battery charging.

### **3.6 Testing Procedure**

Initially, the solar panel underwent experiments to measure the most optimal temperature to produce maximum voltage. The recorded data served as the basis threshold temperature of the sensor for the cooling system. The proposed system has three setups namely: the first setup which is the solar panel with a neuro-fuzzy based MPPT alone, the second setup which is the solar panel with hybrid air-and-water cooling system and lastly, the third setup which has the combination of both the neuro-fuzzy based MPPT solar charge controller and hybrid air-and-water for cooling. The testing procedure covered two main applications specifically, the application of the hybrid air-and-water for cooling system, and the application of the neuro-fuzzy based MPPT charge controller.

Sensors worked on measuring the corresponding parameters such as solar irradiance (Irr), surface temperature (T), current (I), and voltage (V) through the Arduino microcontroller which were the inputs for the buck-boost converter.

The cooling system worked as follows: at a fixed angle of 15 degrees each panel, the air is blown at the back of the solar panel using a fan while the water flows over the front surface of the panel at the same time for both all setups. The recorded actual data for all tests including the parameters were transferred to the computer through the microcontrollers and data-logging software.

On the other hand, the MPPT will serve its purpose of controlling the maximum voltage of the PV module by applying ANFIS method using MATLAB. The actual data can also be compared to the generated data using MATLAB and be evaluated in a statistical analysis. Different shapes are tested to determine the shape that has the least error compared to the gathered actual data. These data will be compared to know the differences of each setup's efficiencies and will be assessed in a cost-benefit analysis.

### 3.7 Evaluation Procedure

Table 3.1 shows the parameters of the data that will be recorded. For the evaluation of the proposed solar PV panel with the constructed cooling system, a comparative analysis will be done to determine the variance in electrical power efficiency of the three setups. The output electrical efficiency and the voltage linearity are the highlights of the evaluation.

**Table 3.1** Data Comparison of 3 Different Setups

Setup	Parameters							
	Time (s)	Solar Irradiance (W/m <sup>2</sup> )	PV Temperature (°C)	Voltage (V)	Current (A)	Input Power (W)	Output Power (W)	Electrical Power Efficiency (%)
Solar PV with MPPT Solar Charge Controller								
Solar PV with Hybrid Cooling System								
Solar PV with Hybrid Cooling System and MPPT Solar Charge Controller								

### 3.8 Gantt Chart

**Table 3.2** Activities from November to March 2020

Activities	Nov	Dec	Jan	Feb	Mar	Apr	May	Jun	Jul	Aug	Sep	Oct	Nov	Dec	Jan	Feb	Mar
Lecture and Research																	
Project Topic																	
Research																	
Research on RRL																	
Drafting of Chapters 1,2 and 3																	
Title Defense																	
Canvassing of Materials																	
Project Proposal Submission																	
Purchasing of Materials																	
Prototyping Hardware Design																	
Programming																	
Progress Defense																	
Adjustments for the Prototype																	
Data Gathering																	
Pre- Final Defense																	
Trouble-shooting and Revising of Program Prototype																	
Deployment																	
Data Gathering of Device																	
Drafting Chapters 1 to 5																	
Final Defense																	
Finalization of Paper																	
Book Submission																	

Table 3.4 shows the Gantt chart of monthly activities of the group throughout the study. It serves as the schedule of the proposed tasks to be finished for the development of the project.

## Chapter 4

### RESULTS AND DISCUSSION

This chapter presents the project's technical description, project structure, interpretation of data, and analysis of findings relative to the tests conducted.

#### **4.1 Project Technical Description**

The 150 W solar panel system is composed of two major parts: the hybrid air-and water-cooling system and the ANFIS-based MPPT charge controller. The cooling system is composed of an Arduino microcontroller which is in charge of the activation of the air- and water-cooling mechanism, namely the DC brushless fans and water sprinkles which both use 12 V to operate. A temperature sensor DS18B20 is used to detect if the solar PV panel surface temperature exceeds the set operating temperature limit that will trigger the on/off duration of the cooling system.

The MPPT controller used ANFIS algorithm to determine the output duty cycle to charge the deep cycle battery through a buck-boost converter circuit. The ANFIS is uploaded into Arduino microcontroller, using voltage, current, temperature and lux sensors as its input which utilizes 5 V operating voltage.

#### **4.2 Project Structural Organization**

##### **4.2.1 Cooling System**

Figure 4.1 shows the water sprinkler from the hybrid cooling system, it allowed the water to flow from the top portion until it covered the whole panel. The water coolant provided the necessary change in temperature that directly affected the current generation of the solar panel.



**Figure 4.1** Front Side of the Panel

Figure 4.2 shows rear side of the panel which contains the brushless DC fan, water vessel, and the receptacles for the sensors and microcontroller. The brushless DC fan from the hybrid cooling system also provided the cooling effect on rear side of the solar panel which operated simultaneously with the water sprinkler at the front side of the panel. The plastic chamber contains the microcontroller which served as the brain of the system. It was responsible for the activation of the cooling system, data logging and processing of data.



**Figure 4.2** Rear Side of the Panel

Figure 4.3 shows the water collector which is located at the bottom part of the rear side of the panel. It was responsible for the water reclamation process which provided less water consumption.



**Fig. 4.3 Solar Panel Setups**

#### **4.2.2 ANFIS-MPPT Controller**

The developed MPPT controller is composed of voltage sensor, current sensor, temperature sensor, lux sensor for the data accumulation, and buck-boost converter to regulate the output voltage.

### **4.3 Project Capabilities and Limitations**

This study focused on the development of the neuro-fuzzy based MPPT charge controller for the hybrid air- and water-cooling system of solar PV panels. The cooling system used the PV system as its power source. The activation was optimized to operate after reaching more than 35 degrees Celsius. In consideration with the geographic location, the panel was set to a fixed angle of 15 degrees but due to Earth's rotation, there is lesser light radiation compared to a movable one that uses

a tracking system. Included in this research is the comparison of the efficiencies of the three setups.

#### 4.4 Project Evaluation

The efficiency of each setup is compared to each other through testing and data gathering. Figure 4.4 shows the plotted data of output power over time of setup 1 (MPPT), setup 2 (SCC and cooling system) and setup 3 (MPPT and cooling system).

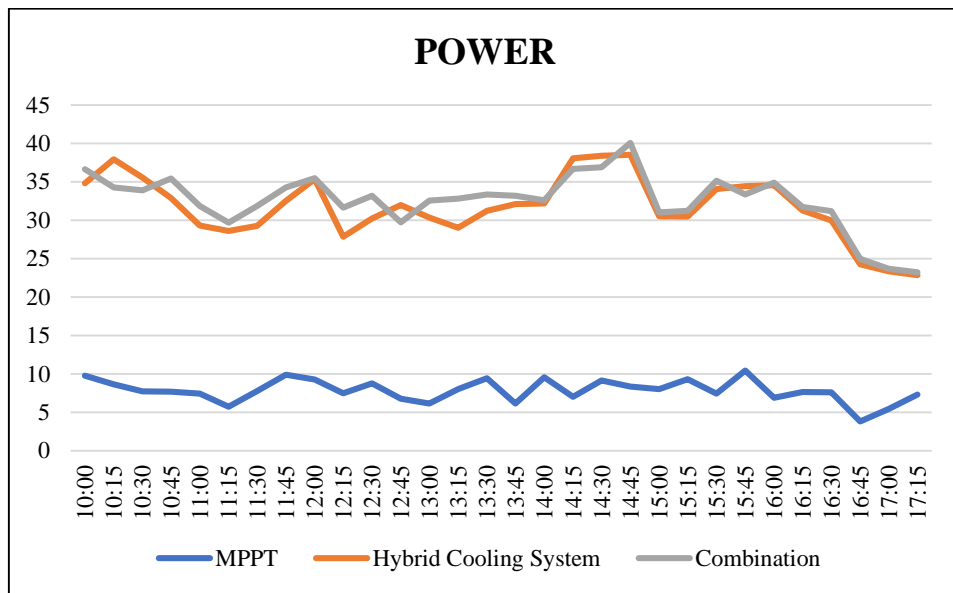


**Figure 4.4** Power output of setups 1, 2 & 3

Table 4.1 and Table 4.2 shows the power efficiency of each setup and the computed efficiency between them. The data used is from 10:00 AM to 5:15PM with 15-minute increment. Setup 3 with the ANFIS-MPPT controller and cooling system has the highest efficiency of 24.005 %. Efficiency significantly increased when the setup has a cooling system.

**Table 4.1** Summary of efficiency per setup

Setup	Average Power (W)	Efficiency (%)
1	7.395	4.930
2	33.754	22.503
3	36.008	24.005

**Table 4.2** Summary of efficiency comparison

Setups Compared	Efficiency (%)
1 & 2	17.50
1 & 3	20
2 & 3	1.5

## 4.5 Tabulation of Results and Interpretation

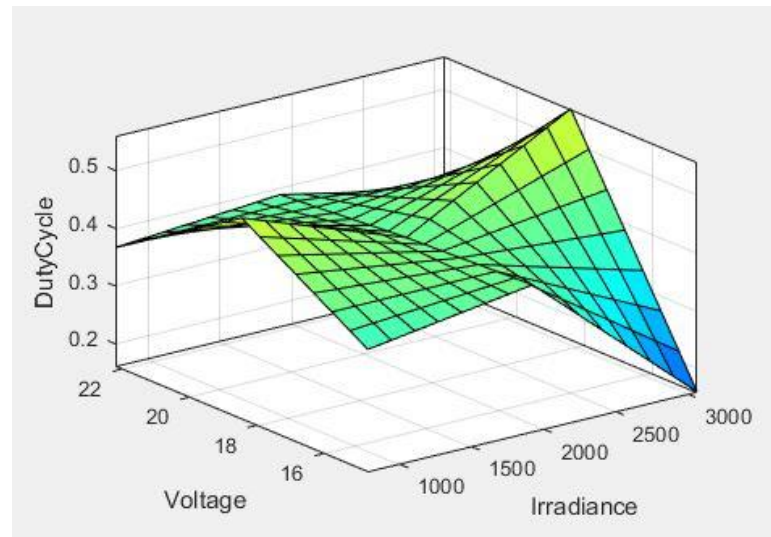
### 4.5.1 ANFIS Algorithm

Table 4.3 shows the data obtained by training different FIS functions. Based on the results, trimf shows lowest linear error rate. As such, trimf was chosen to be the membership function for training the ANFIS algorithm.

**Table 4.3** Training Data for different FIS Functions

Run	FIS Type	Fuzzy Rules	Training Error (%)
1	trimf	81	0.0015666
2	trapmf	81	0.21363
3	gbellmf	81	0.026759
4	gaussmf	81	0.010623
5	gauss2mf	81	0.06068
6	pimf	81	0.27228
7	dsigmf	81	0.092819
8	psigmf	81	0.092819

The output characteristics can easily be estimated by looking at the surface plots. Figure 4.5 shows that as the irradiance increases, the output voltage also increases while as the temperature increases, the output current decreases as shown in Figure 4.6.



**Figure 4.5** Surface Plot of Duty Cycle with respect to Voltage and Irradiance

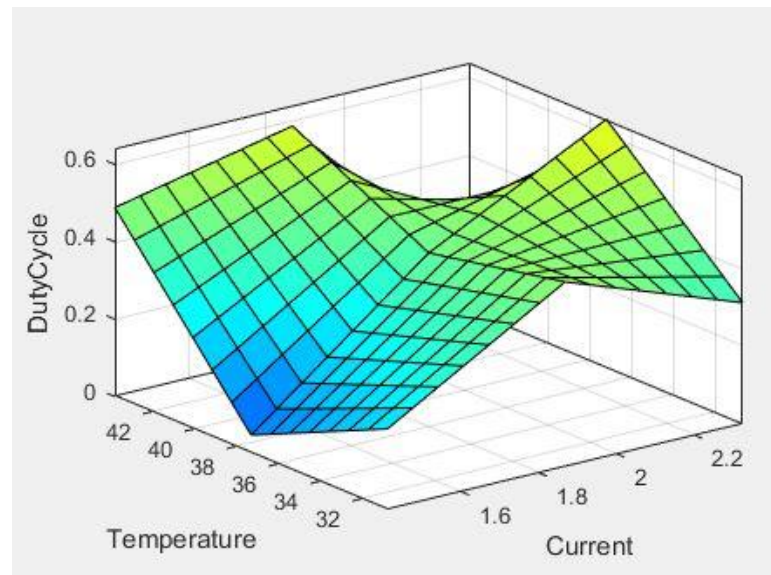


**Figure 4.6** Surface Plot of Duty Cycle with respect to Current and Temperature

#### 4.5.2 Accuracy Test

To test the accuracy of predictive model, RMSE was used to obtain the absolute fit of the model to the computed data. Comparing the computed duty cycle to the FIS generated output is a way to evaluate the accuracy of the FIS system. Figure 4.7 shows the test plot of thirty (30) samples of the training data represented as "o" over the FIS output represented as "\*".

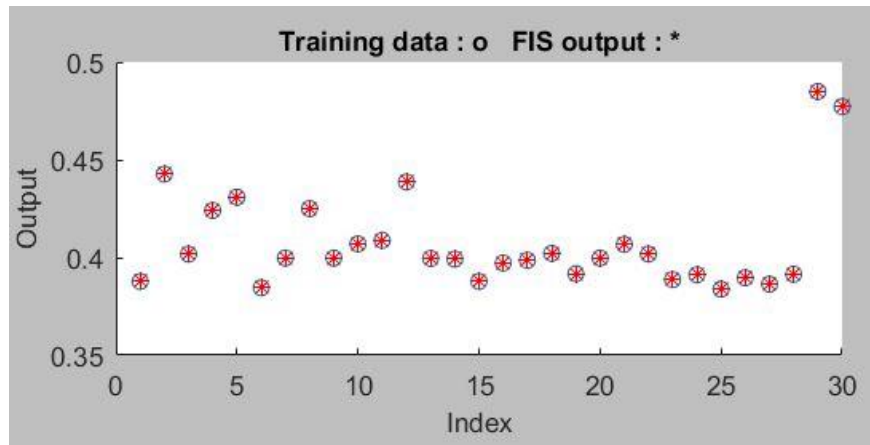


**Figure 4.7** Test Plot

#### 4.5.3 Cost Analysis

Table 4.4 shows the summary of monthly and yearly costs saved for each setup. The energy generated is computed over 10 hours of data collected by each setup. A Meralco rating of ₱8.8901/kWh was used to determine the electricity bill equivalent.

**Table 4.4** Cost saved for each setup

Setup	Energy Generated	Monthly Saved	Yearly Saved
1	0.074 kW	₱19.73	₱240.12
2	0.338 kW	₱90.14	₱1096.77
3	0.360 kW	₱96.01	₱1168.15

For an average of 10 hours/day,

$$Savings = E_G \times D \times R_M$$

Where,

$E_G$  = Energy generated per day (kW)

$D$  = number of days

$R_M$  = Meralco rating (Peso/kWh)

Setup 1:

$$\text{Monthly Saved} = 0.074 \text{ kW} \times 30 \text{ days} \times 8.8901 \text{ php/kWh}$$

₱ 19.73

$$\text{Yearly Saved} = 0.074 \text{ kW} \times 365 \text{ days} \times 8.8901 \text{ php/kWh}$$

₱ 240.12

Setup 2:

$$\text{Monthly Saved} = 0.338 \text{ kW} \times 30 \text{ days} \times 8.8901 \text{ php/kWh}$$

₱ 90.14

$$\text{Yearly Saved} = 0.338 \text{ kW} \times 365 \text{ days} \times 8.8901 \text{ php/kWh}$$

₱ 1096.77

Setup 3:

$$\text{Monthly Saved} = 0.360 \text{ kW} \times 30 \text{ days} \times 8.8901 \text{ php/kWh}$$

₱ 96.01

$$\text{Yearly Saved} = 0.360 \text{ kW} \times 365 \text{ days} \times 8.8901 \text{ php/kWh}$$

₱ 1168.15

## **Chapter 5**

### **SUMMARY OF FINDINGS, CONCLUSIONS, AND RECOMMENDATIONS**

This chapter presents the summary of findings, conclusions, and recommendations relative to the results conducted on the duration of this research.

#### **5.1 Summary of findings**

The developed hybrid air- and water-cooling system used the Arduino to optimize the activation of the air- and water-cooling mechanism by using fans and sprinklers. To ensure the accuracy of each data parameter namely voltage, current, lux, and temperature, each sensor was tested repeatedly and was verified using an actual measuring device of each parameter. The results were then recorded to the data logger. These data gathered were evaluated using Z-Test to attest significant change in each parameter of apiece setup.

These set of data are trained to be used for ANFIS predictive modelling. The accuracy of the FIS system was attained using RMSE wherein the computed duty cycle was compared to the FIS generated output.

#### **5.2 Conclusions**

Based on the results and findings of the research, the following conclusions were inferred:

1. The utilization of Adaptive Neuro-Fuzzy Inference System (setup 1), Hybrid Cooling System (setup 2), and the combination of both (setup 3), have 4.93 %, 22.503 %, and 24.005 % increase of efficiency, respectively, compared to the original setup of a solar panel with a solar charge controller alone.

2. The AI-based prediction model using the ANFIS Grid Partition to implement maximum power point obtained a low root mean square error (RMSE) value of 1.5666e-05 by comparing the computed duty cycle to the FIS generated output, indicating a better fit.
3. The use of ANFIS algorithm for switching pulses of the Buck-Boost Converter Circuit has an average output voltage efficiency of 99.92 % compared to the reference voltage.

### **5.3 Recommendations**

For further improvement of the study, the researchers recommend the following:

1. To create a new algorithm to improve the efficiency of the system's maximum power point tracking capability likewise, the output voltage of the buck-boost converter.
2. To develop a container design maintaining the temperature and can hold larger capacity.
3. To consider using a solar tracker to capture more light which is one base factor for increase of solar panel efficiency.
4. To develop a mobile or website application that allows easy access to the end user.

## REFERENCES

- [1] Y.M.Irwan, W.Z.Leow, M.Irwanto, Fareq.M, A.R.Amelia, N.Gomesh and I.Safwati, "Indoor Test Performance of PV Panel through Water Cooling Method," in *Energy Procedia*, Malaysia, 2015.
- [2] S. Chander, A. Purohit, A. Sharma, Arvind, S. Nehra and M. Dhaka, "A study on photovoltaic parameters of mono-crystalline silicon solar cell with cell temperature," *Energy Reports*, 2015.
- [3] R. Ali and S. Celik, "Effect of Cooling on Solar Panel Performance," vol. 100, 2017.
- [4] S. Wu, F. Guo and L. Xiao, "A review on the methodology for calculating heat and exergy losses of a conventional solar PV/T system," *International Journal of Green Energy*, pp. 379-397, 2014.
- [5] A. Bianchini, A. Guzzini, M. Pellegrini and C. Saccani, "Photovoltaic/thermal (PV/T) solar system: Experimental measurements, performance analysis and economic assessment," *Renewable Energy*, pp. 543-555, 2017.
- [6] L.-H. Yang, J.-D. Liang, C.-Y. Hsu, T.-H. Yang and S.-L. Chen, "Enhanced Efficiency of Photovoltaic Panels by Integrating a Spray Cooling System with Shallow Geothermal Energy Heat Exchanger," *Renewable Energy*, 2018.
- [7] Y.M.Irwan, W.Z.Leow, M.Irwanto, Fareq.M, N.Gomesh and I.Safwati, "Comparison between DC Brushless Fan and DC Hybrid Solar Panel," *Applied Mechanics and Materials*, vol. 793, no. 1662-7482, pp. 373-377, 2015.
- [8] H. Wang, L. Vinayagam, H. Jiang and Z. Q. Cai, "New MPPT Solar Generation Implemented with Constant-Voltage Constant-Current DC/DC Converter," 2016.
- [9] D. Popescu, R. C. Dinu and C. Bratu, "Fuzzy control of cooling water pumps related to a power plant," in *International Conference on Electromechanical and Power Systems (SIELMEN)*, Iasi, Romania, 2017.
- [10] İ. Ceyla, O. Erkaymaz, E. Gedik and A. E. Gürel, "The prediction of photovoltaic module temperature with artificial neural networks," *Case Studies in Thermal Engineering*, vol. 3, pp. 11-20, 2014.

- [11] A. H. Ali and A. A. Abdulrazzaq, "Evaluating the performance and efficiency of MPPT algorithm for PV systems," *International Journal of Engineering & Technology*, vol. 7, no. 4, pp. 2122-2126, 2018.
- [12] L. K. S. Tolentino, F. R. G. Cruz, R. G. Garcia and W.-Y. Chung, "Maximum Power Point Tracking Controller IC Based on Ripple Correlation Control Algorithm," in *8th IEEE International Conference Humanoid, Nanotechnology, Information Technology Communication and Control, Environment and Management (HNICEM)*, Cebu, Philippines, 2015.
- [13] J.-C. Wang, M.-S. Liao, Y.-C. Lee, C.-Y. Liu and K.-C. Kuo, "On enhancing energy harvesting performance of the photovoltaic modules," *Journal of Power Sources*, vol. 376, pp. 55-65, 2018.
- [14] A. Bianchini, A. Guzzini, M. Pellegrini and C. Saccani, "Photovoltaic/thermal (PV/T) solar system: Experimental measurements, performance analysis and economic assessment," *Renewable Energy*, pp. 543-555, 2017.
- [15] V. N. Amalnath and R. Zachariah, "A Simple Control Unit for Temperature Dependent Forced Water Cooling in Solar CPV/T Collector," 2017.
- [16] N. A. Zainal, A. R. Yusoff and A. Apen, "Integrated cooling systems and maximum power point tracking of fuzzy logic controller for improving photovoltaic performances," *Measurement*, vol. 131, pp. 100-108, 2018.
- [17] A. K. Tiwari and V. R. Kalamkar, "Effects of total head and solar radiation on the performance of solar water pumping system," *Renewable Energy*, vol. 118, pp. 919-927, 2018.
- [18] A. Karafil, H. Ozbay and M. Kesler, "Temperature and Solar Radiation Effects on Photovoltaic Panel Power," *New Results in Science*, vol. 12, pp. 48-58, 2016.
- [19] A. Amhani and H. A. Attia, "The performance of a combined solar photovoltaic (PV) and thermoelectric generator (TEG) system," in *International Conference on Electrical and Computing Technologies and Applications (ICECTA)*, 2017.
- [20] A. Sahu, N. Yadav and K. Sudhakar, "Floating photovoltaic powerplant: A review," *RenewableandSustainableEnergyReviews*, pp. 815-824, 2016.

- [21] M. Rahman, M. Hasanuzzaman and N. Rahim, "Effects of various parameters on PV-module power and efficiency," *Energy Conversion and Management*, pp. 348-358, 2015.
- [22] Chaichan, H. A. Kazem and M. T., "Effect of Humidity on Photovoltaic Performance Based on Experimental Study," *International Journal of Applied Engineering Research*, vol. 10, pp. 43572-43577, 2015.
- [23] F. Jafarkazemi, S. A. Saadabadi and H. Pasdarshahri, "The optimum tilt angle for flat-plate solar collectors in Iran," *Renewable Sustainable Energy*, 2014.
- [24] M. Hosenuzzaman, N. Rahim, J. Selvaraj, M. Hasanuzzaman, A. Malek and A. Nahar, "Global prospects, progress, policies, and environmental impact of solar," *Renewable and Sustainable Energy Reviews*, vol. 41, pp. 284-297, 2014.
- [25] N. Karami, N. Moubayed and R. Outbib, "General review and classification of different MPPT Techniques," *Renewable and Sustainable Energy Reviews*, vol. 68, no. 1, pp. 1-18, 2017.
- [26] D. S. Suryawanshi and S. S. Khairnar, "Perturb and observe based MPPT for solar power generation connected to AC load," in *2nd IEEE International Conference On Recent Trends in Electronics Information & Communication Technology (RTEICT)*, 2017.
- [27] L. Zhua, A. P. Ramanb and S. Fanb, "Radiative cooling of solar absorbers using a visibly," 2015.
- [28] Z. Peng, M. R. Herfatmanesh and Y. Liu, "Cooled solar PV panels for output energy efficiency optimisation," *Energy Conversion and Management*, vol. 150, pp. 949-955, 2017.
- [29] N. A. S. Elminshawy, A. M. I. Mohamed, K. Morad, Y. Elhenawy and A. A. Alrobaian, "Performance of PV panel coupled with geothermal air cooling system," *Applied Thermal Engineering*, vol. 148, pp. 1-9, 2019.
- [30] R. Stropnik and U. Stritih, "Increasing the efficiency of PV panel with the use of PCM," *Renewable Energy*, vol. 97, pp. 671-679, 2016.
- [31] B. M. Zilli, A. M. Lenz, S. N. M. d. Souza, D. Secco, C. E. C. Nogueira, O. H. A. Junior, W. Cézar, J. A. C. Siqueira and F. Gurgacz, "Performance and effect of

- water-cooling on a microgeneration system of," *Journal of Cleaner Production*, vol. 192, pp. 477-485, 2017.
- [32] F. L. Tofoli, W. J. De Paula and D. d. C. Pereira, "Comparative Study of Maximum Power Point Tracking Techniques for Photovoltaic Systems," *International Journal of Photoenergy*, 2015.
- [33] R. Blange, C. Mahanta and A. K. Gogoi, "MPPT of Solar Photovoltaic Cell Using Perturb & Observe and Fuzzy Logic controller Algorithm for Buck-Boost DC-DC Converter," 2015.
- [34] S. Malathy and R. Ramaprabha, "Maximum Power Point Tracking Algorithm of SPVA under Inhomogeneous Irradiation Conditions: A Modified Fibonacci Search Based Approach," 2017.
- [35] R. Ramaprabha, M.Balaji and B.L.Mathur, "Maximum power point tracking of partially shaded solar PV system using modified Fibonacci search method with fuzzy controller," *International Journal of Electrical Power & Energy Systems*, vol. 43, no. 1, pp. 754-765, 2012.
- [36] M. Makhloifi, Y. Abdessemed and M. Khireddine, "An Efficient ANN-Based MPPT Optimal Controller of a DC/DC Boost Converter for Photovoltaic Systems," *AUTOMATIKA*, vol. 57, pp. 109-119, 2016.
- [37] S. Shabaan, M. I. A. El-Sebah and P. Bekhit, "Maximum power point tracking for photovoltaic solar pump based on ANFIS tuning system," *Electrical Systems and Information Technology*, pp. 11-22, 2018.
- [38] Z. Ying, W. Jun, H. Dezhi, W. Huafeng and Z. Rundong, "Fuzzy-Logic Based Distributed Energy-Efficient Clustering Algorithm for Wireless Sensor Networks," *Sensors*, vol. 17, pp. 1-21, 2017.
- [39] T.Shanthi and A.S.Vanmukhil, "ANFIS Controller based MPPT Control of Photovoltaic," *International Journal of Computer Applications* , 2013 .
- [40] R. Ali and S. Celik, "Effect of Cooling on Solar Panel Performance," in *International Proceedings of Chemical, Biological and Environmental Engineering*, Illinois, 2017.
- [41] N. Sasidharan, W. Ongsakul, M. P. Varghese, A. VS and A. R, "Efficient improvement of solar photovoltaic system using artificial cooling methods," in

*2018 International Conference on Power, Signals, Control and Computation (EPSCICON),* 2018.

- [42] D. Nebbali, R. Nebbali and A. Ouibrahim, "Enhanced Efficiency of a Solar Photovoltaic Concentration System Cooled by a Pulsed Air," in *International Renewable and Sustainable Energy Conference (IRSEC)*, 2015.
- [43] Z. A. Haidar, J. Orfi and Z. Kaneesamkandi, "Experimental investigation of evaporative cooling for enhancing photovoltaic panels efficiency," *Results in Physics*, vol. 11, pp. 690-697, 2018.
- [44] A. S. Keron, A. B. Sikder, Sama-E-Shan and D. A. Zerin, "Fabrication and experimental analysis of solar panel water cooling system," in *International Conference on Mechanical Engineering and Renewable Energy (ICMERE2017)*, Chittagong, Bangladesh, 2017.
- [45] Y. Irwan, W. Leow, M. Irwanto, F. M, N. Gomesh and I. Safwati, "Comparison between DC Brushless Fan and DC Hybrid Solar Panel Cooling System," *Applied Mechanics and Materials*, vol. 793, pp. 373-377, 2015.
- [46] G. Zanlorenzi, A. L. Szejka and O. Cancigliani, "Hybrid Photovoltaic Module for efficiency improvement through an automatic," *Cleaner Production*, pp. 535-546, 2018.
- [47] Q. Xuefei and M. Lingling, "The Research of Cooling Water Temperature and Flow Rate Control System Based on Heat transfer and Neural Network," in *International Conference on Instrumentation and Measurement, Computer, Communication and Control (IMCCC)*, 2015.
- [48] K. Hazarika and P. K. Choudhury, "Automatic monitoring of solar photovoltaic (SPV) module," *materials today proceedings*, vol. 4, no. 14, pp. 12606-12609, 2017.
- [49] J.-C. Wang, M.-S. Liao, Y.-C. Lee, Cheng-YueLiu, K.-C. Kuo, C.-Y. Chou, C.-K. Huang and J.-A. Jiang, "On enhancing energy harvesting performance of the photovoltaic modules using an automatic cooling system and assessing its economic benefits of mitigating greenhouse effects on the environment," *Journal of Power Sources*, vol. 376, pp. 55-65, 2017.

- [50] R. Rawat and S. S. Chandel, "Maximum Power Point Tracking Techniques in Solar Photovoltaic Systems-A Review," *Energy Technology*, vol. 1, no. 8, 2013.
- [51] C. R. Algarín, J. T. Giraldo and O. R. Álvarez, "Fuzzy Logic Based MPPT Controller for a PV System," *Progress in Photovoltaics Research and Applications*, 2017.
- [52] S. A. Rizzo and G. Scelba, "ANN based MPPT method for rapidly variable shading conditions," *Applied Energy*, vol. 145, pp. 124-132, 2015.
- [53] A. M. Noman, K. E. Addoweesh and A. I. Alolah, "Simulation and Practical Implementation of ANFIS-Based MPPT Method for PV Applications Using Isolated Ćuk Converter," *International Journal of Photoenergy*, vol. 2017, pp. 1-15, 2017.
- [54] A. M., M. Tariq, M. M. and I. Ashraf, "An improved constant voltage based MPPT technique for PMDC motor," *International Journal of Power Electronics and Drive System (IJPEDS)*, vol. 7, no. 4, pp. 1330-1336, 2016.
- [55] U. Yilmaza, K. A. and S. Borekcib, "PV system fuzzy logic MPPT method and PI control as a charge controller," *Renewable and Sustainable Energy Reviews*, vol. 81, pp. 994-1001, 2018.
- [56] H. A. Sher, A. F. Murtaza, K. E. Addoweesh, K. AlHaddad and M. Chiaberge, "A New Sensorless Hybrid MPPT Algorithm Based on Fractional Short-Circuit Current Measurement and P&O MPPT," *IEEE Transactions on Sustainable Energy*, vol. 6, no. 4, pp. 1426-1434, 2015.
- [57] P. S. Gavhane, S. Krishnamurthy, R. Dixit, P. Rama and N. Rajasekar, "EL-PSO based MPPT for Solar PV under Partial Shaded Condition," *Energy Procedia*, vol. 117, pp. 1047-1053, 2017.
- [58] D. C. Huynh and M. W. Dunnigan, "Development and Comparison of an Improved Incremental Conductance Algorithm for Tracking the MPP of a Solar PV Panel," *IEEE Transactions on Sustainable Energy*, vol. 7, no. 4, pp. 1421-1429, 2016.
- [59] A. M. S. Aldobhani and R. John, "Maximum Power Point Tracking of PV System Using ANFIS Prediction and Fuzzy Logic Tracking," *Proceedings of the*

*International MultiConference of Engineers and Computer Scientists*, vol. II, 2008.

- [60] J. A.-A. W. A., W. K. Saad, Y. Hashim, N. B. Zaharudin and M. F. B. Z. Abidin, "Arduino-based Buck Boost Converter for PV Solar System," *2018 IEEE Student Conference on Research and Development (SCOReD)*, 2018.
- [61] F. S. Dinniyah, W. Wahab and M. Alif, "Simulation of Buck-Boost Converter for Solar Panels using PID Controller," *Energy Procedia*, vol. 115, pp. 10-113, 2017.
- [62] R. Ali and S. Celik, "Effect of Cooling on Solar Panel Performance," *International Proceedings of Chemical, Biological and Environmental Engineering*, vol. 100, 2017.
- [63] G. Zanlorenzi, A. L. Szejka and O. C. Junior, "Hybrid photovoltaic module for efficiency improvement through an automatic water cooling system: A prototype case study," *Journal of Cleaner Production*, vol. 196, pp. 535-546, 2018.
- [64] A. Amelia, M. I. Yusoff, M. Irwanto, L. W. Zhe, G. Nair, S. Ibrahim and M. Anuar, "Cooling on Photovoltaic Panel Using Forced Air Convection Induced by DC Fan," *International Journal of Electrical and Computer Engineering (IJECE)*, vol. 6, no. 2, pp. 526-534, 2016.

**APPENDIX A**  
**BILL OF MATERIALS**

Item	Unit	Quantity	Unit Cost	Amount
Restar Solar Panel 150W	pcs.	3	3800	11400
Buck-Boost Converter	pcs.	2	250	500
Solar Charge Controller	pcs.	1	400	400
Battery	pcs.	3	1100	3300
Mega ATmega2560-16AU CH340G	pcs.	3	530	1590
Voltage Detection Sensor Module	pcs.	3	49.75	149.25
Current Sensor ACS712T-20A	pcs.	3	199.75	599.25
Waterproof Temperature Sensor DS18B20	pcs.	3	129.75	389.25
Adafruit TSL2591 High Dynamic Range Digital Light Sensor	pcs.	3	429.75	1289.25
DC 12V Ultra Quiet Mini IP68 800L/H 19W Brushless Submersible Water Pump	pcs.	2	478	956
Dell OEM Foxconn DC Brushless Fan PV123812DSPF	pcs.	2	600	1200
DS1307 RTC Module	pcs.	3	149.75	449.25
16gb SD-Card	pcs.	3	180	540
Adjustable Brass Spray Mising Nozzle Fitting	pcs	30	20.2	606
PVC Pipe 1/2"	pcs.	9	75	675
Water Collector	pcs.	2	200	400
Stranded Wires (Red & Black) 20m	pcs.	3	200	600
Angle Bar 8ft.	pcs.	15	350	5250
Ceramic Clay Pot	pcs.	2	180	360
DC12V Bulb SL 9W	pcs.	11	104	1144
Bulb Socket	pcs.	11	10	110
<b>Total:</b>				31607.25

**APPENDIX B**  
**PROGRAM CODES**

## FIS\_HEADER.H

---

```
////////////////////////////////////////////////////////////////////////
/*
// Matlab .fis to arduino C converter v2.0.1.25122016
// - Karthik Nadig, USA
// Please report bugs to: karthiknadig@gmail.com
////////////////////////////////////////////////////////////////////////
*
#define FIS_TYPE float
#define FIS_RESOLUTION 101
#define FIS_MIN -3.4028235E+38
#define FIS_MAX 3.4028235E+38
typedef FIS_TYPE(*_FIS_MF)(FIS_TYPE, FIS_TYPE*);
typedef FIS_TYPE(*_FIS_ARR_OP)(FIS_TYPE, FIS_TYPE);
typedef FIS_TYPE(*_FIS_ARR)(FIS_TYPE*, int, _FIS_ARR_OP);
```

## ARDUINO MAIN SCRIPT

---

```
#include <SD.h>
#include <LiquidCrystal.h>
#include <RTClib.h>
#include <OneWire.h>
#include <DallasTemperature.h>
LiquidCrystal lcd(2, 3, 4, 5, 6, 7);

// ****
// ANFIS
// ****
#include "fis_header.h"

const int fis_gcI = 4;
const int fis_gcO = 1;
const int fis_gcR = 81;

FIS_TYPE g_fisInput[fis_gcI];
FIS_TYPE g_fisOutput[fis_gcO];

// ****
// Initialize RTC Library
// ****
RTC_DS3231 rtc;
DateTime now;

#define button1 A1
#define button2 A2
#define DS18B20_PIN A3
#define VIN A4
const float VCC = 5.0;
const int model = 2;
#define ONE_WIRE_BUS 2
OneWire oneWire(ONE_WIRE_BUS);
DallasTemperature sensors(&oneWire);

int offset =0;

File dataLog;
boolean sd_ok = 0;

void setup()
{
    pinMode(button1, INPUT_PULLUP);
    pinMode(button2, INPUT_PULLUP);
    pinMode(10, OUTPUT);

    rtc.begin();
    lcd.begin(20, 4);
    lcd.setCursor(0, 3);
    lcd.print("Temp:");

    Serial.begin(9600);
    sensors.begin();
    Serial.print("Initializing SD card...");
}
```

```

if ( !SD.begin() )
    Serial.println("initialization failed!");

else {
    sd_ok = 1;
    Serial.println("initialization done.");
    if( SD.exists("OutputData.csv") == 0 )
    {
        Serial.print("\r\nCreate 'OutputData.csv' file ... ");
        dataLog = SD.open("OutputData.csv", FILE_WRITE);
        if(dataLog) {
            Serial.println("OK");
            dataLog.println("_ DATE TIME TEMPERATURE VOLTAGE CURRENT POWER");
            dataLog.close();
        }
        else
            Serial.println("error creating file.");
    }
}

Serial.println("\r\n  DATE |  TIME | TEMPERATURE | VOLTAGE | CURRENT |  POWER ");
Serial.println("(dd-mm-yyyy)|(hh:mm:ss)|");
}

void loop()
{
// ****
// RTC Void Loop
// ****
    now = rtc.now();
    RTC_display();

    if( !digitalRead(button1) )
    if( debounce() )
    {
        while( debounce() );

        byte hour = edit( now.hour() );
        byte minute = edit( now.minute() );
        byte day = edit( now.day() );
        byte month = edit( now.month() );
        byte year = edit( now.year() );
        rtc.adjust(DateTime(year, month, day, hour, minute, 0));

        while(debounce());
    }

// ****
// Temperature DS18B20 Void Loop
// ****
    static byte p_second;
    if( (now.second() % 3 == 0) && (p_second != now.second()) )
    {
        unsigned int ds18b20_temp;
        char buffer1[12], buffer2[26];

```

```

bool sensor_ok = 0;
p_second = now.second();
if( ds18b20_read(&ds18b20_temp) )
{
    sensor_ok = 1;
    if(ds18b20_temp & 0x8000)
    {
        ds18b20_temp = ~ds18b20_temp + 1;
        sprintf(buffer1, "-%02u.%04u%cC", (ds18b20_temp/16) % 100, (ds18b20_temp & 0x0F) * 625, 223);
    }
    else
    {
        if (ds18b20_temp/16 >= 100)
            sprintf(buffer1, "%03u.%04u%cC", ds18b20_temp/16, (ds18b20_temp & 0x0F) * 625, 223);
        else
            sprintf(buffer1, "%02u.%04u%cC", ds18b20_temp/16, (ds18b20_temp & 0x0F) * 625, 223);
    }
}
else
    sprintf(buffer1, " ERROR ");

lcd.setCursor(5, 3);
lcd.print(buffer1);

sprintf( buffer2, " %02u-%02u-%04u %02u:%02u:%02u ", now.day(), now.month(), now.year(),
         now.hour(), now.minute(), now.second() );
if(sensor_ok) {
    buffer1[8] = 194;
    buffer1[9] = 176;
    buffer1[10] = 'C';
    buffer1[11] = '0';
}

// ****
// Voltage Sensor Void Loop
// ****
int volt = analogRead(A0);
double voltagee = map(volt,0,1023, 0, 2500) + offset;
voltagee /=100;

// ****
// Current Sensor Void Loop
// ****
unsigned int x=0;
float AcsValue=0.0,Samples=0.0,AvgAcs=0.0,AcsValueF=0.0;

for (int x = 0; x < 150; x++){
    AcsValue = analogRead(A4);
    Samples = Samples + AcsValue;
    delay (3);
}
AvgAcs=Samples/150.0;
AcsValueF = ((2.5 - (AvgAcs * (5.0 / 1024.0)) )/0.100)+0.6;

// ****
// Cooling System Trigger

```

```

// ****
sensors.requestTemperatures();
if (sensors.getTempCByIndex(0) >= 35)
{
    digitalWrite(10, HIGH);
}
if (sensors.getTempCByIndex(0) <= 33)
{
    digitalWrite(10, LOW);
}

Serial.print(buffer2);
Serial.print("");
Serial.print(buffer1);
Serial.print(" ");
Serial.print(voltagee,3);
Serial.print("V");
Serial.print(" ");
Serial.print(AcsValueF,3);
Serial.print("A");
Serial.print(" ");
Serial.print(voltagee*AcsValueF,3);
Serial.println("W");

if(sd_ok)
{
    dataLog = SD.open("OutputData.csv", FILE_WRITE);
    dataLog.print(buffer2);
    dataLog.print("");
    dataLog.print(buffer1);
    dataLog.print(" ");
    dataLog.print(voltagee,3);
    dataLog.print(" ");
    dataLog.print(AcsValueF,3);
    dataLog.print(" ");
    dataLog.println(voltagee*AcsValueF,3);
    dataLog.close();
}

}

delay(100);
}

// ****
// RTC Functions
// ****
void RTC_display()
{
    char _buffer[17];
    char dow_matrix[7][10] = {" SUNDAY ", " MONDAY ", " TUESDAY ", " WEDNESDAY ",
                            " THURSDAY ", " FRIDAY ", " SATURDAY "};
    lcd.setCursor(4, 0);
    lcd.print( dow_matrix[now.dayOfTheWeek() ] );
}

```

```

sprintf( _buffer, "TIME: %02u:%02u:%02u", now.hour(), now.minute(), now.second() );
lcd.setCursor(0, 1);
lcd.print(_buffer);
sprintf( _buffer, "DATE: %02u-%02u-%04u", now.day(), now.month(), now.year() );
lcd.setCursor(0, 2);
lcd.print(_buffer);
}

byte edit(byte parameter)
{
    static byte i = 0, y_pos,
               x_pos[5] = {6, 9, 6, 9, 14};
    char text[3];
    sprintf(text,"%02u", parameter);

    if(i < 2)
        y_pos = 1;
    else
        y_pos = 2;

    while( debounce() );

    while(true) {
        while( !digitalRead(button2) ) {
            parameter++;
            if(i == 0 && parameter > 23)
                parameter = 0;
            if(i == 1 && parameter > 59)
                parameter = 0;
            if(i == 2 && parameter > 31)
                parameter = 1;
            if(i == 3 && parameter > 12)
                parameter = 1;
            if(i == 4 && parameter > 99)
                parameter = 0;

            sprintf(text,"%02u", parameter);
            lcd.setCursor(x_pos[i], y_pos);
            lcd.print(text);
            delay(200);
        }

        lcd.setCursor(x_pos[i], y_pos);
        lcd.print(" ");
        unsigned long previous_m = millis();
        while( (millis() - previous_m < 250) && digitalRead(button1) && digitalRead(button2) );
        lcd.setCursor(x_pos[i], y_pos);
        lcd.print(text);
        previous_m = millis();
        while( (millis() - previous_m < 250) && digitalRead(button1) && digitalRead(button2) );

        if(!digitalRead(button1))
        {
            i = (i + 1) % 5;
            return parameter;
        }
    }
}

```

```

        }

    }

bool debounce ()
{
    byte count = 0;
    for(byte i = 0; i < 5; i++)
    {
        if ( !digitalRead(button1) )
            count++;
        delay(10);
    }

    if(count > 2) return 1;
    else      return 0;
}

// ****
// DS18B20 Sensor Functions
// ****

bool ds18b20_start()
{
    bool ret = 0;
    digitalWrite(DS18B20_PIN, LOW);
    pinMode(DS18B20_PIN, OUTPUT);
    delayMicroseconds(500);
    pinMode(DS18B20_PIN, INPUT);
    delayMicroseconds(100);
    if (!digitalRead(DS18B20_PIN))
    {
        ret = 1;
        delayMicroseconds(400);
    }
    return(ret);
}

void ds18b20_write_bit(bool value)
{
    digitalWrite(DS18B20_PIN, LOW);
    pinMode(DS18B20_PIN, OUTPUT);
    delayMicroseconds(2);
    digitalWrite(DS18B20_PIN, value);
    delayMicroseconds(80);
    pinMode(DS18B20_PIN, INPUT);
    delayMicroseconds(2);
}

void ds18b20_write_byte(byte value)
{
    byte i;
    for(i = 0; i < 8; i++)
        ds18b20_write_bit(bitRead(value, i));
}

bool ds18b20_read_bit(void)
{

```

```

    bool value;
    digitalWrite(DS18B20_PIN, LOW);
    pinMode(DS18B20_PIN, OUTPUT);
    delayMicroseconds(2);
    pinMode(DS18B20_PIN, INPUT);
    delayMicroseconds(5);
    value = digitalRead(DS18B20_PIN);
    delayMicroseconds(100);
    return value;
}

byte ds18b20_read_byte(void)
{
    byte i, value;
    for(i = 0; i < 8; i++)
        bitWrite(value, i, ds18b20_read_bit());
    return value;
}

bool ds18b20_read(int *raw_temp_value)
{
    if (!ds18b20_start())
        return(0);
    ds18b20_write_byte(0xCC);
    ds18b20_write_byte(0x44);
    while(ds18b20_read_byte() == 0);
    if (!ds18b20_start())
        return(0);
    ds18b20_write_byte(0xCC);
    ds18b20_write_byte(0xBE);

    *raw_temp_value = ds18b20_read_byte();
    *raw_temp_value |= (unsigned int)(ds18b20_read_byte() << 8);

    return(1);
}

// ****
// ANFIS
// ****
void loop()
{
    g_fisInput[0] = analogRead(A3);
    g_fisInput[1] = analogRead(A0);
    g_fisInput[2] = analogRead(A4);
    g_fisInput[3] = analogRead(A20);
    g_fisOutput[0] = 0;
    fis_evaluate();
    analogWrite(13, g_fisOutput[0]);
}

// ****
// Support functions for Fuzzy Inference System
// ****
// Triangular Member Function

```

```

FIS_TYPE fis_trimf(FIS_TYPE x, FIS_TYPE* p)
{
    FIS_TYPE a = p[0], b = p[1], c = p[2];
    FIS_TYPE t1 = (x - a) / (b - a);
    FIS_TYPE t2 = (c - x) / (c - b);
    if ((a == b) && (b == c)) return (FIS_TYPE) (x == a);
    if (a == b) return (FIS_TYPE) (t2*(b <= x)*(x <= c));
    if (b == c) return (FIS_TYPE) (t1*(a <= x)*(x <= b));
    t1 = min(t1, t2);
    return (FIS_TYPE) max(t1, 0);
}

FIS_TYPE fis_prod(FIS_TYPE a, FIS_TYPE b)
{
    return (a * b);
}

FIS_TYPE fis_prob0r(FIS_TYPE a, FIS_TYPE b)
{
    return (a + b - (a * b));
}

FIS_TYPE fis_sum(FIS_TYPE a, FIS_TYPE b)
{
    return (a + b);
}

FIS_TYPE fis_array_operation(FIS_TYPE *array, int size, _FIS_ARR_OP pfnOp)
{
    int i;
    FIS_TYPE ret = 0;

    if (size == 0) return ret;
    if (size == 1) return array[0];

    ret = array[0];
    for (i = 1; i < size; i++)
    {
        ret = (*pfnOp)(ret, array[i]);
    }

    return ret;
}

// *****
// Data for Fuzzy Inference System
// *****
// Pointers to the implementations of member functions
_FIS_MF fis_gMF[] =
{
    fis_trimf
};

// Count of member function for each Input
int fis_gIMFCCount[] = { 3, 3, 3, 3 };

```

```

// Count of member function for each Output
int fis_gOMFCount[] = { 81 };

// Coefficients for the Input Member Functions
FIS_TYPE fis_gMFI0Coeff1[] = { 27.875, 30.5000663989489, 33.1252189328918 };
FIS_TYPE fis_gMFI0Coeff2[] = { 30.5000439379362, 33.1250899337137, 35.7500146985529 };
FIS_TYPE fis_gMFI0Coeff3[] = { 33.1250589022324, 35.7500235347648, 38.375 };
FIS_TYPE* fis_gMFI0Coeff[] = { fis_gMFI0Coeff1, fis_gMFI0Coeff2, fis_gMFI0Coeff3 };
FIS_TYPE fis_gMFI1Coeff1[] = { 16.03, 18.0399946189546, 20.0497285480447 };
FIS_TYPE fis_gMFI1Coeff2[] = { 18.0401438606359, 20.0499154970376, 22.0599719005212 };
FIS_TYPE fis_gMFI1Coeff3[] = { 20.0500007735391, 22.059920878083, 24.07 };
FIS_TYPE* fis_gMFI1Coeff[] = { fis_gMFI1Coeff1, fis_gMFI1Coeff2, fis_gMFI1Coeff3 };
FIS_TYPE fis_gMFI2Coeff1[] = { 0.967, 1.26018344550299, 1.55368995285112 };
FIS_TYPE fis_gMFI2Coeff2[] = { 1.26144894352548, 1.55374184293707, 1.84506582343562 };
FIS_TYPE fis_gMFI2Coeff3[] = { 1.54322857042615, 1.84655839743408, 2.139 };
FIS_TYPE* fis_gMFI2Coeff[] = { fis_gMFI2Coeff1, fis_gMFI2Coeff2, fis_gMFI2Coeff3 };
FIS_TYPE fis_gMFI3Coeff1[] = { 730.87, 1309.9099994367, 1888.94999632606 };
FIS_TYPE fis_gMFI3Coeff2[] = { 1309.90999977533, 1888.94999935973, 2467.98999995868 };
FIS_TYPE fis_gMFI3Coeff3[] = { 1888.95000034305, 2467.98999992303, 3047.03 };
FIS_TYPE* fis_gMFI3Coeff[] = { fis_gMFI3Coeff1, fis_gMFI3Coeff2, fis_gMFI3Coeff3 };
FIS_TYPE** fis_gMFICoeff[] = { fis_gMFI0Coeff, fis_gMFI1Coeff, fis_gMFI2Coeff, fis_gMFI3Coeff };

// Coefficients for the Output Member Functions
FIS_TYPE fis_gMFO0Coeff1[] = { 0, 0, 0, 0, 0.441175368472831 };
FIS_TYPE fis_gMFO0Coeff2[] = { 0, 0, 0, 0, 0.576091819588048 };
FIS_TYPE fis_gMFO0Coeff3[] = { 0, 0, 0, 0, 0 };
FIS_TYPE fis_gMFO0Coeff4[] = { 0, 0, 0, 0, 0.0343856393508999 };
FIS_TYPE fis_gMFO0Coeff5[] = { 0, 0, 0, 0, 0.186668030104236 };
FIS_TYPE fis_gMFO0Coeff6[] = { 0, 0, 0, 0, 0.000495415622027392 };
FIS_TYPE fis_gMFO0Coeff7[] = { 0, 0, 0, 0, 0.00480489086238222 };
FIS_TYPE fis_gMFO0Coeff8[] = { 0, 0, 0, 0, 0.0577714052542009 };
FIS_TYPE fis_gMFO0Coeff9[] = { 0, 0, 0, 0, 0.00138774636884471 };
FIS_TYPE fis_gMFO0Coeff10[] = { 0, 0, 0, 0, 0.124339853124378 };
FIS_TYPE fis_gMFO0Coeff11[] = { 0, 0, 0, 0, 0.426548684285438 };
FIS_TYPE fis_gMFO0Coeff12[] = { 0, 0, 0, 0, 0.000338785894935949 };
FIS_TYPE fis_gMFO0Coeff13[] = { 0, 0, 0, 0, 0.0785885829139632 };
FIS_TYPE fis_gMFO0Coeff14[] = { 0, 0, 0, 0, 0.638042492226812 };
FIS_TYPE fis_gMFO0Coeff15[] = { 0, 0, 0, 0, 0.0770447797054661 };
FIS_TYPE fis_gMFO0Coeff16[] = { 0, 0, 0, 0, 0.0173840628949225 };
FIS_TYPE fis_gMFO0Coeff17[] = { 0, 0, 0, 0, 0.261906666524588 };
FIS_TYPE fis_gMFO0Coeff18[] = { 0, 0, 0, 0, 0.296369382577245 };
FIS_TYPE fis_gMFO0Coeff19[] = { 0, 0, 0, 0, 0 };
FIS_TYPE fis_gMFO0Coeff20[] = { 0, 0, 0, 0, 0.0219233553380202 };
FIS_TYPE fis_gMFO0Coeff21[] = { 0, 0, 0, 0, 0.00249900690409632 };
FIS_TYPE fis_gMFO0Coeff22[] = { 0, 0, 0, 0, 0 };
FIS_TYPE fis_gMFO0Coeff23[] = { 0, 0, 0, 0, 0.394249874051082 };
FIS_TYPE fis_gMFO0Coeff24[] = { 0, 0, 0, 0, 0.11769470277916 };
FIS_TYPE fis_gMFO0Coeff25[] = { 0, 0, 0, 0, 0 };
FIS_TYPE fis_gMFO0Coeff26[] = { 0, 0, 0, 0, 0.39642830147097 };
FIS_TYPE fis_gMFO0Coeff27[] = { 0, 0, 0, 0, 0.588791214796149 };
FIS_TYPE fis_gMFO0Coeff28[] = { 0, 0, 0, 0, 0.234554412086707 };
FIS_TYPE fis_gMFO0Coeff29[] = { 0, 0, 0, 0, 0.528716873359858 };
FIS_TYPE fis_gMFO0Coeff30[] = { 0, 0, 0, 0, 0 };
FIS_TYPE fis_gMFO0Coeff31[] = { 0, 0, 0, 0, 0.0656900468933169 };
FIS_TYPE fis_gMFO0Coeff32[] = { 0, 0, 0, 0, 0.470274718881957 };

```

```

FIS_TYPE fis_gMFO0Coeff33[] = { 0, 0, 0, 0, 0.00470243427797067 };
FIS_TYPE fis_gMFO0Coeff34[] = { 0, 0, 0, 0, 0.0259867106992945 };
FIS_TYPE fis_gMFO0Coeff35[] = { 0, 0, 0, 0, 0.315115711223068 };
FIS_TYPE fis_gMFO0Coeff36[] = { 0, 0, 0, 0, 0.0131723462153707 };
FIS_TYPE fis_gMFO0Coeff37[] = { 0, 0, 0, 0, 0.136849229758324 };
FIS_TYPE fis_gMFO0Coeff38[] = { 0, 0, 0, 0, 0.387795816668998 };
FIS_TYPE fis_gMFO0Coeff39[] = { 0, 0, 0, 0, 0.33202000627421 };
FIS_TYPE fis_gMFO0Coeff40[] = { 0, 0, 0, 0, 0.407418277581095 };
FIS_TYPE fis_gMFO0Coeff41[] = { 0, 0, 0, 0, 0.414568572593905 };
FIS_TYPE fis_gMFO0Coeff42[] = { 0, 0, 0, 0, 0.423019608889371 };
FIS_TYPE fis_gMFO0Coeff43[] = { 0, 0, 0, 0, 0.100688308483084 };
FIS_TYPE fis_gMFO0Coeff44[] = { 0, 0, 0, 0, 0.38932528435611 };
FIS_TYPE fis_gMFO0Coeff45[] = { 0, 0, 0, 0, 0.487250145949307 };
FIS_TYPE fis_gMFO0Coeff46[] = { 0, 0, 0, 0, 0 };
FIS_TYPE fis_gMFO0Coeff47[] = { 0, 0, 0, 0, 0.407615439692223 };
FIS_TYPE fis_gMFO0Coeff48[] = { 0, 0, 0, 0, 0.50091748292092 };
FIS_TYPE fis_gMFO0Coeff49[] = { 0, 0, 0, 0, 0 };
FIS_TYPE fis_gMFO0Coeff50[] = { 0, 0, 0, 0, 0.383402387578369 };
FIS_TYPE fis_gMFO0Coeff51[] = { 0, 0, 0, 0, 0.363641237723895 };
FIS_TYPE fis_gMFO0Coeff52[] = { 0, 0, 0, 0, 0 };
FIS_TYPE fis_gMFO0Coeff53[] = { 0, 0, 0, 0, 0.385458494423994 };
FIS_TYPE fis_gMFO0Coeff54[] = { 0, 0, 0, 0, 0.325703099095019 };
FIS_TYPE fis_gMFO0Coeff55[] = { 0, 0, 0, 0, 0 };
FIS_TYPE fis_gMFO0Coeff56[] = { 0, 0, 0, 0, 0 };
FIS_TYPE fis_gMFO0Coeff57[] = { 0, 0, 0, 0, 0 };
FIS_TYPE fis_gMFO0Coeff58[] = { 0, 0, 0, 0, 0 };
FIS_TYPE fis_gMFO0Coeff59[] = { 0, 0, 0, 0, 0 };
FIS_TYPE fis_gMFO0Coeff60[] = { 0, 0, 0, 0, 0 };
FIS_TYPE fis_gMFO0Coeff61[] = { 0, 0, 0, 0, 0 };
FIS_TYPE fis_gMFO0Coeff62[] = { 0, 0, 0, 0, 0 };
FIS_TYPE fis_gMFO0Coeff63[] = { 0, 0, 0, 0, 0 };
FIS_TYPE fis_gMFO0Coeff64[] = { 0, 0, 0, 0, 0 };
FIS_TYPE fis_gMFO0Coeff65[] = { 0, 0, 0, 0, 0.460203523556557 };
FIS_TYPE fis_gMFO0Coeff66[] = { 0, 0, 0, 0, 0.494347131044095 };
FIS_TYPE fis_gMFO0Coeff67[] = { 0, 0, 0, 0, 0 };
FIS_TYPE fis_gMFO0Coeff68[] = { 0, 0, 0, 0, 0.366898203538557 };
FIS_TYPE fis_gMFO0Coeff69[] = { 0, 0, 0, 0, 0.397341466920896 };
FIS_TYPE fis_gMFO0Coeff70[] = { 0, 0, 0, 0, 0 };
FIS_TYPE fis_gMFO0Coeff71[] = { 0, 0, 0, 0, 0.0231679874578922 };
FIS_TYPE fis_gMFO0Coeff72[] = { 0, 0, 0, 0, -0.0343869933800284 };
FIS_TYPE fis_gMFO0Coeff73[] = { 0, 0, 0, 0, 0 };
FIS_TYPE fis_gMFO0Coeff74[] = { 0, 0, 0, 0, 0.276347006716441 };
FIS_TYPE fis_gMFO0Coeff75[] = { 0, 0, 0, 0, 0.263096667597814 };
FIS_TYPE fis_gMFO0Coeff76[] = { 0, 0, 0, 0, 0 };
FIS_TYPE fis_gMFO0Coeff77[] = { 0, 0, 0, 0, 0.472490687138172 };
FIS_TYPE fis_gMFO0Coeff78[] = { 0, 0, 0, 0, 0.385377829580878 };
FIS_TYPE fis_gMFO0Coeff79[] = { 0, 0, 0, 0, 0 };
FIS_TYPE fis_gMFO0Coeff80[] = { 0, 0, 0, 0, 0.145855032237677 };
FIS_TYPE fis_gMFO0Coeff81[] = { 0, 0, 0, 0, 0.0268749375022401 };

FIS_TYPE* fis_gMFO0Coeff[] = { fis_gMFO0Coeff1, fis_gMFO0Coeff2, fis_gMFO0Coeff3,
fis_gMFO0Coeff4, fis_gMFO0Coeff5, fis_gMFO0Coeff6, fis_gMFO0Coeff7, fis_gMFO0Coeff8,
fis_gMFO0Coeff9, fis_gMFO0Coeff10, fis_gMFO0Coeff11, fis_gMFO0Coeff12, fis_gMFO0Coeff13,
fis_gMFO0Coeff14, fis_gMFO0Coeff15, fis_gMFO0Coeff16, fis_gMFO0Coeff17, fis_gMFO0Coeff18,
fis_gMFO0Coeff19, fis_gMFO0Coeff20, fis_gMFO0Coeff21, fis_gMFO0Coeff22, fis_gMFO0Coeff23,
fis_gMFO0Coeff24, fis_gMFO0Coeff25, fis_gMFO0Coeff26, fis_gMFO0Coeff27, fis_gMFO0Coeff28,
fis_gMFO0Coeff29, fis_gMFO0Coeff30, fis_gMFO0Coeff31, fis_gMFO0Coeff32, fis_gMFO0Coeff33,

```



```

int fis_gRI22[] = { 1, 3, 2, 2 };
int fis_gRI23[] = { 1, 3, 2, 3 };
int fis_gRI24[] = { 1, 3, 3, 1 };
int fis_gRI25[] = { 1, 3, 3, 2 };
int fis_gRI26[] = { 1, 3, 3, 3 };
int fis_gRI27[] = { 2, 1, 1, 1 };
int fis_gRI28[] = { 2, 1, 1, 2 };
int fis_gRI29[] = { 2, 1, 1, 3 };
int fis_gRI30[] = { 2, 1, 2, 1 };
int fis_gRI31[] = { 2, 1, 2, 2 };
int fis_gRI32[] = { 2, 1, 2, 3 };
int fis_gRI33[] = { 2, 1, 3, 1 };
int fis_gRI34[] = { 2, 1, 3, 2 };
int fis_gRI35[] = { 2, 1, 3, 3 };
int fis_gRI36[] = { 2, 2, 1, 1 };
int fis_gRI37[] = { 2, 2, 1, 2 };
int fis_gRI38[] = { 2, 2, 1, 3 };
int fis_gRI39[] = { 2, 2, 2, 1 };
int fis_gRI40[] = { 2, 2, 2, 2 };
int fis_gRI41[] = { 2, 2, 2, 3 };
int fis_gRI42[] = { 2, 2, 3, 1 };
int fis_gRI43[] = { 2, 2, 3, 2 };
int fis_gRI44[] = { 2, 2, 3, 3 };
int fis_gRI45[] = { 2, 3, 1, 1 };
int fis_gRI46[] = { 2, 3, 1, 2 };
int fis_gRI47[] = { 2, 3, 1, 3 };
int fis_gRI48[] = { 2, 3, 2, 1 };
int fis_gRI49[] = { 2, 3, 2, 2 };
int fis_gRI50[] = { 2, 3, 2, 3 };
int fis_gRI51[] = { 2, 3, 3, 1 };
int fis_gRI52[] = { 2, 3, 3, 2 };
int fis_gRI53[] = { 2, 3, 3, 3 };
int fis_gRI54[] = { 3, 1, 1, 1 };
int fis_gRI55[] = { 3, 1, 1, 2 };
int fis_gRI56[] = { 3, 1, 1, 3 };
int fis_gRI57[] = { 3, 1, 2, 1 };
int fis_gRI58[] = { 3, 1, 2, 2 };
int fis_gRI59[] = { 3, 1, 2, 3 };
int fis_gRI60[] = { 3, 1, 3, 1 };
int fis_gRI61[] = { 3, 1, 3, 2 };
int fis_gRI62[] = { 3, 1, 3, 3 };
int fis_gRI63[] = { 3, 2, 1, 1 };
int fis_gRI64[] = { 3, 2, 1, 2 };
int fis_gRI65[] = { 3, 2, 1, 3 };
int fis_gRI66[] = { 3, 2, 2, 1 };
int fis_gRI67[] = { 3, 2, 2, 2 };
int fis_gRI68[] = { 3, 2, 2, 3 };
int fis_gRI69[] = { 3, 2, 3, 1 };
int fis_gRI70[] = { 3, 2, 3, 2 };
int fis_gRI71[] = { 3, 2, 3, 3 };
int fis_gRI72[] = { 3, 3, 1, 1 };
int fis_gRI73[] = { 3, 3, 1, 2 };
int fis_gRI74[] = { 3, 3, 1, 3 };
int fis_gRI75[] = { 3, 3, 2, 1 };
int fis_gRI76[] = { 3, 3, 2, 2 };
int fis_gRI77[] = { 3, 3, 2, 3 };

```

```

int fis_gRI78[] = { 3, 3, 3, 1 };
int fis_gRI79[] = { 3, 3, 3, 2 };
int fis_gRI80[] = { 3, 3, 3, 3 };
int* fis_gRI[] = { fis_gRI0, fis_gRI1, fis_gRI2, fis_gRI3, fis_gRI4, fis_gRI5, fis_gRI6, fis_gRI7, fis_gRI8,
fis_gRI9, fis_gRI10, fis_gRI11, fis_gRI12, fis_gRI13, fis_gRI14, fis_gRI15, fis_gRI16, fis_gRI17,
fis_gRI18, fis_gRI19, fis_gRI20, fis_gRI21, fis_gRI22, fis_gRI23, fis_gRI24, fis_gRI25, fis_gRI26,
fis_gRI27, fis_gRI28, fis_gRI29, fis_gRI30, fis_gRI31, fis_gRI32, fis_gRI33, fis_gRI34, fis_gRI35,
fis_gRI36, fis_gRI37, fis_gRI38, fis_gRI39, fis_gRI40, fis_gRI41, fis_gRI42, fis_gRI43, fis_gRI44,
fis_gRI45, fis_gRI46, fis_gRI47, fis_gRI48, fis_gRI49, fis_gRI50, fis_gRI51, fis_gRI52, fis_gRI53,
fis_gRI54, fis_gRI55, fis_gRI56, fis_gRI57, fis_gRI58, fis_gRI59, fis_gRI60, fis_gRI61, fis_gRI62,
fis_gRI63, fis_gRI64, fis_gRI65, fis_gRI66, fis_gRI67, fis_gRI68, fis_gRI69, fis_gRI70, fis_gRI71,
fis_gRI72, fis_gRI73, fis_gRI74, fis_gRI75, fis_gRI76, fis_gRI77, fis_gRI78, fis_gRI79, fis_gRI80 };

// Rule Outputs
int fis_gRO0[] = { 1 };
int fis_gRO1[] = { 2 };
int fis_gRO2[] = { 3 };
int fis_gRO3[] = { 4 };
int fis_gRO4[] = { 5 };
int fis_gRO5[] = { 6 };
int fis_gRO6[] = { 7 };
int fis_gRO7[] = { 8 };
int fis_gRO8[] = { 9 };
int fis_gRO9[] = { 10 };
int fis_gRO10[] = { 11 };
int fis_gRO11[] = { 12 };
int fis_gRO12[] = { 13 };
int fis_gRO13[] = { 14 };
int fis_gRO14[] = { 15 };
int fis_gRO15[] = { 16 };
int fis_gRO16[] = { 17 };
int fis_gRO17[] = { 18 };
int fis_gRO18[] = { 19 };
int fis_gRO19[] = { 20 };
int fis_gRO20[] = { 21 };
int fis_gRO21[] = { 22 };
int fis_gRO22[] = { 23 };
int fis_gRO23[] = { 24 };
int fis_gRO24[] = { 25 };
int fis_gRO25[] = { 26 };
int fis_gRO26[] = { 27 };
int fis_gRO27[] = { 28 };
int fis_gRO28[] = { 29 };
int fis_gRO29[] = { 30 };
int fis_gRO30[] = { 31 };
int fis_gRO31[] = { 32 };
int fis_gRO32[] = { 33 };
int fis_gRO33[] = { 34 };
int fis_gRO34[] = { 35 };
int fis_gRO35[] = { 36 };
int fis_gRO36[] = { 37 };
int fis_gRO37[] = { 38 };
int fis_gRO38[] = { 39 };
int fis_gRO39[] = { 40 };
int fis_gRO40[] = { 41 };
int fis_gRO41[] = { 42 };

```

```

int fis_gRO42[] = { 43 };
int fis_gRO43[] = { 44 };
int fis_gRO44[] = { 45 };
int fis_gRO45[] = { 46 };
int fis_gRO46[] = { 47 };
int fis_gRO47[] = { 48 };
int fis_gRO48[] = { 49 };
int fis_gRO49[] = { 50 };
int fis_gRO50[] = { 51 };
int fis_gRO51[] = { 52 };
int fis_gRO52[] = { 53 };
int fis_gRO53[] = { 54 };
int fis_gRO54[] = { 55 };
int fis_gRO55[] = { 56 };
int fis_gRO56[] = { 57 };
int fis_gRO57[] = { 58 };
int fis_gRO58[] = { 59 };
int fis_gRO59[] = { 60 };
int fis_gRO60[] = { 61 };
int fis_gRO61[] = { 62 };
int fis_gRO62[] = { 63 };
int fis_gRO63[] = { 64 };
int fis_gRO64[] = { 65 };
int fis_gRO65[] = { 66 };
int fis_gRO66[] = { 67 };
int fis_gRO67[] = { 68 };
int fis_gRO68[] = { 69 };
int fis_gRO69[] = { 70 };
int fis_gRO70[] = { 71 };
int fis_gRO71[] = { 72 };
int fis_gRO72[] = { 73 };
int fis_gRO73[] = { 74 };
int fis_gRO74[] = { 75 };
int fis_gRO75[] = { 76 };
int fis_gRO76[] = { 77 };
int fis_gRO77[] = { 78 };
int fis_gRO78[] = { 79 };
int fis_gRO79[] = { 80 };
int fis_gRO80[] = { 81 };
int* fis_gRO[] = { fis_gRO0, fis_gRO1, fis_gRO2, fis_gRO3, fis_gRO4, fis_gRO5, fis_gRO6, fis_gRO7,
fis_gRO8, fis_gRO9, fis_gRO10, fis_gRO11, fis_gRO12, fis_gRO13, fis_gRO14, fis_gRO15, fis_gRO16,
fis_gRO17, fis_gRO18, fis_gRO19, fis_gRO20, fis_gRO21, fis_gRO22, fis_gRO23, fis_gRO24,
fis_gRO25, fis_gRO26, fis_gRO27, fis_gRO28, fis_gRO29, fis_gRO30, fis_gRO31, fis_gRO32,
fis_gRO33, fis_gRO34, fis_gRO35, fis_gRO36, fis_gRO37, fis_gRO38, fis_gRO39, fis_gRO40,
fis_gRO41, fis_gRO42, fis_gRO43, fis_gRO44, fis_gRO45, fis_gRO46, fis_gRO47, fis_gRO48,
fis_gRO49, fis_gRO50, fis_gRO51, fis_gRO52, fis_gRO53, fis_gRO54, fis_gRO55, fis_gRO56,
fis_gRO57, fis_gRO58, fis_gRO59, fis_gRO60, fis_gRO61, fis_gRO62, fis_gRO63, fis_gRO64,
fis_gRO65, fis_gRO66, fis_gRO67, fis_gRO68, fis_gRO69, fis_gRO70, fis_gRO71, fis_gRO72,
fis_gRO73, fis_gRO74, fis_gRO75, fis_gRO76, fis_gRO77, fis_gRO78, fis_gRO79, fis_gRO80 };

// Input range Min
FIS_TYPE fis_gIMin[] = { 30.5, 18.04, 1.26, 1309.91 };

// Input range Max
FIS_TYPE fis_gIMax[] = { 35.75, 22.06, 1.846, 2467.99 };

```



```

        }
    }
else
{
    fuzzyFires[r] = 0;
    for (i = 0; i < fis_gcI; ++i)
    {
        index = fis_gRI[r][i];
        if (index > 0)
            fuzzyFires[r] = fis_prob0(fuzzyFires[r], fuzzyInput[i][index - 1]);
        else if (index < 0)
            fuzzyFires[r] = fis_prob0(fuzzyFires[r], 1 - fuzzyInput[i][-index - 1]);
        else
            fuzzyFires[r] = fis_prob0(fuzzyFires[r], 0);
    }
}

fuzzyFires[r] = fis_gRWeight[r] * fuzzyFires[r];
sW += fuzzyFires[r];
}

if (sW == 0)
{
    for (o = 0; o < fis_gcO; ++o)
    {
        g_fisOutput[o] = ((fis_gOMax[o] + fis_gOMin[o]) / 2);
    }
}
else
{
    for (o = 0; o < fis_gcO; ++o)
    {
        FIS_TYPE sWI = 0.0;
        for (j = 0; j < fis_gOMFCount[o]; ++j)
        {
            fuzzyOutput[o][j] = fis_gMFOCoeff[o][j][fis_gcI];
            for (i = 0; i < fis_gcI; ++i)
            {
                fuzzyOutput[o][j] += g_fisInput[i] * fis_gMFOCoeff[o][j][i];
            }
        }

        for (r = 0; r < fis_gcR; ++r)
        {
            index = fis_gRO[r][o] - 1;
            sWI += fuzzyFires[r] * fuzzyOutput[o][index];
        }

        g_fisOutput[o] = sWI / sW;
    }
}
}

```

**APPENDIX C**  
**SPECIFICATIONS AND DATASHEET**



GLOBAL PROFESSIONAL PV PRODUCTS INTEGRATED SOLUTIONS SUPPLIER

## RT6E-150M

**36 Cells**

Mono-crystalline

**150W**

Power output

**15.16%**

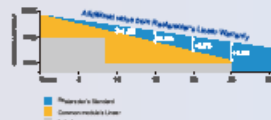
The Highest Efficiency

**0~+5W**

Tolerance



**0.5% Annual Degradation over 30 years**



**LINEAR PERFORMANCE WARRANTY**  
(Type Product Warranty / Max Power Decaying)

WWW.RESTARSLAR.COM



RT6E-150M is a robust solar module with 36 solar cells. These modules can be used for on-grid solar applications. Our meticulous design and production techniques ensure a high-yield, long-term performance for every module produced. Our rigorous quality control and in-house testing facilities guarantee Restarsolar's modules meet the highest quality standards possible.



High module conversion efficiency (up to 15.16%), through superior manufacturing technology



Guaranteed 0~+5W positive power output tolerance ensures high reliability



Anti-reflective, hydrophobic coating improves light absorption and reduces surface dust



Excellent performance under low light environments (mornings, evenings and cloudy days)



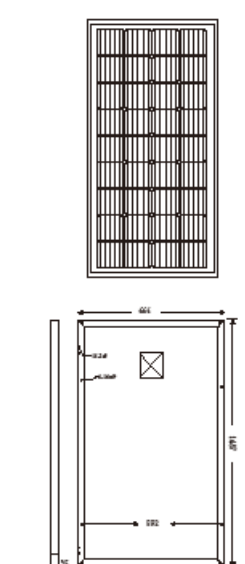
Suitable for harsh environments, such as coasts, deserts and lakes. Withstand high level of wind loads(2400pa) and snow loads(5400pa)

### Full range of products and certification systems

ISO 9001 TUV PID-FREE CE IEC61215/61730/61701/62716



Dimensions of PV Module Unit:mm



#### ELECTRICAL DATA(STC)

Rated Power in Watt-Peak(Wp)	160W
Open Circuit Voltage-Voc(V)	22.7V
Short Circuit Current-Isc(A)	8.98A
Module Power Voltage-Vmp (V)	18.4V
Module Power Current-Imp(A)	8.16A
Module Efficiency (%)	15.16%

STC: Irradiance 1000 W/m<sup>2</sup>, Cell Temp 25°C, Air Mass 1.5 according to EN 60804-2.

#### ELECTRICAL DATA(MOCT)

Max/short Power-Pmax (Wp)	112W
Open Circuit Voltage-Voc (V)	20.62V
Short Circuit Current-Isc (A)	7.12A
Module Power Voltage-Vmp (V)	17.14V
Module Power Current-Imp (A)	6.55A

NOTE: Irradiance of 800 W/m<sup>2</sup>, Ambient Temperature 20°C, Wind Speed 1 m/s

#### MECHANICAL DATA

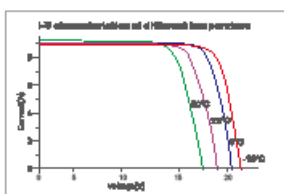
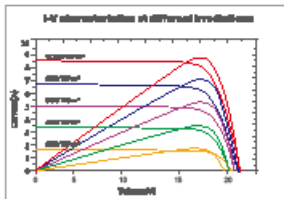
Solar cells	Mono-crystalline 156x156mm, 4 or 5 Bus bars
Dell configuration	36 cells(4x9)
Module dimensions	1487x566x35mm
Weight	11.5KGS
Front Cover	3.2mm Tempered Glass
Frame Material	Anodized Aluminum Alloy
J-BOX	IP65 or IP67, 6 Diodes
Cable	4mm <sup>2</sup> (IEC)12AWG(UL), 900mm
Connectors	MCA or MC4 Comparable
Standard Packaging	2pcs/carton box

#### TEMPERATURE & MAXIMUM RATINGS

Nominal Operating Cell Temperature (NOCT)	41°C±2°C
Temperature Coefficient of V <sub>oc</sub>	-0.32%/°C
Temperature Coefficient of I <sub>sc</sub>	0.05%/°C
Temperature Coefficient of P <sub>max</sub>	-0.36%/°C
Operational Temperature	-40→85°C
Maximum System Voltage	1000V(IEC)/600V(UL)
Max Series Fuse Rating	12A
Limiting Reverse Current	12A

#### PACKAGING CONFIGURATION

	40HQ	200P
Number of modules per container	1680pcs	660pcs
Package	2pcs/carton box	2pcs/carton box
Package Weight	23kg/carton box	23kg/carton box
Package Number	840/carton boxes	330/carton boxes
Package Dimension	1500*700*80mm/carton box	1500*700*80mm/carton box



# Technical Specification

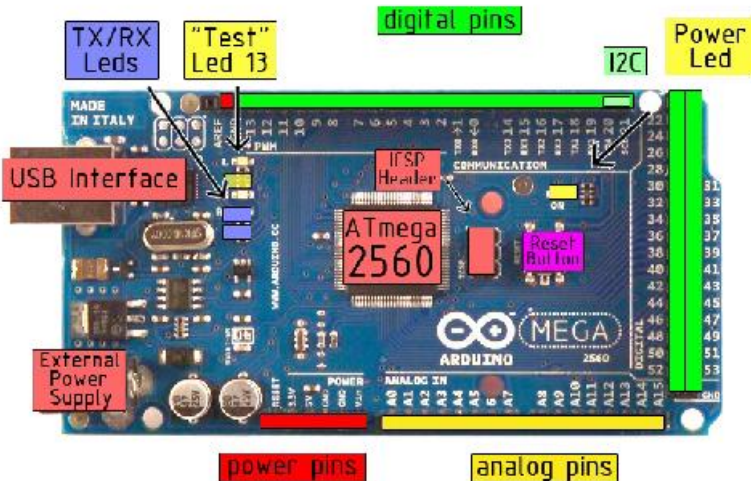


EAGLE files: [arduino-mega2560-reference-design.zip](#) Schematic: [arduino-mega2560-schematic.pdf](#)

## Summary

Microcontroller	ATmega2560
Operating Voltage	5V
Input Voltage (recommended)	7-12V
Input Voltage (limits)	6-20V
Digital I/O Pins	54 (of which 14 provide PWM output)
Analog Input Pins	16
DC Current per I/O Pin	40 mA
DC Current for 3.3V Pin	50 mA
Flash Memory	256 KB of which 8 KB used by bootloader
SRAM	8 KB
EEPROM	4 KB
Clock Speed	16 MHz

## the board



**radiospares** **RADIONICS**



## Power

The Arduino Mega2560 can be powered via the USB connection or with an external power supply. The power source is selected automatically. External (non-USB) power can come either from an AC-to-DC adapter (wall-wart) or battery. The adapter can be connected by plugging a 2.1mm center-positive plug into the board's power jack. Leads from a battery can be inserted in the Gnd and Vin pin headers of the POWER connector.

The board can operate on an external supply of 6 to 20 volts. If supplied with less than 7V, however, the 5V pin may supply less than five volts and the board may be unstable. If using more than 12V, the voltage regulator may overheat and damage the board. The recommended range is 7 to 12 volts.

The Mega2560 differs from all preceding boards in that it does not use the FTDI USB-to-serial driver chip. Instead, it features the Atmega8U2 programmed as a USB-to-serial converter.

The power pins are as follows:

- **VIN**. The input voltage to the Arduino board when it's using an external power source (as opposed to 5 volts from the USB connection or other regulated power source). You can supply voltage through this pin, or, if supplying voltage via the power jack, access it through this pin.
- **5V**. The regulated power supply used to power the microcontroller and other components on the board. This can come either from VIN via an on-board regulator, or be supplied by USB or another regulated 5V supply.
- **3V3**. A 3.3 volt supply generated by the on-board regulator. Maximum current draw is 50 mA.
- **GND**. Ground pins.

## Memory

The ATmega2560 has 256 KB of flash memory for storing code (of which 8 KB is used for the bootloader), 8 KB of SRAM and 4 KB of EEPROM (which can be read and written with the [EEPROM library](#)).

## Input and Output

Each of the 54 digital pins on the Mega can be used as an input or output, using [pinMode\(\)](#), [digitalWrite\(\)](#), and [digitalRead\(\)](#) functions. They operate at 5 volts. Each pin can provide or receive a maximum of 40 mA and has an internal pull-up resistor (disconnected by default) of 20-50 kOhms. In addition, some pins have specialized functions:

- **Serial**: 0 (RX) and 1 (TX); **Serial 1**: 19 (RX) and 18 (TX); **Serial 2**: 17 (RX) and 16 (TX); **Serial 3**: 15 (RX) and 14 (TX). Used to receive (RX) and transmit (TX) TTL serial data. Pins 0 and 1 are also connected to the corresponding pins of the ATmega8U2 USB-to-TTL Serial chip.
- **External Interrupts**: 2 (interrupt 0), 3 (interrupt 1), 18 (interrupt 5), 19 (interrupt 4), 20 (interrupt 3), and 21 (interrupt 2). These pins can be configured to trigger an interrupt on a low value, a rising or falling edge, or a change in value. See the [attachInterrupt\(\)](#) function for details.
- **PWM**: 0 to 13. Provide 8-bit PWM output with the [analogWrite\(\)](#) function.
- **SPI**: 50 (MISO), 51 (MOSI), 52 (SCK), 53 (SS). These pins support SPI communication, which, although provided by the underlying hardware, is not currently included in the Arduino language. The SPI pins are also broken out on the ICSP header, which is physically compatible with the Duemilanove and Diecimila.
- **LED**: 13. There is a built-in LED connected to digital pin 13. When the pin is HIGH value, the LED is on, when the pin is LOW, it's off.
- **I<sup>C</sup>**: 20 (**SDA**) and 21 (**SCL**). Support I<sup>C</sup> (TWI) communication using the [Wire library](#) (documentation on the Wiring website). Note that these pins are not in the same location as the I<sup>C</sup> pins on the Duemilanove.

The Mega2560 has 16 analog inputs, each of which provide 10 bits of resolution (i.e. 1024 different values). By default they measure from ground to 5 volts, though it is possible to change the upper end of their range using the AREF pin and [analogReference\(\)](#) function.

There are a couple of other pins on the board:

- **AREF**. Reference voltage for the analog inputs. Used with [analogReference\(\)](#).
- **Reset**. Bring this line LOW to reset the microcontroller. Typically used to add a reset button to shields which block the one on the board.



**radiospares**

**RADIOMICS**



## Communication

The Arduino Mega2560 has a number of facilities for communicating with a computer, another Arduino, or other microcontrollers. The ATmega2560 provides four hardware UARTs for TTL (5V) serial communication. An ATmega8U2 on the board channels one of these over USB and provides a virtual com port to software on the computer (Windows machines will need a .inf file, but OSX and Linux machines will recognize the board as a COM port automatically). The Arduino software includes a serial monitor which allows simple textual data to be sent to and from the board. The RX and TX LEDs on the board will flash when data is being transmitted via the ATmega8U2 chip and USB connection to the computer (but not for serial communication on pins 0 and 1).

A [SoftwareSerial library](#) allows for serial communication on any of the Mega's digital pins.

The ATmega2560 also supports I2C (TWI) and SPI communication. The Arduino software includes a Wire library to simplify use of the I2C bus; see the [documentation on the Wiring website](#) for details. To use the SPI communication, please see the ATmega2560 datasheet.

## Programming

The Arduino Mega2560 can be programmed with the Arduino software ([download](#)). For details, see the [reference](#) and [tutorials](#).

The Atmega2560 on the Arduino Mega comes preburned with a [bootloader](#) that allows you to upload new code to it without the use of an external hardware programmer. It communicates using the original STK500 protocol ([reference](#), [C header files](#)).

You can also bypass the bootloader and program the microcontroller through the ICSP (In-Circuit Serial Programming) header; see [these instructions](#) for details.



**radiospares**

**RADIONICS**



## Automatic (Software) Reset

Rather than requiring a physical press of the reset button before an upload, the Arduino Mega2560 is designed in a way that allows it to be reset by software running on a connected computer. One of the hardware flow control lines (DTR) of the ATmega8U2 is connected to the reset line of the ATmega2560 via a 100 nanofarad capacitor. When this line is asserted (taken low), the reset line drops long enough to reset the chip. The Arduino software uses this capability to allow you to upload code by simply pressing the upload button in the Arduino environment. This means that the bootloader can have a shorter timeout, as the lowering of DTR can be well-coordinated with the start of the upload.

This setup has other implications. When the Mega2560 is connected to either a computer running Mac OS X or Linux, it resets each time a connection is made to it from software (via USB). For the following half-second or so, the bootloader is running on the Mega2560. While it is programmed to ignore malformed data (i.e. anything besides an upload of new code), it will intercept the first few bytes of data sent to the board after a connection is opened. If a sketch running on the board receives one-time configuration or other data when it first starts, make sure that the software with which it communicates waits a second after opening the connection and before sending this data.

The Mega contains a trace that can be cut to disable the auto-reset. The pads on either side of the trace can be soldered together to re-enable it. It's labeled "RESET-EN". You may also be able to disable the auto-reset by connecting a 110 ohm resistor from 5V to the reset line; see [this forum thread](#) for details.

## USB Overcurrent Protection

The Arduino Mega has a resettable polyfuse that protects your computer's USB ports from shorts and overcurrent. Although most computers provide their own internal protection, the fuse provides an extra layer of protection. If more than 500 mA is applied to the USB port, the fuse will automatically break the connection until the short or overload is removed.

## Physical Characteristics and Shield Compatibility

The maximum length and width of the Mega PCB are 4 and 2.1 inches respectively, with the USB connector and power jack extending beyond the former dimension. Three screw holes allow the board to be attached to a surface or case. Note that the distance between digital pins 7 and 8 is 160 mil (0.16"), not an even multiple of the 100 mil spacing of the other pins.

The Mega is designed to be compatible with most shields designed for the Diecimila or Duemilanove. Digital pins 0 to 13 (and the adjacent AREF and GND pins), analog inputs 0 to 5, the power header, and ICSP header are all in equivalent locations. Further the main UART (serial port) is located on the same pins (0 and 1), as are external interrupts 0 and 1 (pins 2 and 3 respectively). SPI is available through the ICSP header on both the Mega and Duemilanove / Diecimila. Please note that I<sup>C</sup> is not located on the same pins on the Mega (20 and 21) as the Duemilanove / Diecimila (analog inputs 4 and 5).



**radiospares**

**RADIONICS**



# How to use Arduino



Arduino can sense the environment by receiving input from a variety of sensors and can affect its surroundings by controlling lights, motors, and other actuators. The microcontroller on the board is programmed using the [Arduino programming language](#) (based on [Wiring](#)) and the Arduino development environment (based on [Processing](#)). Arduino projects can be stand-alone or they can communicate with software running on a computer (e.g. Flash, Processing, MaxMSP).

Arduino is a cross-platform program. You'll have to follow different instructions for your personal OS. Check on the [Arduino site](#) for the latest instructions. <http://arduino.cc/en/Guide/HomePage>

## Linux Install

## Windows Install

## Mac Install

Once you have downloaded/unzipped the arduino IDE, you can Plug the Arduino to your PC via USB cable.

### Blink led

Now you're actually ready to "burn" your first program on the arduino board. To select "blink led", the physical translation of the well known programming "hello world", select

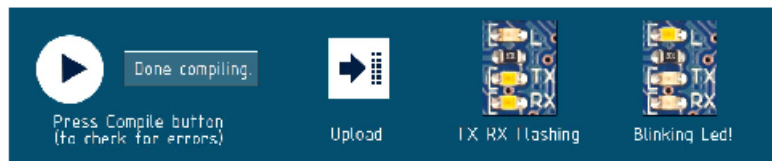
**File>Sketchbook>  
Arduino-0017>Examples>  
Digital>Blink**

Once you have your sketch you'll see something very close to the screenshot on the right.

In **Tools>Board** select MEGA

Now you have to go to **Tools>SerialPort** and select the right serial port, the one arduino is attached to.

```
void setup() {  
  // initialize digital pin 13 as an output.  
  pinMode(13, OUTPUT);  
}  
  
void loop() {  
  digitalWrite(13, HIGH); // Set the LED on  
  delay(1000); // Wait a second  
  digitalWrite(13, LOW); // Set the LED off  
  delay(1000); // Wait a second  
}
```



Done compiling.

Press Compile button  
(to check for errors)



Upload



TX RX Flashing



Blinking Led!



**radiospares**

**RADIONICS**





Shenzhen Global Technology Co., Ltd

Voltage Sensor / Divider Board for ARDUINO developments

Model: Voltage Sensor / 170640

**Description:** This module is designed based on the principle of resistor divider to reduce the input voltage of the terminal interface by 5 times. The maximum input voltage of the Arduino is 5V. The input voltage of the voltage detection module cannot be greater than  $5V \times 5 = 25V$  (if 3.3V is used). System, the input voltage can not be greater than  $3.3V \times 5 = 16.5V$ . Because the AVR chip used by Arduino is 10-bit AD, the analog resolution of this module is  $0.00489V$  ( $5V/1023$ ), so the voltage detection module detects that the input minimum voltage is  $0.00489V \times 5 = 0.02445V$ .  
parameter:  
Voltage input range max: DC0-25V  
Voltage detection range: DC0.02445V - 25V  
Voltage simulation resolution: 0.00489V  
DC Input Interface: terminal positive terminal is connected to VCC, negative terminal is connected to GND  
Output Interface: "-" is connected to 5V3.3V, "+" is connected to GND, and "s" is connected to the AD pin of Arduino.

Reference Code:

```
#include
```

```
int val1;  
int val2;  
  
void setup()  
{  
    pinMode(LED1,OUTPUT);  
    Serial.begin(9600);  
    Serial.println("Emartee.Com");  
    Serial.println("Voltage: ");  
    Serial.print("v");  
}  
void loop()  
{  
    float temp;  
    val1=analogRead(0);  
    temp=val1/4.092;  
    val1=(int)temp//  
    val2=(val1*100)/10;  
    Serial.println(val2);  
    delay(1000);  
}
```



Shenzhen City, Guangdong Science and Technology Co., Ltd. Address: China's Shenzhen Futian District, Shenzhen Huaiqiang North Road  
Copyright © 2010-2015 1688.com All rights reserved. Copyright and Trademark Notices

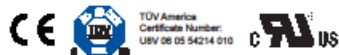


ACS712

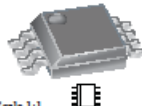
**Fully Integrated, Hall Effect-Based Linear Current Sensor IC  
with 2.1 kVRMS Isolation and a Low-Resistance Current Conductor**

**Features and Benefits**

- Low-noise analog signal path
- Device bandwidth is set via the new FILTER pin
- 5  $\mu$ s output rise time in response to step input current
- 80 kHz bandwidth
- Total output error 1.5% at  $T_A = 25^\circ\text{C}$
- Small footprint, low-profile SOIC8 package
- 1.2 m $\Omega$  internal conductor resistance
- 2.1 kVRMS minimum isolation voltage from pins 1-4 to pins 5-8
- 5.0 V, single supply operation
- 66 to 185 mV/A output sensitivity
- Output voltage proportional to AC or DC currents
- Factory-trimmed for accuracy
- Extremely stable output offset voltage
- Nearly zero magnetic hysteresis
- Ratiometric output from supply voltage



**Package: 8 Lead SOIC (suffix LC)**



Approximate Scale 1:1

**Description**

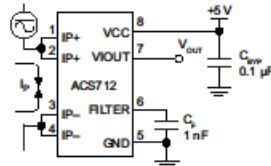
The Allegro® ACS712 provides economical and precise solutions for AC or DC current sensing in industrial, commercial, and communications systems. The device package allows for easy implementation by the customer. Typical applications include motor control, load detection and management, switch-mode power supplies, and overcurrent fault protection. The device is not intended for automotive applications.

The device consists of a precise, low-offset, linear Hall circuit with a copper conduction path located near the surface of the die. Applied current flowing through this copper conduction path generates a magnetic field which the Hall IC converts into a proportional voltage. Device accuracy is optimized through the close proximity of the magnetic signal to the Hall transducer. A precise, proportional voltage is provided by the low-offset, chopper-stabilized BiCMOS Hall IC, which is programmed for accuracy after packaging.

The output of the device has a positive slope ( $>V_{IOUT(Q)}$ ) when an increasing current flows through the primary copper conduction path (from pins 1 and 2, to pins 3 and 4), which is the path used for current sampling. The internal resistance of this conductive path is 1.2 m $\Omega$  typical, providing low power loss. The thickness of the copper conductor allows survival of

*Continued on the next page...*

**Typical Application**



Application 1. The ACS712 outputs an analog signal,  $V_{OUT}$ , that varies linearly with the uni- or bi-directional AC or DC primary sampled current,  $I_p$ , within the range specified.  $C_F$  is recommended for noise management, with values that depend on the application.

ACS712-DS, Rev. 14

## ACS712

*Fully Integrated, Hall Effect-Based Linear Current Sensor IC  
with 2.1 kVRMS Isolation and a Low-Resistance Current Conductor*

### Description (continued)

the device at up to 5 $\times$  overcurrent conditions. The terminals of the conductive path are electrically isolated from the signal leads (pins 5 through 8). This allows the ACS712 to be used in applications requiring electrical isolation without the use of opto-isolators or other costly isolation techniques.

The ACS712 is provided in a small, surface mount SOIC8 package. The leadframe is plated with 100% matte tin, which is compatible with standard lead (Pb) free printed circuit board assembly processes. Internally, the device is Pb-free, except for flip-chip high-temperature Pb-based solder balls, currently exempt from RoHS. The device is fully calibrated prior to shipment from the factory.

### Selection Guide

Part Number	Packing*	T <sub>A</sub> (°C)	Optimized Range, I <sub>P</sub> (A)	Sensitivity, S <sub>ens</sub> (Typ) (mV/A)
ACS712ELCTR-05B-T	Tape and reel, 3000 pieces/reel	-40 to 85	$\pm 5$	185
ACS712ELCTR-20A-T	Tape and reel, 3000 pieces/reel	-40 to 85	$\pm 20$	100
ACS712ELCTR-30A-T	Tape and reel, 3000 pieces/reel	-40 to 85	$\pm 30$	66

\*Contact Allegro for additional packing options.

### Absolute Maximum Ratings

Characteristic	Symbol	Notes	Rating	Units
Supply Voltage	V <sub>CC</sub>		8	V
Reverse Supply Voltage	V <sub>RCC</sub>		-0.1	V
Output Voltage	V <sub>IOUT</sub>		8	V
Reverse Output Voltage	V <sub>RIOUT</sub>		-0.1	V
Reinforced Isolation Voltage	V <sub>ISO</sub>	Pins 1-4 and 5-8; 60 Hz, 1 minute, T <sub>A</sub> =25°C Maximum working voltage according to UL60950-1	2100	VAC
Basic Isolation Voltage	V <sub>ISO(basic)</sub>	Pins 1-4 and 5-8; 60 Hz, 1 minute, T <sub>A</sub> =25°C Maximum working voltage according to UL60950-1	1500	VAC
Output Current Source	I <sub>IOUT(Source)</sub>		3	mA
Output Current Sink	I <sub>IOUT(Sink)</sub>		10	mA
Overcurrent Transient Tolerance	I <sub>P</sub>	1 pulse, 100 ms	100	A
Nominal Operating Ambient Temperature	T <sub>A</sub>	Range E	-40 to 85	°C
Maximum Junction Temperature	T <sub>J(max)</sub>		165	°C
Storage Temperature	T <sub>stg</sub>		-65 to 170	°C

Parameter	Specification
Fire and Electric Shock	CAN/CSA-C22.2 No. 60950-1-03 UL 60950-1:2003 EN 60950-1:2001



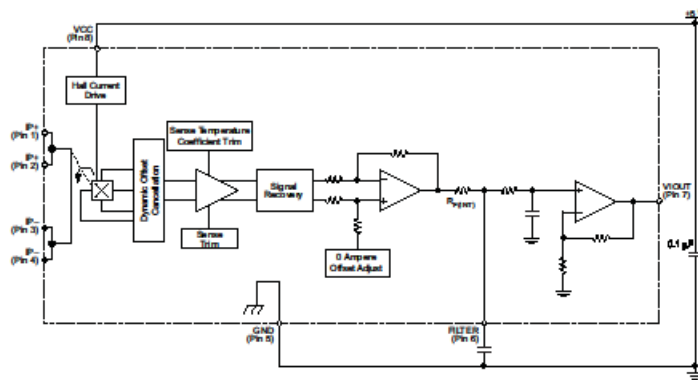
Allegro MicroSystems, Inc.  
115 Northwest Cutoff  
Worcester, Massachusetts 01615-0038 U.S.A.  
1.508.853.5000; www.allegromicro.com

2

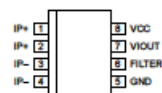
## ACS712

Fully Integrated, Hall Effect-Based Linear Current Sensor IC  
with 2.1 kVRMS Isolation and a Low-Resistance Current Conductor

Functional Block Diagram



Pin-out Diagram



Terminal List Table

Number	Name	Description
1 and 2	IP+	Terminals for current being sampled; fused Internally
3 and 4	IP-	Terminals for current being sampled; fused Internally
5	GND	Signal ground terminal
6	FILTER	Terminal for external capacitor that sets bandwidth
7	VIOUT	Analog output signal
8	VCC	Device power supply terminal



Allegro MicroSystems, Inc.  
115 Northwest Cutoff  
Worcester, Massachusetts 01615-0038 U.S.A.  
1.508.853.5000; [www.allegromicro.com](http://www.allegromicro.com)

3

## ACS712

Fully Integrated, Hall Effect-Based Linear Current Sensor IC  
with 2.1 kVRMS Isolation and a Low-Resistance Current Conductor

**COMMON OPERATING CHARACTERISTICS<sup>1</sup>** over full range of  $T_A$ ,  $C_F = 1 \text{ nF}$ , and  $V_{CC} = 5 \text{ V}$ , unless otherwise specified

Characteristic	Symbol	Test Conditions	Min.	Typ.	Max.	Units
<b>ELECTRICAL CHARACTERISTICS</b>						
Supply Voltage	$V_{CC}$		4.5	5.0	5.5	V
Supply Current	$I_{CC}$	$V_{CC} = 5.0 \text{ V}$ , output open	—	10	13	mA
Output Capacitance Load	$C_{LOAD}$	$V_{OUT}$ to GND	—	—	10	nF
Output Resistive Load	$R_{LOAD}$	$V_{OUT}$ to GND	4.7	—	—	kΩ
Primary Conductor Resistance	$R_{PRIMARY}$	$T_A = 25^\circ\text{C}$	—	1.2	—	mΩ
Rise Time	$t_r$	$I_p = I_p(\text{max})$ , $T_A = 25^\circ\text{C}$ , $C_{OUT}$ = open	—	5	—	μs
Frequency Bandwidth	$f$	–3 dB, $T_A = 25^\circ\text{C}$ ; $I_p$ is 10 A peak-to-peak	—	80	—	kHz
Nonlinearity	$E_{UN}$	Over full range of $I_p$	—	1.5	—	%
Symmetry	$E_{SYM}$	Over full range of $I_p$	98	100	102	%
Zero Current Output Voltage	$V_{OUT(0)}$	Bidirectional; $I_p = 0 \text{ A}$ , $T_A = 25^\circ\text{C}$	—	$V_{CC} \times 0.5$	—	V
Power-On Time	$t_{PO}$	Output reaches 90% of steady-state level, $T_J = 25^\circ\text{C}$ , 20 A present on leadframe	—	35	—	μs
Magnetic Coupling <sup>2</sup>			—	12	—	GA
Internal Filter Resistance <sup>3</sup>	$R_{F(INT)}$			1.7	—	kΩ

<sup>1</sup>Device may be operated at higher primary current levels,  $I_p$ , and ambient,  $T_A$ , and internal leadframe temperatures,  $T_J$ , provided that the Maximum Junction Temperature,  $T_J(\text{max})$ , is not exceeded.

<sup>2</sup>1G = 0.1 mT.

<sup>3</sup> $R_{F(INT)}$  forms an RC circuit via the FILTER pin.

**COMMON THERMAL CHARACTERISTICS<sup>1</sup>**

		Min.	Typ.	Max.	Units
Operating Internal Leadframe Temperature	$T_A$ E range	—40	—	85	°C
			Value		Units
Junction-to-Lead Thermal Resistance <sup>2</sup>	$R_{JL}$	Mounted on the Allegro ASEK 712 evaluation board			5 °C/W
Junction-to-Ambient Thermal Resistance	$R_{JA}$	Mounted on the Allegro 85-0322 evaluation board, Includes the power consumed by the board			23 °C/W

<sup>1</sup>Additional thermal information is available on the Allegro website.

<sup>2</sup>The Allegro evaluation board has 1500 mm<sup>2</sup> of 2 oz. copper on each side, connected to pins 1 and 2, and to pins 3 and 4, with thermal vias connecting the layers. Performance values include the power consumed by the PCB. Further details on the board are available from the Frequently Asked Questions document on our website. Further information about board design and thermal performance also can be found in the Applications Information section of this datasheet.



Allegro MicroSystems, Inc.  
115 Northwest Cutoff  
Worcester, Massachusetts 01615-0038 U.S.A.  
1.508.853.5000; www.allegromicro.com

4

## ACS712

Fully Integrated, Hall Effect-Based Linear Current Sensor IC  
with 2.1 kVRMS Isolation and a Low-Resistance Current Conductor

x05B PERFORMANCE CHARACTERISTICS<sup>1</sup>  $T_A = -40^\circ\text{C}$  to  $85^\circ\text{C}$ ,  $C_F = 1\text{nF}$ , and  $V_{CC} = 5\text{V}$ , unless otherwise specified

Characteristic	Symbol	Test Conditions	Min.	Typ.	Max.	Units
Optimized Accuracy Range	$I_p$		-5	-	5	A
Sensitivity	Sens	Over full range of $I_p$ , $T_A = 25^\circ\text{C}$	180	185	190	mV/A
Noise	$V_{NOISE(PP)}$	Peak-to-peak, $T_A = 25^\circ\text{C}$ , 185 mV/A programmed Sensitivity, $C_F = 47\text{nF}$ , $C_{OUT} = \text{open}$ , 2 kHz bandwidth	-	21	-	mV
Zero Current Output Slope	$\Delta I_{OUT(0)}$	$T_A = -40^\circ\text{C}$ to $25^\circ\text{C}$	-	-0.26	-	mV/ $^\circ\text{C}$
		$T_A = 25^\circ\text{C}$ to $150^\circ\text{C}$	-	-0.08	-	mV/ $^\circ\text{C}$
Sensitivity Slope	$\Delta S_{Sens}$	$T_A = -40^\circ\text{C}$ to $25^\circ\text{C}$	-	0.054	-	mV/A/ $^\circ\text{C}$
		$T_A = 25^\circ\text{C}$ to $150^\circ\text{C}$	-	-0.008	-	mV/A/ $^\circ\text{C}$
Total Output Error <sup>2</sup>	$E_{TOT}$	$I_p = \pm 5\text{A}$ , $T_A = 25^\circ\text{C}$	-	$\pm 1.5$	-	%

<sup>1</sup>Device may be operated at higher primary current levels,  $I_p$ , and ambient temperatures,  $T_A$ , provided that the Maximum Junction Temperature,  $T_{J(max)}$ , is not exceeded.

<sup>2</sup>Percentage of  $I_p$ , with  $I_p = 5\text{A}$ . Output filtered.

x20A PERFORMANCE CHARACTERISTICS<sup>1</sup>  $T_A = -40^\circ\text{C}$  to  $85^\circ\text{C}$ ,  $C_F = 1\text{nF}$ , and  $V_{CC} = 5\text{V}$ , unless otherwise specified

Characteristic	Symbol	Test Conditions	Min.	Typ.	Max.	Units
Optimized Accuracy Range	$I_p$		-20	-	20	A
Sensitivity	Sens	Over full range of $I_p$ , $T_A = 25^\circ\text{C}$	96	100	104	mV/A
Noise	$V_{NOISE(PP)}$	Peak-to-peak, $T_A = 25^\circ\text{C}$ , 100 mV/A programmed Sensitivity, $C_F = 47\text{nF}$ , $C_{OUT} = \text{open}$ , 2 kHz bandwidth	-	11	-	mV
Zero Current Output Slope	$\Delta I_{OUT(0)}$	$T_A = -40^\circ\text{C}$ to $25^\circ\text{C}$	-	-0.34	-	mV/ $^\circ\text{C}$
		$T_A = 25^\circ\text{C}$ to $150^\circ\text{C}$	-	-0.07	-	mV/ $^\circ\text{C}$
Sensitivity Slope	$\Delta S_{Sens}$	$T_A = -40^\circ\text{C}$ to $25^\circ\text{C}$	-	0.017	-	mV/A/ $^\circ\text{C}$
		$T_A = 25^\circ\text{C}$ to $150^\circ\text{C}$	-	-0.004	-	mV/A/ $^\circ\text{C}$
Total Output Error <sup>2</sup>	$E_{TOT}$	$I_p = \pm 20\text{A}$ , $T_A = 25^\circ\text{C}$	-	$\pm 1.5$	-	%

<sup>1</sup>Device may be operated at higher primary current levels,  $I_p$ , and ambient temperatures,  $T_A$ , provided that the Maximum Junction Temperature,  $T_{J(max)}$ , is not exceeded.

<sup>2</sup>Percentage of  $I_p$ , with  $I_p = 20\text{A}$ . Output filtered.

x30A PERFORMANCE CHARACTERISTICS<sup>1</sup>  $T_A = -40^\circ\text{C}$  to  $85^\circ\text{C}$ ,  $C_F = 1\text{nF}$ , and  $V_{CC} = 5\text{V}$ , unless otherwise specified

Characteristic	Symbol	Test Conditions	Min.	Typ.	Max.	Units
Optimized Accuracy Range	$I_p$		-30	-	30	A
Sensitivity	Sens	Over full range of $I_p$ , $T_A = 25^\circ\text{C}$	63	66	69	mV/A
Noise	$V_{NOISE(PP)}$	Peak-to-peak, $T_A = 25^\circ\text{C}$ , 66 mV/A programmed Sensitivity, $C_F = 47\text{nF}$ , $C_{OUT} = \text{open}$ , 2 kHz bandwidth	-	7	-	mV
Zero Current Output Slope	$\Delta I_{OUT(0)}$	$T_A = -40^\circ\text{C}$ to $25^\circ\text{C}$	-	-0.35	-	mV/ $^\circ\text{C}$
		$T_A = 25^\circ\text{C}$ to $150^\circ\text{C}$	-	-0.08	-	mV/ $^\circ\text{C}$
Sensitivity Slope	$\Delta S_{Sens}$	$T_A = -40^\circ\text{C}$ to $25^\circ\text{C}$	-	0.007	-	mV/A/ $^\circ\text{C}$
		$T_A = 25^\circ\text{C}$ to $150^\circ\text{C}$	-	-0.002	-	mV/A/ $^\circ\text{C}$
Total Output Error <sup>2</sup>	$E_{TOT}$	$I_p = \pm 30\text{A}$ , $T_A = 25^\circ\text{C}$	-	$\pm 1.5$	-	%

<sup>1</sup>Device may be operated at higher primary current levels,  $I_p$ , and ambient temperatures,  $T_A$ , provided that the Maximum Junction Temperature,  $T_{J(max)}$ , is not exceeded.

<sup>2</sup>Percentage of  $I_p$ , with  $I_p = 30\text{A}$ . Output filtered.



Allegro MicroSystems, Inc.  
115 Northwest Cutoff  
Worcester, Massachusetts 01615-0038 U.S.A.  
1.508.853.5000; www.allegromicro.com

5

## DS18B20 Waterproof Temperature Sensor Cable



### Product Description

This Maxim-made item is a digital thermo probe or sensor that employs DALLAS DS18B20. Its unique 1-wire interface makes it easy to communicate with devices. It can converts temperature to a 12-bit digital word in 750ms (max). Besides, it can measures temperatures from -55°C to +125°C (-67F to +257F). In addition, this thermo probe doesn't require any external power supply since it draws power from data line. Last but not least, like other common thermo probe, its stainless steel probe head makes it suitable for any wet or harsh environment.

The datasheet of this DS18B20 Sensor can be found from:

<https://dl.nmh9io6v2uc.cloudfront.net/datasheets/Sensors/Temperature/DS18B20.pdf>

### Feature:

Power supply range:	3.0V to 5.5V
Operating temperature range:	-55°C to +125°C (-67F to +257F)
Storage temperature range:	-55°C to +125°C (-67F to +257F)
Accuracy over the range of -10°C to +85°C:	±0.5°C
3-pin 2510 Female Header Housing	

Waterproof Stainless steel sheath	
Stainless steel sheath	
Size of Sheath:	6*50mm
Connector:	RJ11/RJ12, 3P-2510, USB.
Pin Definition:	RED: VCC Yellow: DATA Black: GND
Cable length:	1meter, 2m, 3m, 4m are available upon request.

**Application:**

The DS18B20 Digital Temperature Probe provides 9 to 12 bit (configurable) temperature readings which indicate the temperature of the device. Information is sent to/from the DS18B20 over a 1-Wire interface, so that only one wire (and ground) needs to be connected from a central microprocessor to a DS18B20. Power for reading, writing, and performing temperature conversions can be derived from the data line itself with no need for an external power source.

Because each DS18B20 contains a unique silicon serial number, multiple DS18B20s can exist on the same 1Wire bus. This allows for placing temperature sensors in many different places. Applications where this feature is useful include HVAC environmental controls, sensing temperatures inside buildings, equipment or machinery, and process monitoring and control.

**Details:**



Figure 1

Quick-teck Electronics Components datasheet

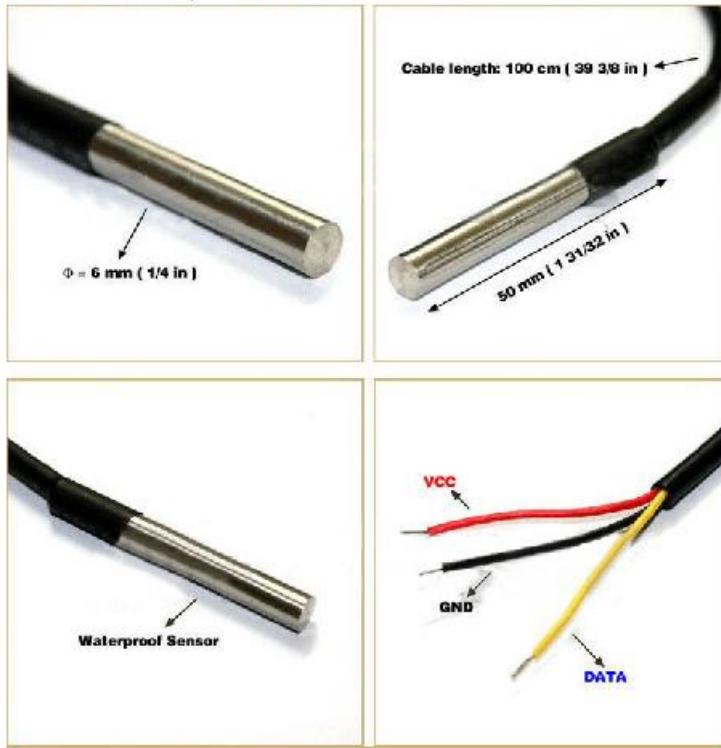


Figure 2

## Overview

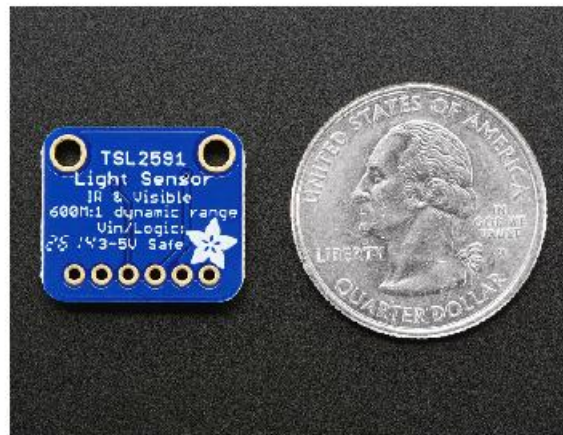
**Adafruit TSL2591 High Dynamic Range Digital Light Sensor**

Created by lady ada

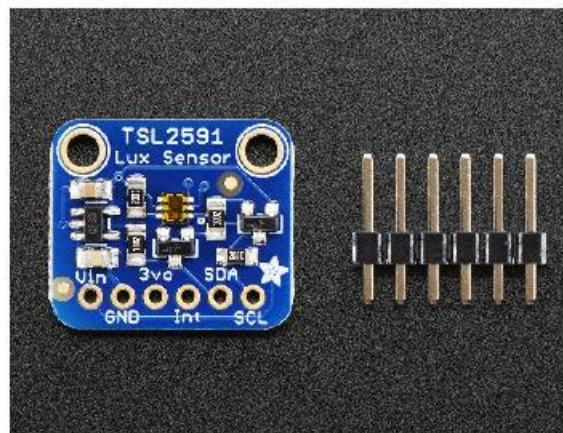


When the future is dazzlingly-bright, this ultra-high-range luminosity sensor will help you measure it. The TSL2591 luminosity sensor is an advanced digital light sensor, ideal for use in a wide range of light situations. Compared to low cost CdS cells, this sensor is more precise, allowing for exact lux calculations and can be configured for different gain/timing ranges to detect light ranges from up to 188uLux up to 88,000 Lux on the fly.

The best part of this sensor is that it contains both infrared and full spectrum diodes! That means you can separately measure infrared, full-spectrum or human-visible light. Most sensors can only detect one or the other, which does not accurately represent what human eyes see (since we cannot perceive the IR light that is detected by most photo diodes)



This sensor is much like the TSL2561 but with a wider range (and the interface code is different). This sensor has a massive 600,000,000:1 dynamic range! Unlike the TSL2561 you cannot change the I<sub>C</sub> address either, so keep that in mind.



The built in ADC means you can use this with any microcontroller, even if it doesn't have analog inputs. The current draw is extremely low, so its great for low power data-logging systems. about 0.4mA when actively sensing, and less than 5  $\mu$ A when in power-down mode.

## Pinouts

The TSL2591 is a I2C sensor. That means it uses the two I2C data/clock wires available on most microcontrollers, and can share those pins with other sensors as long as they don't have an address collision. For future reference, the I2C address is `0x29` and you *can't* change it!



### Power Pins:

- ◆ **Vin** - this is the power pin. Since the chip uses 3 VDC, we have included a voltage regulator on board that will take 3-5VDC and safely convert it down. To power the board, give it the same power as the logic level of your microcontroller - e.g. for a 5V micro like Arduino, use 5V
- **3vo** - this is the 3.3V output from the voltage regulator, you can grab up to 100mA from this if you like
- ◆ **GND** - common ground for power and logic

(<https://adafru.it/dGy>)

- **SCL** - I2C clock pin, connect to your microcontrollers I2C clock line.
- **SDA** - I2C data pin, connect to your microcontrollers I2C data line.

### Other Pins:

- **INT** - this is the INTerrupt pin from the sensor. It can be programmed to do a couple different things by noodling with the I2C registers. For example trigger when a conversion is done, or when the light level has changed a lot, etc. We don't have library support for this pin.

**APPENDIX D**  
**DOCUMENTATION**



Project Presentation



IEEE HNICEM 2019



Deployment at MRF Balangkas, Valenzuela City

**APPENDIX E**  
**CURRICULUM VITAE**



Seeking a challenging career with a progressive organization to share and gain knowledge by performing the assigned task according to company's standard.

## EDUCATION

### Bachelor of Science in Electronics Engineering

Technological University of the Philippines  
A.Y. 2016 – 2020

#### Thesis

Neuro-Fuzzy based MPPT for Solar PV Panel Hybrid Cooling System

Published Paper at IEEE HNICEM 2019

## AFFILIATION

A.Y. 2018-2019

#### Junior Committee Head

at Commission on Student Election (COMSELEC)

A.Y. 2018-2020

#### Vice President

at Association of Student Assistants

2018 – Present

#### ECT Associate Member

at Institute of Electronics Engineers of the Philippines

# RICKRIC O. GRATELA

📍 Lancaster New City General Trias, Cavite

📞 09226705827/09350152240

✉️ Rickricgratela@gmail.com

## SKILLS

### TECHNICAL

1. Calibration and Preventive maintenance of specific handlers.
2. Knowledgeable on basic hardware troubleshooting, Digital Electronics and PCB Designing.
3. Electronic Circuit Analysis, Basic R Programming and C++.

### PERSONAL

1. Self-motivated, initiative, high level of energy.
2. Quick learner of advance technologies.
3. Adaptability and ability to work under pressure.

## LICENSE & CERTIFICATION

October 2018    **Electronics Technician (ECT)**

## EXPERIENCE

(April 2019 – June 2019)

### PROCESS ENGINEER (INTERN)

[ANALOG DEVICES INC.](#)

Gateway Business Park 4107, General Trias, Cavite

- Basic process mapping, analysis and issue investigation.
- Material standard qualification monitoring process and Technical Review Board endorsing, Engineering Report.
- Material specification organizing and revision.
- Failure Mode Effect Analysis (FMEA)
- MSOP and SOIC Measuring equipment programming

(June 2015 – October 2015)

### TECHNICAL SUPPORT (INTERN)

[MAXIM INTEGRATED PHILIPPINES](#)

Gateway Business Park 4107, General Trias, Cavite

- Handler and Prober calibration
- Handler and Prober preventive maintenance
- Delta 8000 and Rasco 1500 plunging distance monitoring



To seek career development opportunities where my capacity and knowledge could be best subjected and utilized to support the growth of myself and the organization.

## EDUCATION

### Bachelor of Science in Electronics Engineering

Technological University of the Philippines  
A.Y. 2014 – 2020

#### Thesis

Neuro-Fuzzy based MPPT for Solar PV Panel Hybrid Cooling System

Published Paper at IEEE HNICEM 2019

## AFFILIATION

A.Y. 2019-2020

### TUP Manila Board of Directors – Head

at Institute of Electronics Engineers of the Philippines Manila Student Chapter

A.Y. 2018-2019

### TUP Manila Board of Directors – Member

at Institute of Electronics Engineers of the Philippines Manila Student Chapter

2018 – Present

### Member

at Institute of Electronics Engineers of the Philippines

# JOYCE ANN S. MARTES

📍 136 Kings Street, Manuyo Dos, Las Piñas City, Manila

📞 09612422275

✉️ joyceann.martes@tup.edu.ph

## SKILLS

### TECHNICAL

1. Basic Data Analysis, Electronic Circuit Analysis, and Circuitry Troubleshooting.
2. Basic R Programming, Digital Signal Processing using MATLAB.
3. Familiar with software such as LABVIEW and Virtuoso.
4. Good communication skills and technical writing.

### PERSONAL

1. Exceptionally versatile and adaptable.
2. Adaptive of new concepts quickly and efficiently.
3. Self-motivated to learn new skills and techniques.

## LICENSE & CERTIFICATION

2018 - Present **Tertiary Education Subsidy (TES) Scholar**

October 2018 **Electronics Technician (ECT)**

2014 - 2017 **Department of Science and Technology – Science Education Institute (DOST-SEI) Scholar**

## EXPERIENCE

(April 2019 – June 2019)

### TECHNICAL SUPPORT (INTERN)

[Glacier South Refrigeration Services Corporation](#)

Amvel Business Park, San Dionisio, Parañaque City

- Installation of CCTV Surveillance Systems.
- Monitoring of the daily total energy consumption.
- Maintenance/Troubleshooting of Electronic Equipment.
- Learning Electromechanical Disciplines and Applications: Refrigeration and Air Conditioning Technology.



To obtain employment with a company that offers a positive atmosphere to learn and implement new skills and technologies for the betterment of the organization

## EDUCATION

### Bachelor of Science in Electronics Engineering

Technological University of the Philippines  
A.Y. 2016 – 2020

#### Thesis

Neuro-Fuzzy based MPPT for Solar PV Panel Hybrid Cooling System

Published Paper at IEEE HNICEM 2019

## AFFILIATION

A.Y. 2017-2019

**Awards and Certifications Committee – Chairperson**  
at Annual Presentation of Project Research in Engineering

A.Y. 2017-2018

**Publication and Certification Senior Committee Head**  
at Organization of Electronics Engineering Students

2018 – Present

**Member**  
at Institute of Electronics Engineers of the Philippines

# GEROME I. PAGATPATAN

📍 Don Mariano Academe Residences San Miguel, Manila

📞 09771100698

✉️ pagatpatangerome@gmail.com

## SKILLS

### TECHNICAL

1. Competent in Adobe Photoshop and MS Office Applications.
2. Electronic Circuit Analysis, Basic R Programming, and Digital Signal Processing using MATLAB.
3. Good communication skills and proficient in English language both written and oral.

### PERSONAL

1. Exceptionally versatile and adaptable.
2. Quick learner of advance technologies.
3. Self-motivated to learn new skills and techniques.

## LICENSE & CERTIFICATION

October 2018      **Electronics Technician (ECT)**

April 2018      **IT Passport (IP) Certification Examination**

## EXPERIENCE

(April 2019 – June 2019)

### NETWORK ENGINEER (INTERN)

#### ASIA UNITED BANK – HEAD OFFICE

Joy-Nostalg Center, 17 ADB Ave, San Antonio, Mandaluyong City

- Configuration of Router, Switches and VoIP.
- Troubleshooting, diagnosing and resolving hardware, software, and other network and system problems.
- Conferring with network users about solving existing system problems.

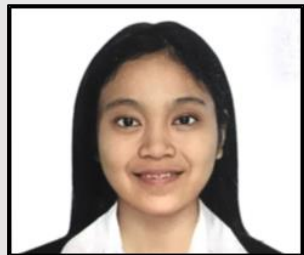
(May 2015 – October 2015)

### TECHNICAL SUPPORT (INTERN)

#### EXPOSE SECURITY & ELECTRONICS

1629 Laguna St, Santa Cruz, Manila, 1003 Metro Manila

- Installation of CCTV Surveillance Systems.
- DNS and Port Forwarding Configuration.
- Maintenance/Troubleshooting of Electronic Equipment.



# JESSA P. PAGKALIWANGAN

Las Pinas City, Manila

09451542489

pjessap@gmail.com

## SKILLS

### TECHNICAL

1. Competent in MS Office Applications.
2. Electronic Circuit Analysis, Basic R Programming, and Digital Signal Processing using MATLAB.
3. Good communication skills and proficient in English language both written and oral.

### PERSONAL

1. Exceptionally versatile and adaptable.
2. Quick learner of advance technologies.
3. Self-motivated to learn new skills and techniques.

## LICENSE & CERTIFICATION

October 2018 **Electronics Technician (ECT)**

October 2018 **IT Passport (IP) Certification Examination**

February 2020 **Cisco Certified Network Associate CCNA**

## AFFILIATION

A.Y. 2016-2020

### Member

at Organization of Electronics Engineering Students

2018 – Present

### Member

at Institute of Electronics Engineers of the Philippines



To seek a job where I can hone my knowledge and skills in order to contribute to the company's success as well as my personal development through work.

## EDUCATION

### Bachelor of Science in Electronics Engineering

Technological University of the Philippines  
A.Y. 2016 – 2020

#### Thesis

Neuro-Fuzzy based MPPT for Solar PV Panel Hybrid Cooling System

Published Paper at IEEE HNICEM 2019

## AFFILIATION

A.Y. 2017-2018

### Conference Secretariat – Co-Chairperson

at Annual Presentation of Project Research in Engineering

A.Y. 2017-2018

### Public Relations Officer

at Organization of Electronics Engineering Students

2018 – Present

### Member

at Institute of Electronics Engineers of the Philippines

# DIETHER KYLE A. TORCUATO

📍 2216 Rd. 15 Fabie Estate Sta.Ana, Manila

📞 09272112244

✉ dkatorcuato@gmail.com

## SKILLS

### TECHNICAL

1. Proficient in MS Office Applications.
2. Electronic Circuit Analysis, Basic R Programming, and Digital Signal Processing using MATLAB.
3. Good communication skills and proficient in English language both written and oral.

### PERSONAL

1. Exceptionally versatile and adaptable.
2. Quick learner of advance technologies.
3. Self-motivated to learn new skills and techniques.

## LICENSE & CERTIFICATION

October 2018      **Electronics Technician (ECT)**

April 2018      **IT Passport (IP) Certification Examination**

## EXPERIENCE

(April 2015 – October 2015)

(April 2019-May 2019)

### SERVICE TECHNICIAN (INTERN)

#### Golden Cup Exim Marketing Corporation

2437 Tejeron St. Sta.Anna, Manila, Metro Manila

- Configuration of different Photocopy Machines.
- Troubleshooting, diagnosing and resolving hardware problems of Photocopy Machines.

## PROOFREADER'S CERTIFICATE

This is to certify that the undersigned has reviewed and went through all the pages of the proposed project study manuscript / research entitled "**NEURO-FUZZY BASED MPPT FOR SOLAR PV PANEL HYBRID COOLING SYSTEM**" developed by **RICKRIC O. GRATELA, JOYCE ANN S. MARTES, GEROME I. PAGATPATAN, JESSA P. PAGKALIWANGAN, AND DIETHER KYLE A. TORCUATO** aligned with the set of structural rules that govern the composition of *sentences, phrases, and words* in the English language.

Signed:



Jenny Rose B. Mazo, LPT

Date Signed:

December 13, 2020